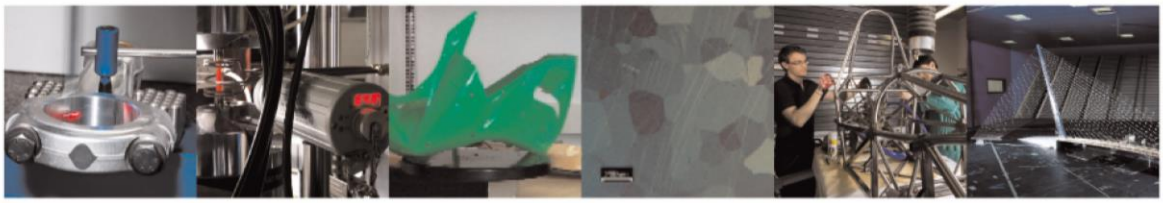

Learning to deep learning: statistics and a paradigm test in selecting a UNet architecture to enhance MRI

Sharma, R.; Tsiamyrtzis, P.; Webb, A. G.; Leiss, E. L.; Tsekos, N. V.

This is a post-peer-review, pre-copyedit version of an article published in MAGNETIC RESONANCE MATERIALS IN PHYSICS BIOLOGY AND MEDICINE. The final authenticated version is available online at: http://dx.doi.org/10.1007/s10334-023-01127-6

Learning to deep-learning: statistics and a paradigm test in selecting a UNet architecture to enhance MRI

Rishabh Sharma[1], Panagiotis Tsiamyrtzis[2], Andrew G. Webb[3], Ernst L. Leiss[4], Nikolaos V. Tsekos[1,*]

[1]Medical Robotics and Imaging Lab, Department of Computer Science, University of Houston, Houston, TX, USA
[2]Department of Mechanical Engineering, Politecnico di Milano, Milan, Italy & Department of Statistics, Athens University of Economics and Business, Greece
[3]C.J. Gorter Center for High Field MRI, Department of Radiology, Leiden University Medical Center, Leiden, The Netherlands
[4]Department of Computer Science, University of Houston, Houston, TX, USA
[*]Corresponding Author at: 501, Philip G. Hoffman Hall, University of Houston, 4800 Calhoun Road, Houston, TX 77204, United States of America

Abstract

Objective: This study aims to assess the statistical significance of training parameters in 240 dense UNets (DUNets) used for enhancing low Signal-to-Noise Ratio (SNR) and undersampled MRI in various acquisition protocols. The objective is to determine the validity of differences between different DUNet configurations and their impact on image quality metrics.
Methods: To achieve this, we trained all DUNets using the same learning rate and number of epochs, with variations in 5 acquisition protocols, 24 loss function weightings, and 2 ground truths. We calculated evaluation metrics for two metric regions of interest (ROI). We employed both Analysis of Variance (ANOVA) and Mixed Effects Model (MEM) to assess the statistical significance of the independent parameters, aiming to compare their efficacy in revealing differences and interactions among fixed parameters.
Results: ANOVA analysis showed that, except for the acquisition protocol, fixed variables were statistically insignificant. In contrast, MEM analysis revealed that all fixed parameters and their interactions held statistical significance. This emphasizes the need for advanced statistical analysis in comparative studies, where MEM can uncover finer distinctions often overlooked by ANOVA.
Discussion: These findings highlight the importance of utilizing appropriate statistical analysis when comparing different deep learning models. Additionally, the surprising effectiveness of the UNet architecture in enhancing various acquisition protocols underscores the potential for developing improved methods for characterizing and training deep learning models. This study serves as a stepping stone toward enhancing the transparency and comparability of deep learning techniques for medical imaging applications.

Keywords

Deep learning, UNet, statistical significance, mixed effects modeling, enhance, undersampled

Introduction

In the field of Magnetic Resonance (MR), there is an ever-growing body of work in deep learning (DL) techniques [1–5], including feed-forward convolutional neural networks (CNN) [5–7], UNets [4, 8–14], and generative adversarial networks (GANs) [15–17]. Among the most common applications are the use of DL in reconstructing undersampled k-space data [3–5, 18] and the enhancement of low resolution and/or low signal-to-noise ratio (SNR) images or spectroscopic scans [19–21]. The growing number and the inherently complex nature of DL techniques underscore the challenge of selecting the appropriate architecture, as well as its training pipeline, which includes training data sets [22], ground truths [23], loss functions [24], and metrics of performance [25].

Introducing a new or modified neural network typically includes comparisons with other DL and non-DL methods [23, 26–28], most usually based on average image quality metrics calculated over the test populations [29, 30]. In such studies, relying on empirical results emphasizes the importance of testing for statistical significance to ensure that results are not coincidental [31, 32]. Statistical analysis and significance testing can be critical when the reported differences in means are small relative to their standard deviations or distributions of the metrics; such findings are common in MRI DL studies [11, 12, 33], and subjective evaluation is eventually used as the determinant [5]. While a significant portion of surveyed works does not assess statistical significance when comparing methods, some works use analysis of variance (ANOVA) [34, 35]. However, in typical DL studies where the comparison is based on testing the networks on the same data set, ANOVA is not the appropriate statistical model since it does not consider repeated measures (ANOVA assumes different data sets with the same distribution). In these cases, the appropriate statistical analysis is the mixed effects model (MEM) based analysis on the same set [36].

These observations have led us to conduct the present study, which aims to evaluate whether, and to what extent, statistical analysis can capture differences in the performance of networks in terms of their training and outcomes characterized with the commonly used image quality metrics. To investigate this, a simple scenario of implementing a neural network for enhancing undersampled and/or low SNR MR images was replicated. Then, statistical analysis is conducted to evaluate whether, and to what extent, significant conclusions can be drawn regarding the operator- and user-selectable aspects of implementing the network that represents network training and characterization. While the aforementioned matters relate to virtually any neural architecture, here we focus on UNets that were designed for elucidating imaging features [37], including image-to-image translations such as post-acquisition enhancement of low quality MRI images [19, 38–44]. In particular, we utilized a version of Dense UNet (DUNet) that was employed before to enhance image quality [45–49]. We chose a few significant parameters that affect network performance, specifically related to training and metric calculation, from the countless options available. Our investigation of this DUNet focuses on two training features (loss function and ground truth) and outcomes (metrics calculated on the entire image or a specific area).

The first training-related aspect investigated in this work is the loss function [24, 50]. A characteristic of the multifaceted nature of DL training is that loss functions can be even more important than the details of the network architecture [51]. From the wide range of used loss functions, we trained the DUNet with simple pixel-to-pixel ones: (a) the fundamental functions L1 [50, 52], L2 [6–10, 14], structural similarity index measure (SSIM) [50, 52–55], and (b) composite loss functions (CLFs), i.e., weighted additions of the aforelisted fundamental ones [24, 56–59]. CLFs are used to train networks to improve multiple image properties concurrently. As an example, in UNets, the inclusion of edge information [60] or SSIM [58] along with pixel-to-pixel

loss (L1 or L2), incorporates the presence of structural information that is also optimized during network training. The second training-related aspect was the ground truth (GT), which also determines the features of the image the network will transform. Manipulated GT were used before, including sharpening GT, simulating GT images, acquiring GT using scanners, and averaging signals to create GT with different SNRs [23, 61, 62]. Recently, the pioneering concept of using undersampled MRI as GT in self-supervised MRI reconstruction was introduced by Korkmaz et al. [63]. The third aspect evaluated image metrics calculated on the entire image or a targeted area. Metrics measured over the entire image can present challenges for implementing suitable DL, so focusing on a region of interest (ROI) may be necessary to optimize performance. Sun et al. suggest that training networks on ROI tend to optimize ROIs better and that networks affect specific regions of the image differently [64]. In this work, we added a synthetic high intensity lesion during the data augmentation phase; this artificial lesion was used to prescribe the ROI for focused metrics.

The tested statistical analysis models were applied in comparing the performance of the aforelisted DUNets to enhance MRI images with a variety of Signal-to-Noise Ratio (SNR) and image structural information. Those images were in silico generated using five different acquisition protocols (AcqPr) corresponding to different combinations of k-space sampling and repetitions per k-space line. Since the objective of this work was to assess the statistical analysis, we implemented those AcqPr with: (a) simple Cartesian undersampling (i.e., along the phase encoding of a conventional pulse sequence), (b) all AcqPr had the same total number of k-space lines (i.e., same duration of acquisition), (c) variations of image quality was secondary to adjusting k-space sampling pattern and repetitions per k-space line. It is noted that this work, does not entail evaluation of reconstruction algorithms, rather investigates a simple UNet-based image enhancement of reconstructed MRI images. The design of this study focuses first on assessing the statistical analysis in investigating the impact of various factors (like loss function, GT, and AcqPr) that contribute to the overall training and the AI model.

We compared the performance of a DUNet using four commonly used image quality metrics: mean squared error (MSE), mean absolute error (MAE), peak signal-to-noise ratio (PSNR), and structural similarity index measure (SSIM) [65]. Statistical analysis was based on descriptive statistics (i.e., mean ± standard deviation) on the test set and testing for statistical significance using both ANOVA and MEM. Descriptive analysis was performed for 480 cases corresponding to all possible combinations of the twenty four CLFs, the two GT, the five AcqPr, and the two measurement regions of interest (MeROI). Our significance tests focused on identifying the contributions of weightings in composite loss functions, acquisition protocols, and their interaction. By conducting significance tests on AI components, such as loss functions and AcqPr, we aim to improve interpretability and create more explainable AI systems.

Materials and Methods

Study Design

In this study, we utilized an appropriately trained DUNet to enhance low SNR and undersampled images. The image quality was then evaluated using conventional image evaluation metrics. The study was conducted in three steps, which are summarized in Table 1: (I) data acquisition, i.e., generation of the acquired images (IMacq), using specific acquisition protocols (AcqPr). The IMacq were then used as input to the DUNet. (II) DL step that included (a) training of the DUNet, with the IMacq and GT training sets, matching GT and LF, and (b) applying the DUNet on the test set of IMacq to generate the enhanced images (IMenh), and (III) processing the IMenh for statistical analysis of the evaluation metrics. These in silico studies need networks to be trained and tested with spatially matched pairs of IMacq and corresponding GT, which are not publicly

available and hard to collect. So, we synthesized them from the publicly available OASIS project [66] (as discussed below).

A simple cartesian scanning approach is utilized, with k-space undersampling along the phase encoding axis, followed by a weighted k-space acquisition which determines the distribution (or number) of repetitions (Nreps) per k-space line; this is the acquisition protocol (AcqPr). In suboptimal conditions, an AcqPr of Nreps = 100 is assumed to be the best choice to improve SNR for all lines of the complete (100%) k-space (matrix size of the OASIS images 176x208). The time required to collect such an image is (100%)x100xTR = TR×10^4. These images serve as one of the types of tested GT, the acquired ground truth (GTacq). Assuming a 10-fold reduction in acquisition duration, AcqPr with a time cost of TR×10^3 can be prescribed. Table 1 reports the five AcqPr used to acquire the IMacq, and Fig. 1 illustrates the simulated IMacq for each AcqPr and their difference with GTacq.

Table 1 lists the 240 in silico experiments, each one corresponding to a combination of an AcqPr (x5), an LF/CLF (x24), and a GT (x2). Each experiment entailed training, testing, and validation of a DUnet dedicated to a particular combination of parameters. The testing outcomes of the 240 experiments were used to calculate the evaluation metrics for the two cases of meROI. This resulted in 480 cases, and these cases were analyzed using ANOVA and MEM to statistically evaluate the differences in performance between independent parameters.

To generate the input IMacq, we simulated the acquisition of the k-space for each experiment using five different AcqPr (N=5), keeping the total number of collected k-space lines constant. These protocols produce images with varying degrees of blurring artifacts and SNR, as shown in Table 1 and visualized in Fig. 1.

Twenty four loss functions composed of three single and two composite functions were tested. The single functions consisted of two pixel-to-pixel loss functions (I) L1 [50, 52] and (II) L2 [6–10, 14], and a perceptual metric loss function to measure image similarity, (III) the SSIM loss (LSSIM) [50, 52–55] computed with window sizes 3 and 7 (LSSIMw3 and LSSIMw7). The LSSIM is defined as

$$\mathrm{LSSIM} = \frac{1}{\mathrm{N}} \times \sum_{\mathrm{n=1}}^{\mathrm{N}} 1 - \mathrm{SSIM(n)} \tag{1}$$

where ‘N’ is the number of total pixels in the image, and ‘n’ is any given pixel location in the image.

The two composite loss functions that combined pixel-to-pixel and structural information were (IV) CLF1 = κ×L1+(1-κ)×$L1_{Canny}$, where κ ∈ [0.0,0.9] in steps of 0.1 [56]. CLF1 combines pixel-to-pixel L1 loss over the entire image and the edge map loss component $L1_{Canny}$ calculated as shown in equation 2, and (V) CLF2 = L1+λ×LSSIM, where λ ∈ [0.0 – 0.5] in steps of 0.1 and LSSIM window sizes are 3 and 7 [58].

$$\mathrm{L1_{Canny}} = \frac{1}{\mathrm{N}} \times \sum_{\mathrm{i=0}}^{\mathrm{N}} \left| \mathrm{Edge_{Y_{True}}} \times \mathrm{Y_{True}} - \mathrm{Edge_{Y_{True}}} \times \mathrm{Y_{Pred}} \right| \tag{2}$$

where ‘N’ is the number of total pixels in the image. Y_{True} and Y_{Pred} are the GT and IMenh, respectively. $\mathrm{Edge_{Y_{True}}}$ is the edge map of the ground truth generated using the Canny filter. To calculate $L1_{Canny}$, $\mathrm{Edge_{Y_{True}}}$ is multiplied on a pixel-by-pixel basis with both Y_{True} and Y_{Pred}. It is

important to note that only the edge map of the Y_{True} is used for pixel-by-pixel multiplication for both Y_{True} and Y_{Pred} because $\mathrm{Edge}_{Y_{True}}$ represents the true edges expected in the GT image.

We tested two types of ground truth. The first, GTsyn, was the outcome of the augmentations step (i.e., steps corresponding to random rotations and the hyperintense lesion shown in Fig. 2) applied to the images from the OASIS dataset with complete k-space data; as such, it corresponds to zeroing the signal of the empty space. The process to generate GTsyn involved rotations, addition of hyperintense lesions with random attributes, and elastic deformation applied to white and gray matter regions. Additionally, Gaussian noise was introduced to the resulting images. The combination of rotated gray matter (GM), white matter (WM), and cerebrospinal fluid (CSF) images produced synthetic MRI (synMRI) images, serving as the Ground Truth with a resolution of 176 × 208. A more detailed description of GTsyn generation can be found from the work of Sharma et al. [49]. The second, GTacq, was generated by averaging Nreps = 100 images synthesized from the complete k-space (each with random Gaussian noise applied to its k-space), replicating the scenario where ground truth is experimentally determined. The performance of the 240 DUNets was assessed by measuring evaluation metrics MSE, MAE, PSNR, and SSIM on (I) the entire image and (II) lesion-focused ROI.

Training and Testing Dataset

These in silico studies used brain MRI from the OASIS project dataset [66]; originally tailored for investigations related to Alzheimer's disease and brain aging. It comprises high-quality structural MRI scans of the brain from a diverse group of participants, encompassing both healthy individuals and those diagnosed with Alzheimer's disease. We started with 436 T1 weighted MRI images randomly selected from the OASIS project (in gif format included in the database) [66] and synthesized 2616 synthetic images based on the augmentation pipeline reported in previous work [49]. Each synthetic data set (5 images generated with the five AcqPr and the two GTs) comprises ten pairs of unique AcqPr and GT. Fig. 2 illustrates the two steps of the implemented synthesis: (I) Augmentation in the real space by random rotations of segmented WM, GM, and CSF maps, followed by their weighted addition on an empty zero signal matrix. Subsequently, random diameter and position circular hyperintense lesions (subjected to elastic deformation [33]) limited to the WM and GM were added to generate GTsyn. (II) Generation of IMacq and GTacq computed by (a) adding random Gaussian noise, with 0.05-0.01% standard deviation of the maximum k-space SI and applying the AcqPr weighting to the k-space of GTsyn, followed by (b) inverse Fourier transformation to generate the IMacq. The corresponding GTacq was generated by the same pipeline with a complete k-space and 100 Nreps, i.e., 100 repetitions per line.

Network Implementation and Training

The DUNet was implemented using Keras with TensorFlow 2.2, and it was trained and tested on Nvidia V100 tensor core GPUs with an Adam optimizer [67], a batch size of 32, a learning rate of 0.001, and 100 epochs. To ensure consistency throughout the 240 experiments, 2616 images, which comprised of 1680 training images, 516 testing images, and 420 validation images, were split based on patient identification numbers to prevent any data leakage into the testing set. We kept other hyperparameters constant except loss functions to ensure consistency.

Evaluation Metrics and Statistics

In this study, we compared the performance of DUNet-enhanced images to two ground truth datasets using the metrics of MSE, MAE, PSNR, and variable size window SSIM (windows [3x3, 5x5, …, 11x11, 13x13] pixels) [24,49]. These metrics were applied to a sample of 516 testing images for the two MeROI and reported as mean ± standard deviation. We performed statistical analysis using ANOVA and MEM to assess the significance of (1) κ values (i.e., $\kappa \in$ [0.0, 0.1, 0.2,

…, 0.9]) in CLF1 and AcqPr, and (2) λ values (λ ∈ [0.0, 0.1, 0.2, …, 0.5] and LSSIM window sizes (WS) in CLF2, and AcqPr. We selected the SSIM with a window size of 11 to represent the SSIM class in the statistical analysis due to the high correlation with SSIM of different window sizes (Figs. 3 to 6, and Tables 2 and 3, and in relation to Fig. 7). The evaluation metrics (MSE, MAE, PSNR, and SSIMw11) were used as response variables for the statistical analysis. We excluded the two levels of GT from the ANOVA and MEM analysis since the significance of GT was evident from the descriptive statistics and only used data acquired with GTacq for statistical analysis.

Statistical Analysis

In our study, we conducted statistical analysis on two subgroups. Firstly, we tested the effect of κ on the loss function $\kappa \times L1+(1-\kappa)\times L1_{Canny}$ (CLF1), where κ varies from 0.1-1.0 with a step size of 0.1. We excluded κ = 0 (i.e., $L1_{Canny}$ loss function) as it showed significantly inferior performance than other values of κ, as evidenced by the descriptive statistics results. The fixed variables for this subgroup in the mixed effects model were (I) κ with ten distinct levels ranging from [0.1-1.0] with a step size of 0.1 and (II) input AcqPr with five levels (Table 1). Secondly, we tested the effect of λ in L1+λ×LSSIM (CLF2). For this subgroup, the fixed variables were (I) λ with six levels ranging from [0.0-0.5] with a step size of 0.1, (II) window sizes of LSSIM with two levels (3 and 7), and (III) input AcqPR with five levels (Table 1). The test images formed the random effects in the mixed effects model, on which the repeated measures were performed for all possible combinations of fixed variables.

We performed ANOVA and MEM analysis using custom software written in R, version 4.2.2 [68]. The classical ANOVA is capable of treating only fixed effects, that is for every level of the fixed factors considered in the study, we assume that we have a different random sample (i.e., a different data set) from a normal distribution. All the Normal distributions are assumed to have the same variance and the classical ANOVA will examine whether we have any differences in the means. However, in DL studies, we typically have only one data set (i.e., a set of images) and for each level of the fixed factors considered in the study we perform measurements on the exact same images. Therefore, we have a repeated measure design, where the images constitute the random effects, leading to what is known as MEM design. So, the basic difference on the two approaches is that while ANOVA considers that at each level we have a different set of images, the MEM is taking into account that the same image is measured multiple times, i.e., MEM is capable to consider the image to image differences, while ANOVA neglects this.

Results

In our MRI study, we collected a large amount of data by calculating output image metrics for a total of 480 discrete cases. These cases encompassed twenty-four LF, two GT (GTsyn and GTacq), five k-space AcqPr (complete, hat-like, US-1, US2, and US3), and two MeROI (i.e., entire image and lesion-focused ROI). A single case corresponds to the average value per metric for 516 test images calculated for nine evaluation metrics (MSE, MAE, PSNR, and six variable window size SSIM). We found distinct patterns in the data, and therefore, we present selected outcomes in the main body of the manuscript (Tables 2 and Figs. 3 to 6), while the complete set of evaluation metrics is available in the supplemental tables 1 to 20. This comprehensive analysis provides a better understanding of the effects of different combinations of LF, GT, AcqPr, and MeROI on the enhancement of MRI images.

Figs. 3 and 4 summarize the MAE and SSIM descriptive Statistics of images enhanced by DUNets trained with the cost functions $\kappa \times L1+(1-\kappa)\times L1_{Canny}$ (CLF1) and L1+λ×LSSIMw7 (CLF2), respectively. Only the MAE and SSIM are shown as representative results and manifest identical patterns, as in supplemental tables 1-20. Figs. 3 and 4 have identical structures presenting the

results for (i) the two GT, GTacq (100 repetitions of complete k-space) being the graphs in the left column 3/4(a, c, e, g) and GTsyn (signal-zeroed empty space) the graphs in the right column 3/4(b, d, f, h), and (ii) the two MeROI of the entire image in the upper two rows 3/4(a, b, c, d) and the lesion-focused ROI the lower two rows 3/4(e, f, g, h). Inspection of these figures, in accordance with Tables 2 and 3, provides a birds-eye view of the outcomes of these studies that can be summarized in three observations. First, it appears that there is no effect of the κ or λ values of CLF1 and CLF2, respectively, on the performance of the DUNet. Second, differences can only be seen between the outcomes of DUNet trained with GTacq and GTsyn. Third, all LF performed similarly well for all acquisition protocols except US-3 (k-space coverage with 10% central and 10% equidistant lines outside), and this was irrespective of κ or λ values of the loss function or ground truth or on which area of the image the metrics were calculated.

Impact of GT

The choice of GT causes the most observable difference in the results of DUNet. Comparing the two GT in Tables 2 and 3, the five AcqPr had higher SSIM when they were enhanced by a DNUet trained with the GTsyn (five rightmost columns) than those enhanced with the GTacq and no post-acquisition processing (five leftmost columns). For example, Table 2, with L1 loss function (the tan rows), indicates that the SSIMw5 metric for the complete k-space AcqPr is significantly higher with GTsyn (0.9603±0.0093) than with GTacq (0.8501±0.0474), and the standard deviation based ranges do not overlap. This trend can also be observed in all other loss functions and AcqPr in Table 2 and Figs. 3 and 4. Comparing GTsyn with GTacq over the lesion-focused area reveals some different results. In Table 3, with the L1 loss function (tan rows), the SSIMw5 metric for complete AcqPr is 0.9591±0.0313 for GTsyn and 0.9221±0.0469 for GTacq. However, there is an overlap in the standard deviation-based range when metrics are calculated over the lesion-focused ROI area. In Figs. 3 and 4, we observe similar trends, which suggest that the use of an empty-space noiseless GTsyn results in better denoising of empty space by DUNet, as reflected by the improved evaluation metrics. This applies to all other metrics in supplemental tables 1-20. The effect of GT is also evident when comparing image-to-image Figs. 5 and 6, which are enhanced with DUNet trained with GTacq and GTsyn, respectively. For instance, images in Fig. 5(c) or 5(e) exhibit higher errors when correspondingly compared to Fig. 6(c) or 6(e), and this is evident in both the empty space (expected as the GTsyn is trained on a zeroed-empty space) as well as on the tissue area.

Impact of CLF

The effect of the tested CLF can be assessed by inspecting Tables 2 and 3 along any column (each column corresponding to a combination of GT and AcqPr), as well as in Figs. 3 and 4 (in each graph, the same color boxes). It appears that the κ or λ values of the CLF1 and CLF2 have no significant effect; the differences in the means of the metrics lie within a standard deviation. The same is the observation in the visual inspection of the example DUNet outcome images in Figs. 5 and 6; indeed, when comparing outcomes collected with the same AcqPr (i.e., same column), we see no clear visual difference between the two presented λ (Figs. 5(b) vs. 5(d) and Figs. 6(b) vs. 6(d)). The same applies when comparing the error maps, column-wise Figs. 5(c) vs. 5(e) and Figs. 6(c) vs. 6(e). Although there are some high-intensity hotspots in the zoomed-in areas, these differences are relatively small compared to the brightness of the error map, which is five times that of the images. This behavior was quite unexpected as prior works have clearly stated preferred values like for κ=0.7 [56] or λ=0.1 [58].

Impact of AcqPr

The effect of AcqPr can be observed by inspecting Tables 2 and 3 along rows for either of the GTs (rows correspond to one of the 24 LF) that indicate a dependence of enhancement

performance to the AcqPr, especially when considering metrics calculated on the entire image versus the lesion-focused ROI. Table 2, Figs. 3(a) to 3(d), and Figs. 4(a) to 4(d) reveal clearly that images enhanced from undersampled k-space (US-1 and US-2) have a higher SSIMw5 than those enhanced with the complete and hat-like AcqPr. However, when we inspect Table 3, Figs. 3(e) to (h), and Figs. 4(e) to (h), i.e., lesion-focused ROI, the reverse trend is observed: the complete and hat-like AcqPr yields higher SSIMw5 than US-1, US-2, and US-3. One can also observe that the DUNet performs sub-optimally under US-3 acquisition for both entire image and lesion-focused ROI for any combination of LF and GT. Notably, there is no clear difference between the other four AcqPr. This is also supported by the images in Figs. 5 and 6. Comparing the outcomes when the input images were enhanced with the same $\lambda=0$ in Fig. 6(c), we observe differences relative to GT in the zoomed areas as hotspots. These hotspots are relatively brighter among images enhanced from US-1, US-2, and US-3, with US-3 exhibiting the strongest hotspots. Yet, such hotspots are absent in the images enhanced from complete and hat-like k-space acquisitions. Similar results were seen in Figs. 6(e), 5(c), and 5(e).

Fig. 7 shows scatter plots (lower triangle), Pearson's correlation scores (upper triangle), and distribution plots (diagonal) for evaluation metrics on different cost functions. The correlation matrix provides statistical evidence that SSIM with different window sizes is highly correlated (>=0.99). The density plot along the diagonal visually represents the distribution of data by depicting the density of data points along a continuous axis. Every cell in the lower triangular refers to the scatter plots between the two variables that corresponds to the column and the row of that particular cell. For example, row three from the top and column one from the left corresponds to the cell that shows the scatter plot for values obtained for PSNR and MSE for the enhanced images; and, the respective cell on the upper triangle measures the correlation that these two variables have up to a second decimal point. Therefore, the main diagonal reports the individual histogram and density plots for the variables. The lower triangle reports all possible scatter plots among the variables and the respective cell on the upper triangle quantifies the strength of the linear relationship in this scatter plot using Pearson's correlation coefficient.

Fig. 7 serves as a foundational step for response variable reduction in statistical analysis as SSIM with different window sizes is correlated, and an observation made on one is therefore applicable to the other with near-perfectly correlated metrics.

ANOVA vs MEM

Table 4 reports the significance scores as F-ratios (and p-values in square brackets) for ANOVA (Tables 4a and 4b) and mixed effects model (MEM) (Tables 4c and 4d). We conducted a statistical analysis that focused on two factors. Firstly, we tested the impact of kappa values of CLF1, AcqPr, and their interactions (Tables 4a and 4c), referred to as **(1)**. Secondly, we investigated the effect of lambda values and LSSIM window size (WS) in CLF2, AcqPr, and their interactions (Tables 4b and 4d), referred to as **(2)**. The significance level was set to alpha=0.05. The p-values in Tables 4a and 4b demonstrate that AcqPr is a significant component and affects the DUNet enhancement. The mean response values for US-3 are different from other AcqPr, which contributes to this significance. All other factors reported with ANOVA in Tables 4a and 4b are insignificant (p>>0.05). The insignificance of these factors (except AcqPr) is due to the repeated measure design in the studies, which are ignored by classical ANOVA. We use MEM to account for the repeated measure design of this study, and the results of MEM analysis are reported in Tables 4c and 4d. MEM analysis clearly shows that all the factors in **(1)** and **(2)** are highly statistically significant (p<<0.05) except for the WS, which was marginally significant (p=0.055) for the response variable MSE (Table 4d). Observations in Tables 4c and 4d suggest that due to image-to-image variation, we need to look at the interaction plots (reported in Fig. 8). The

interaction plots reveal patterns in the conditional means of the test images (random effects in MEM). Figs. 8(a) and 8(b) display the predicted values for significant interaction of fixed variables in **(1)** and **(2)**, respectively corresponding to different response variables and allowing us to interpret the effect of fixed variables in **(1)** and **(2)** visually.

Visual Representation of Image-to-Image Variation

Four representative examples of individually enhanced IMenh, generated using the US-2 and US-3 protocols, were visually inspected (see Figs. 9 and 10). The results revealed differences among the CLFs that are visually apparent but not captured by ANOVA. Notably, when comparing Figs. 9(a-c), two low-intensity CSF structures (pointed by arrows) appeared to have different widths for the three CLFs, with the smallest one observed in Fig. 9(a). While these differences are relatively minor, when combined with other differences across the image, they may contribute to the different SSIM. For instance, Fig. 9(a) has an SSIM of 0.9014, which was lower than that in Fig. 9(b) (SSIM = 0.9016) and Fig. 9(c) (SSIM = 0.9025). Similarly, the arrow-pointed structures in Figs. 9(d-f) have different sizes in the different CLFs. These differences are apparent in the error map shown in Fig. 9(d), which exhibits higher intensity hotspots than Figs. 9(e) and 9(f). These differences may explain the corresponding SSIM of 0.9074, 0.9082, and 0.9085, respectively. However, since the average SSIM is 0.9021±0.0310, the minor differences are insignificant in ANOVA.

In Fig. 10, we examine the two IMenh cases generated from IMacq obtained from the US-3 outlier. The three different CLFs, used for enhancement cause substantial observable differences in the results. For instance, in Figs. 10(a) to 10(c), the orange arrows in zoomed area 1 highlight differences in the shape and contrast of low-intensity structures. Similar differences are observed in the structure of the synthetic lesion in zoomed area 2. In Fig. 10(d), the thickness of the low-intensity CSF in zoomed area 1 and the white matter in zoomed area 2 were lower than that of Figs. 10(e) and 10(f). These differences are visible in the error maps, where bright hotspots are present. In addition, the SSIM values (reported under each image) vary, as in Fig. 9.

Discussion

Descriptive statistics, ANOVA, and MEM were used in comparing the performance of the 240 tested networks, each providing different perspectives on the effects of the independent parameters, i.e., AcqPr, LF, and GT, on the evaluation metrics. Univariate descriptive statistics, i.e., means and standard deviations (Figs. 3 and 4 and Tables 2 and 3) providing a summary-like perspective, point to some initial observations. First, it is evident that the choice of ground truth affects the network's performance. Therefore, we proceeded to analyze with ANOVA and MEM with other independent parameters for only the case of GTacq. Second, it is also apparent that of all independent parameters, only AcqPr affects the evaluation metrics; and this effect can be clearly attributed to the inclusion of US-3. When compared to the other AcqPr, US-3 evaluation metrics exhibit different mean values and, in most cases, a larger standard deviation. The metrics of the other AcqPr exhibit close mean values with highly overlapping standard deviations (Tables 2 and 3). The observations of descriptive statistics are also evident in the ANOVA analysis.

Indeed, the assessment of the statistical significance of the differences in network performance (Tables 4a and 4b) with ANOVA aligns with the observations from the descriptive statistics. First, the evaluation metrics are not affected by the weightings of the CLF functions (κ in CLF1 and λ in CLF2). However, the independence is a surprise as such composite loss functions were used before to improve image structure. Interestingly, prior works that reported preferred weightings, such as κ or λ values, relied on visual assessment of the enhanced images [56, 58] rather than quantitative metrics. Second, it is only the AcqPr that has any effect on the performance metrics,

and this originates exclusively from the US-3 protocol. This suboptimal performance of the networks can be expected since the input IMacq's come from a suboptimal undersampled k-space (10% k-space lines in the central band and 10% equidistant distribution of k-space lines outside the center band).

We employed descriptive statistics and ANOVA to evaluate the performance of various DUNet models in enhancing low-quality images across different acquisition protocols and cost functions. Our results indicate that all tested models performed equally well. Nevertheless, it is important to note that adjustments to the ground truth can impact the outcome. Notably, while US-3 had lower performance compared to other acquisition protocols, any well-trained version of DUNet could still be used. Despite these findings, two interrelated issues require further consideration. First, previous works used visual inspection to report preferred networks, i.e., choices not based on the statistical significance of the metrics. The second, and related to the former issue, is the appropriateness of descriptive statistics and ANOVA in investigating differences among outcomes of comparative tests.

By definition, ANOVA assumes no repeated measures: practically, each network should have been tested on different test sets with the same distribution of investigated independent parameters. This is not the case in the comparative studies of networks in the literature (including the work presented here): for comparison, the same set of test images is used to compare the outcomes of networks. MEM analysis is the appropriate statistical analysis that, by design, addresses the issue of image-to-image variation [36] that arises by repeatedly observing the effect of different levels of the fixed variables on the same image. After applying MEM to the 100 networks (i.e., 10 CLF1 × 5 AcqPr and 10 CLF2 × 5 AcqPr) and 51600 individual IMenh (100 networks × 516 images), a different pattern emerged: each fixed variable, i.e., κ for CLF1, λ and WS for CLF2, and AcqPr, is significant (MEM results in Tables 4c and 4d). When considering image-to-image variation through MEM analysis, differences among the 100 networks (i.e., 10 CLF1 × 5 AcqPr and 10 CLF2 × 5 AcqPr) and 51600 individual IMenh (100 networks × 516 images) emerge that are not apparent in descriptive statistics (Tables 2 and 3 and Figs. 3 and 4), ANOVA (Tables 4a and 4b), and visual results (Figs. 5 and 6).

MEM offers insights about the interaction among the fixed variables, i.e., the impact of AcqPr, κ, and λ on network performance, as measured by evaluation metrics. The interaction plots in Figs. 8(a) and 8(b) show that errors were highest with the US-3 protocol, regardless of κ, λ, or WS, indicating that the DUNet's performance is primarily influenced by AcqPr rather than CLF1's κ or CLF2's λ or WS values. While descriptive statistics and ANOVA provide evidence supporting the role of US-3 in AcqPr, MEM further reveals the combined effects with other fixed variables. The MEM analysis identified even minor differences resulting from κ, λ, and WS, which can inform decisions about DUNet training given the fixed AcqPr and evaluation metric.

The fact that MEM can reveal effects due to its inherent incorporation of image-to-image variability raises another question: whether the MEM-elucidated small variations relate to the human-defined features that determine the subjective visual inspection outcomes. If such a relationship exists, then MEM may be a stepping stone toward forming means to quantitatively assess and compare network outputs.

In Fig. 10, we display the outputs of three loss functions on US-3 AcqPr images, with arrows pointing to areas of small visual variations. We zoom in on these areas to highlight the differences in local structures. The SSIMw11 values are slightly different (Fig. 10(a) SSIM = 0.8451, Fig. 10(b) SSIM = 0.8460, and Fig. 10(c) SSIM = 0.8494), with a difference of only 0.0034, which is within the reported standard deviation of 0.0310 (supplemental table 5). ANOVA determined the

variations as statistically insignificant, with a p-value of 0.307 and an F-ratio of 1.19 (Table 4b). However, visual inspection of Figs. 10(a) and 10(b) reveals differences in local structures leading to distinct SSIM values. MEM analysis revealed that 'λ' is highly significant, with a p-value of 0.000 and an F-ratio of 155.68 (Table 4d), along with other fixed variables. Similarly, ANOVA reported insignificance for the fixed variable 'κ' with a p-value of 0.950 and an F-ratio of 0.36 (Table 4a). In contrast, MEM reported high significance with a p-value = 0.000 and an F-ratio of 46.80 (Table 4c), indicating that MEM shows closer relation to the visual inspection. The use of MEM has facilitated the detection of subtle variations, which are represented by the interaction plots shown in Figs. 8(a) and 8(b).

Although it is impossible to provide a definitive answer, the differences revealed by MEM analysis may explain the previously reported preferences for κ and λ based on visual inspection [56, 58]. The outcomes of the MEM can be used to optimize the training parameters of the DUNet model for achieving the best outcomes in individual evaluation metrics. Overall, the MEM approach offers a more comprehensive understanding of how loss functions impact model performance, which can be useful in achieving optimal outcomes for image enhancement tasks. However, it is important to note that the practical significance of the minor differences revealed by MEM can only be determined through human feedback. While MEM is effective in capturing small differences and showing high statistical significance, its applicability to real-world scenarios ultimately depends on human feedback.

The interaction plots in Figs. 8(a) and 8(b) suggest that there is no singular optimal value of κ in CLF1 nor of λ or WS in CLF2 that can yield the best results across all response variables. This indicates that alternative metrics are needed to accurately measure the impact of different loss functions and other fixed variables on the overall image quality. As such, previous works have had to rely on visual inspection to find optimal κ and λ. Additionally, our findings suggest that the variability in response variables, points to a potential limitation of evaluation metrics in capturing variation at the pixel-to-pixel level and structural information. To address this limitation, it is important to train the network with appropriate datasets (in this case, accounting for the differences due to AcqPr).

Our study confirms the impact of AcqPr on the performance of DUNet in image enhancement. Both ANOVA (Tables 4a and 4b) and MEM (Tables 4c and 4d) produced a p-value of '0.000' across all evaluation metrics, indicating the significance of AcqPr. However, ANOVA results suggest that the effect of AcqPr is primarily driven by US-3, which has substantially different values than the other AcqPr. In contrast, MEM could detect small differences in SSIM values among the other four AcqPr, where the difference in SSIM is less than 0.0045 (i.e., less than 0.45% with respect to GTacq and L1 loss for supplemental tables 1 to 4). The interaction plots in Fig. 8(a) showed that, for any value of κ, US-1 and US-2 outperformed the other AcqPr with higher mean and confidence intervals under the PSNR or SSIM plot. MEM captured the small differences in the SSIM values of different AcqPr. For instance, in supplemental table 1 for complete AcqPr, the SSIM value was 0.8976, while in supplemental table 2 for hat-like AcqPr, it was 0.8991. The difference between the two values was 0.0015, which is less than 0.15% with respect to GTacq. The F-ratios for SSIM under AcqPr were 562.59 (Table 4a) and 71357.28 (Table 4b) for ANOVA and MEM, respectively. The high difference in F-ratios indicates that MEM reported higher significance than ANOVA, as MEM effectively captured image-to-image differences related to different AcqPr.

While the study design was focused and, in certain aspects, limited to specific AcqPr, loss functions, and GT, these do not affect the generalization of the outcomes. Despite comparing 240 individually trained and tested networks, we only tested a specific UNet architecture, trained and

tested on a small number (24) of rather simple single and composite cost functions (L1, L2, SSIM, and $L1_{Canny}$) and synthetic data. Nevertheless, the underlying capability in assessing differences between the three statistical approaches was clearly seen, with the potential need for more sensitive analysis models, like MEM. The potential of such models can also be seen if we attribute the lack of significant differences in the ANOVA analysis to a possible insensitivity of the used UNet to the loss functions. Even in this case, MEM reported statistically significant differences when comparing the loss functions (F-values and interaction plots).

The MEM analysis (compared to descriptive statistics and ANOVA) further underscores the importance of methodology that considers subject-to-subject variability in identifying the optimal hyperparameters for different imaging problems and considering the uniqueness of every single patient. Moreover, those findings underscore the value of application-driven criteria; an image is as good as its informational content to support the assessment of (patho)physiology and not the degree of visual pleasantness (although the latter does not exclude the former). Under the same context, it also becomes apparent the importance of human input about or enforcement of the quality of the informational content of an image. The latter may be realized as part of network training and/or the introduction of metrics or (composite) loss functions that capture human criteria about the appropriateness of the outcome. We feel that this study lays a foundational step toward explainable AI in imaging and demonstrates the importance of incorporating appropriate statistical methods to better understand DL in imaging.

With primary objective the investigation of statistical analysis methodologies in comparing different DL architectures, in the paradigm of enhancing low quality MRI, certain selections were made in the design and the practical implementation of the study. All tested 240 DL models were based on the UNet architecture (under supervised leraning) selected for its stability in training [69, 70] and its propensity to yield consistent and deterministic outputs [37, 69]. Consequently, UNet enabled improved logistics in the execution of this study that entailed the training of 240 experiments and outcome analysis for 480 cases (cindering the two ROI versions). Moreover, UNet have been used before for the selected paradigm of enhancing low quality MRI images [19, 38–49]. While UNet was a robust and stable choice for these studies, it should be noted that other architectures may offer better image enhancement, such as GANs that generate perceptually improved images [71–75]. It will be important to expand the evaluation for the statistical analysis of the altering the training models also to GAN or other architectures. It should be emphasized that this work does not delve into the reconstruction of undersampled MRI; rather it uses DL to enhance already reconstructed lower-quality MRI images (originating from in silico undersampled scans).

Several other choices were made in the design of this study. In the context of our present investigation, out of the plurality of possible GTs we selected two GT (both generated with the complete k-space). While the current study demonstrated the efficacy of UNet methods in relation to those GTs, it is important to note that alternative DL techniques, such as GANs, maybe more suitable with low-quality GT, as was recently presented in [63]. Notably, while it may be impossible to train a model to surpass the quality limitations of the GT, subtle adjustments to the GT can serve to ameliorate the quality of undersampled GT images, thereby facilitating the training of more suitable DL models. It is noted that the statistical analysis comparison tests in the current study does not include GANs or diffusion models. These DL methods have the potential to introduce more intricate loss functions into the image enhancement process, which, in turn, can contribute to perceptually superior outcomes in the enhanced images. In light of this, we are committed to exploring this intriguing aspect in our future research endeavors. We also employed the use of magnitude images form the OASIS dataset, adopted for simplicity and to keep effort focused on the effects of specific parameters on image enhancement without the complexities

associated with reconstruction. However, it should be noted that using DICOM images, while it serves the research objectives of this work, carries certain limitations. One notable limitation is that it may lead to an overoptimistic evaluation of our model's performance.

In this work, the 240 different DL models were all trained with the same learning rate and number of epochs. It is imperative to emphasize that various DL models, characterized by differing architectural features such as loss functions and their interactions with GT, do not follow the same learning trajectories. Consequently, the ideal approach entails training models until convergence, however, this practice presents a challenge when comparing outcomes. When comparing two or more DL methods, it is imperative to ensure as much methodological consistency as feasible. One approach to achieve this entails enforcing uniformity in various hyperparameters, including the learning rate and epochs as in Bressem et al. [76]. As an essential facet of our forthcoming research, we intend to extend the scope by training models under varied hyperparameter configurations and employing diverse stopping criteria. This extension aims to introduce heightened variability, all while incorporating these parameters into the framework of the MEM. Subsequent significance testing will be conducted through the herein presented statistical methodologies that leverage image-to-image variations, further enhancing the rigor of analysis.

This study serves as a foundational exploration of the impact of parameter variations in image enhancement (and is not intended to provide a one-size-fits-all solution for all MRI applications.) As example, a potentially impactful future research thrust would be the use of statistical analysis for assessing the performance of a wider range of DL methods with distinct parameters (i.e. to discern which parameters hold statistical significance), include but not limited to diffusion-based reconstruction, unrolled architectures and the use of specialized loss functions for reconstruction [77–79]. Consequently, the reconstruction method employed will be integrated into the parameters of the MEM and will play a pivotal role in the subsequent significance analysis. This expansion in methodology will enable us to provide a more comprehensive understanding of the interplay between reconstruction and enhancement, thereby enhancing the robustness and relevance of our study.

Conclusion

In the quest to understand and practically use DL, careful consideration is needed in performing comparison studies to ensure that the sought out improvements are well characterized and not coincidental. Failure to account for image-to-image variability, as is the case with descriptive statistics and ANOVA analysis, may result in the inability to accurately measure differences in imaging features that are instrumental in determining the value of a network's outcome. These pilot studies with MEM analysis indicate that when image-to-image variability is considered, finer differences and interactions among the fixed variables can be captured. Such sensitivity may lead to a more appropriate characterization of the outcomes of a DL method, and incorporating such methods in the training stage of a network can be beneficial. Although it is not possible to provide a definitive answer, differences captured by MEM may account for the human preference for specific network outcomes. In general, we advocate incorporating appropriate statistical analysis when evaluating DL methods (as statistical analysis is often overlooked when comparing different models or hyperparameters in literature). An interesting outcome was that a conventional DL architecture, like the DUNet, can be effectively trained to enhance the outcomes of a range of acquisition protocols. This satisfactory performance raises questions about the effectiveness of the utilized loss functions and metrics, particularly when the improvements/differences correspond to a small percentage. It also reinforces the idea that a human or a human-like metric is needed to evaluate image quality. These are among the perspectives in DL that needs to be carefully and critically studied by MR scientists.

Data Availability

Data used in this study were accessed through the OASIS dataset [66].

References

1. Mazurowski MA, Buda M, Saha A, Bashir MR (2019) Deep learning in radiology: An overview of the concepts and a survey of the state of the art with focus on MRI. Journal of Magnetic Resonance Imaging 49:939–954.
2. Akkus Z, Galimzianova A, Hoogi A, Rubin DL, Erickson BJ (2017) Deep Learning for Brain MRI Segmentation: State of the Art and Future Directions. J Digit Imaging 30:449–459.
3. Ueda T, Ohno Y, Yamamoto K, Iwase A, Fukuba T, Hanamatsu S, Obama Y, Ikeda H, Ikedo M, Yui M, Murayama K, Toyama H (2021) Compressed sensing and deep learning reconstruction for women's pelvic MRI denoising: Utility for improving image quality and examination time in routine clinical practice. Eur J Radiol 134:109430.
4. Do W, Seo S, Han Y, Ye JC, Choi SH, Park S (2020) Reconstruction of multicontrast MR images through deep learning. Med Phys 47:983–997.
5. Sandino CM, Cheng JY, Chen F, Mardani M, Pauly JM, Vasanawala SS (2020) Compressed Sensing: From Research to Clinical Practice With Deep Neural Networks: Shortening Scan Times for Magnetic Resonance Imaging. IEEE Signal Process Mag 37:117–127.
6. Fuin N, Bustin A, Küstner T, Oksuz I, Clough J, King AP, Schnabel JA, Botnar RM, Prieto C (2020) A multi-scale variational neural network for accelerating motion-compensated whole-heart 3D coronary MR angiography. Magn Reson Imaging 70:155–167.
7. Kwon K, Kim D, Park H (2017) A parallel MR imaging method using multilayer perceptron. Med Phys 44:6209–6224.
8. Han Y, Yoo J, Kim HH, Shin HJ, Sung K, Ye JC (2018) Deep learning with domain adaptation for accelerated projection-reconstruction MR. Magn Reson Med 80:1189–1205.
9. Lee D, Yoo J, Tak S, Ye JC (2018) Deep Residual Learning for Accelerated MRI Using Magnitude and Phase Networks. IEEE Trans Biomed Eng 65:1985–1995.
10. Han Y, Sunwoo L, Ye JC (2020) k-Space Deep Learning for Accelerated MRI. IEEE Trans Med Imaging 39:377–386.
11. Ottesen JA, Caan MWA, Groote IR, Bjørnerud A (2023) A densely interconnected network for deep learning accelerated MRI. Magnetic Resonance Materials in Physics, Biology and Medicine 36:65–77.
12. Hashimoto F, Ote K, Oida T, Teramoto A, Ouchi Y (2020) Compressed-Sensing Magnetic Resonance Image Reconstruction Using an Iterative Convolutional Neural Network Approach. Applied Sciences 10:1902.
13. Bustin A, Fuin N, Botnar RM, Prieto C (2020) From Compressed-Sensing to Artificial Intelligence-Based Cardiac MRI Reconstruction. Front Cardiovasc Med. doi: 10.3389/fcvm.2020.00017
14. Hyun CM, Kim HP, Lee SM, Lee S, Seo JK (2018) Deep learning for undersampled MRI reconstruction. Phys Med Biol 63:135007.
15. Chen Y, Shi F, Christodoulou AG, Xie Y, Zhou Z, Li D (2018) Efficient and accurate MRI super-resolution using a generative adversarial network and 3D multi-level densely connected network. Lecture Notes in Computer Science (including subseries Lecture Notes in Artificial Intelligence and Lecture Notes in Bioinformatics). pp 91–99

16. Mahapatra D, Bozorgtabar B, Garnavi R (2019) Image super-resolution using progressive generative adversarial networks for medical image analysis. Computerized Medical Imaging and Graphics 71:30–39.
17. Lyu Q, Shan H, Wang G (2020) MRI Super-Resolution With Ensemble Learning and Complementary Priors. IEEE Trans Comput Imaging 6:615–624.
18. Cole E, Cheng J, Pauly J, Vasanawala S (2021) Analysis of deep complex-valued convolutional neural networks for MRI reconstruction and phase-focused applications. Magn Reson Med 86:1093–1109.
19. Iqbal Z, Nguyen D, Hangel G, Motyka S, Bogner W, Jiang S (2019) Super-Resolution 1H Magnetic Resonance Spectroscopic Imaging Utilizing Deep Learning. Front Oncol. doi: 10.3389/fonc.2019.01010
20. Glang F, Deshmane A, Prokudin S, Martin F, Herz K, Lindig T, Bender B, Scheffler K, Zaiss M (2020) DeepCEST 3T: Robust MRI parameter determination and uncertainty quantification with neural networks—application to CEST imaging of the human brain at 3T. Magn Reson Med 84:450–466.
21. Zaiss M, Deshmane A, Schuppert M, Herz K, Glang F, Ehses P, Lindig T, Bender B, Ernemann U, Scheffler K (2019) DeepCEST: 9.4 T Chemical exchange saturation transfer MRI contrast predicted from 3 T data - a proof of concept study. Magn Reson Med 81:3901–3914.
22. LeCun Y, Bengio Y, Hinton G (2015) Deep learning. Nature 521:436–444.
23. Wang X, Xie L, Dong C, Shan Y (2021) Real-ESRGAN: Training Real-World Blind Super-Resolution With Pure Synthetic Data. Proceedings of the IEEE/CVF International Conference on Computer Vision (ICCV) Workshops. pp 1905–1914
24. Zhao H, Gallo O, Frosio I, Kautz J (2017) Loss Functions for Image Restoration With Neural Networks. IEEE Trans Comput Imaging 3:47–57.
25. Lin DJ, Johnson PM, Knoll F, Lui YW (2021) Artificial Intelligence for MR Image Reconstruction: An Overview for Clinicians. Journal of Magnetic Resonance Imaging 53:1015–1028.
26. He K, Zhang X, Ren S, Sun J (2016) Deep Residual Learning for Image Recognition. Proceedings of the IEEE Conference on Computer Vision and Pattern Recognition (CVPR)
27. Szegedy C, Liu W, Jia Y, Sermanet P, Reed S, Anguelov D, Erhan D, Vanhoucke V, Rabinovich A (2015) Going Deeper With Convolutions. Proceedings of the IEEE Conference on Computer Vision and Pattern Recognition (CVPR)
28. Huang Q, yang D, Xian Y, Wu P, Yi J, Qu H, Metaxas D (2020) Enhanced MRI Reconstruction Network Using Neural Architecture Search. pp 634–643
29. Yang G, Yu S, Dong H, Slabaugh G, Dragotti PL, Ye X, Liu F, Arridge S, Keegan J, Guo Y, Firmin D (2018) DAGAN: Deep De-Aliasing Generative Adversarial Networks for Fast Compressed Sensing MRI Reconstruction. IEEE Trans Med Imaging 37:1310–1321.
30. Luo G, Zhao N, Jiang W, Hui ES, Cao P (2020) MRI reconstruction using deep Bayesian estimation. Magn Reson Med 84:2246–2261.
31. Dror R, Shlomov S, Reichart R (2019) Deep Dominance - How to Properly Compare Deep Neural Models. Proceedings of the 57th Annual Meeting of the Association for Computational Linguistics. Association for Computational Linguistics, Stroudsburg, PA, USA, pp 2773–2785
32. Raschka S (2018) Model Evaluation, Model Selection, and Algorithm Selection in Machine Learning.

33. Menze BH, Jakab A, Bauer S, Kalpathy-Cramer J, Farahani K, Kirby J, Burren Y, Porz N, Slotboom J, Wiest R, Lanczi L, Gerstner E, Weber M-A, Arbel T, Avants BB, Ayache N, Buendia P, Collins DL, Cordier N, Corso JJ, Criminisi A, Das T, Delingette H, Demiralp C, Durst CR, Dojat M, Doyle S, Festa J, Forbes F, Geremia E, Glocker B, Golland P, Guo X, Hamamci A, Iftekharuddin KM, Jena R, John NM, Konukoglu E, Lashkari D, Mariz JA, Meier R, Pereira S, Precup D, Price SJ, Raviv TR, Reza SMS, Ryan M, Sarikaya D, Schwartz L, Shin H-C, Shotton J, Silva CA, Sousa N, Subbanna NK, Szekely G, Taylor TJ, Thomas OM, Tustison NJ, Unal G, Vasseur F, Wintermark M, Ye DH, Zhao L, Zhao B, Zikic D, Prastawa M, Reyes M, Van Leemput K (2015) The Multimodal Brain Tumor Image Segmentation Benchmark (BRATS). IEEE Trans Med Imaging 34:1993–2024.
34. Wahlang I, Maji AK, Saha G, Chakrabarti P, Jasinski M, Leonowicz Z, Jasinska E (2022) Brain Magnetic Resonance Imaging Classification Using Deep Learning Architectures with Gender and Age. Sensors 22:1766.
35. Cuocolo R, Comelli A, Stefano A, Benfante V, Dahiya N, Stanzione A, Castaldo A, De Lucia DR, Yezzi A, Imbriaco M (2021) Deep Learning Whole-Gland and Zonal Prostate Segmentation on a Public MRI Dataset. Journal of Magnetic Resonance Imaging 54:452–459.
36. Pinheiro JC, Bates DM (2000) Mixed-Effects Models in S and S-PLUS. doi: 10.1007/b98882
37. Ronneberger O, Fischer P, Brox T (2015) U-Net: Convolutional Networks for Biomedical Image Segmentation. pp 234–241
38. Hu X, Naiel MA, Wong A, Lamm M, Fieguth P (2019) RUNet: A Robust UNet Architecture for Image Super-Resolution. 2019 IEEE/CVF Conference on Computer Vision and Pattern Recognition Workshops (CVPRW). doi: 10.1109/CVPRW.2019.00073
39. Lin H, Figini M, Tanno R, Blumberg SB, Kaden E, Ogbole G, Brown BJ, D'Arco F, Carmichael DW, Lagunju I, Cross HJ, Fernandez-Reyes D, Alexander DC (2019) Deep Learning for Low-Field to High-Field MR: Image Quality Transfer with Probabilistic Decimation Simulator. pp 58–70
40. Masutani EM, Bahrami N, Hsiao A (2020) Deep Learning Single-Frame and Multiframe Super-Resolution for Cardiac MRI. Radiology 295:552–561.
41. Chatterjee S, Sarasaen C, Rose G, Nürnberger A, Speck O (2022) DDoS-UNet: Incorporating temporal information using Dynamic Dual-channel UNet for enhancing super-resolution of dynamic MRI.
42. Chatterjee S, Sciarra A, Dunnwald M, Mushunuri RV, Podishetti R, Rao RN, Gopinath GD, Oeltze-Jafra S, Speck O, Nurnberger A (2021) ShuffleUNet: Super resolution of diffusion-weighted MRIs using deep learning. 2021 29th European Signal Processing Conference (EUSIPCO). IEEE, pp 940–944
43. Ding PLK, Li Z, Zhou Y, Li B (2019) Deep residual dense U-Net for resolution enhancement in accelerated MRI acquisition. In: Angelini ED, Landman BA (eds) Medical Imaging 2019: Image Processing. SPIE, p 14
44. Nasrin S, Alom MZ, Burada R, Taha TM, Asari VK (2019) Medical Image Denoising with Recurrent Residual U-Net (R2U-Net) base Auto-Encoder. 2019 IEEE National Aerospace and Electronics Conference (NAECON). IEEE, pp 345–350
45. Guan S, Khan AA, Sikdar S, Chitnis P V. (2020) Fully Dense UNet for 2-D Sparse Photoacoustic Tomography Artifact Removal. IEEE J Biomed Health Inform 24:568–576.

46. Kolarik M, Burget R, Uher V, Povoda L (2019) Superresolution of MRI brain images using unbalanced 3D Dense-U-Net network. 2019 42nd International Conference on Telecommunications and Signal Processing (TSP). IEEE, Budapest, Hungary, pp 643–646
47. Aghabiglou A, Eksioglu EM (2021) MR image reconstruction using densely connected residual convolutional networks. Comput Biol Med 139:105010.
48. Acar V, Eksioglu EM (2021) Scale Input Adapted Attention for Image Denoising Using a Densely Connected U-Net: SADE-Net. pp 792–801
49. Sharma R, Tsiamyrtzis P, Webb AG, Seimenis I, Loukas C, Leiss E, Tsekos N V. (2022) A Deep Learning Approach to Upscaling "Low-Quality" MR Images: An In Silico Comparison Study Based on the UNet Framework. Applied Sciences 12:11758.
50. Ghodrati V, Shao J, Bydder M, Zhou Z, Yin W, Nguyen K-L, Yang Y, Hu P (2019) MR image reconstruction using deep learning: evaluation of network structure and loss functions. Quant Imaging Med Surg 9:1516–1527.
51. Isensee F, Kickingereder P, Wick W, Bendszus M, Maier-Hein KH (2019) No New-Net. pp 234–244
52. Li H, Liu J (2021) Edge, Structure and Texture Refinement for Retrospective High Quality MRI Restoration using Deep Learning.
53. Moran S, Marza P, McDonagh S, Parisot S, Slabaugh G (2020) DeepLPF: Deep Local Parametric Filters for Image Enhancement. Proceedings of the IEEE/CVF Conference on Computer Vision and Pattern Recognition (CVPR)
54. Tao L, Zhu C, Xiang G, Li Y, Jia H, Xie X (2017) LLCNN: A convolutional neural network for low-light image enhancement. 2017 IEEE Visual Communications and Image Processing (VCIP). IEEE, St. Petersburg, FL, USA, pp 1–4
55. Ignatov A, Timofte R, van Vu T, Luu TM, Pham TX, van Nguyen C, Kim Y, Choi J-S, Kim M, Huang J, Ran J, Xing C, Zhou X, Zhu P, Geng M, Li Y, Agustsson E, Gu S, van Gool L, de Stoutz E, Kobyshev N, Nie K, Zhao Y, Li G, Tong T, Gao Q, Hanwen L, Michelini PN, Dan Z, Fengshuo H, Hui Z, Wang X, Deng L, Meng R, Qin J, Shi Y, Wen W, Lin L, Feng R, Wu S, Dong C, Qiao Y, Vasu S, Thekke Madam N, Kandula P, Rajagopalan AN, Liu J, Jung C (2019) PIRM Challenge on Perceptual Image Enhancement on Smartphones: Report. Computer Vision -- ECCV 2018 Workshops. Springer International Publishing, pp 315–333
56. Seif G, Androutsos D (2018) Edge-Based Loss Function for Single Image Super-Resolution. 2018 IEEE International Conference on Acoustics, Speech and Signal Processing (ICASSP). IEEE, Calgary, AB, Canada, pp 1468–1472
57. Lyu Q, Shan H, Steber C, Helis C, Whitlow C, Chan M, Wang G (2020) Multi-Contrast Super-Resolution MRI Through a Progressive Network. IEEE Trans Med Imaging 39:2738–2749.
58. Qiu S, Chen Y, Ma S, Fan Z, Moser FG, Maya MM, Christodoulou AG, Xie Y, Li D (2022) Multiparametric mapping in the brain from conventional contrast-weighted images using deep learning. Magn Reson Med 87:488–495.
59. Li C, Anwar S, Porikli F (2020) Underwater scene prior inspired deep underwater image and video enhancement. Pattern Recognit 98:107038.
60. Abdollahi A, Pradhan B (2021) Integrating semantic edges and segmentation information for building extraction from aerial images using UNet. Machine Learning with Applications 6:100194.

61. Lauzon CB, Asman AJ, Crainiceanu C, Caffo BC, Landman BA (2011) Assessment of Bias for MRI Diffusion Tensor Imaging Using SIMEX. In: Fichtinger G, Martel A, Peters T (eds) Medical Image Computing and Computer-Assisted Intervention -- MICCAI 2011. Springer Berlin Heidelberg, Berlin, Heidelberg, pp 107–115
62. Koonjoo N, Zhu B, Bagnall GC, Bhutto D, Rosen MS (2021) Boosting the signal-to-noise of low-field MRI with deep learning image reconstruction. Sci Rep. doi: 10.1038/s41598-021-87482-7
63. Korkmaz Y, Cukur T, Patel V (2023) Self-Supervised MRI Reconstruction with Unrolled Diffusion Models.
64. Sun L, Fan Z, Ding X, Huang Y, Paisley J (2019) Region-of-interest undersampled MRI reconstruction: A deep convolutional neural network approach. Magn Reson Imaging 63:185–192.
65. Wang Z, Bovik AC, Sheikh HR, Simoncelli EP (2004) Image Quality Assessment: From Error Visibility to Structural Similarity. IEEE Transactions on Image Processing 13:600–612.
66. Marcus DS, Wang TH, Parker J, Csernansky JG, Morris JC, Buckner RL (2007) Open Access Series of Imaging Studies (OASIS): Cross-sectional MRI Data in Young, Middle Aged, Nondemented, and Demented Older Adults. J Cogn Neurosci 19:1498–1507.
67. Kingma DP, Ba J (2014) Adam: A Method for Stochastic Optimization.
68. R Core Team (2022) R: A language and environment for statistical computing. R Foundation for Statistical Computing, Vienna, Austria. URL https://www.R-project.org/.
69. Cai S, Tian Y, Lui H, Zeng H, Wu Y, Chen G (2020) Dense-UNet: a novel multiphoton in vivo cellular image segmentation model based on a convolutional neural network. Quant Imaging Med Surg 10:1275–1285.
70. Kodali N, Abernethy J, Hays J, Kira Z (2017) On Convergence and Stability of GANs.
71. Lucas A, Tapia SL, Molina R, Katsaggelos AK (2018) Generative Adversarial Networks and Perceptual Losses for Video Super-Resolution. doi: 10.1109/TIP.2019.2895768
72. Borji A (2022) Pros and cons of GAN evaluation measures: New developments. Computer Vision and Image Understanding 215:103329.
73. Chen Y, Christodoulou AG, Zhou Z, Shi F, Xie Y, Li D (2020) MRI Super-Resolution with GAN and 3D Multi-Level DenseNet: Smaller, Faster, and Better.
74. Goodfellow IJ, Pouget-Abadie J, Mirza M, Xu B, Warde-Farley D, Ozair S, Courville A, Bengio Y (2014) Generative Adversarial Networks.
75. Sanchez I, Vilaplana V (2018) Brain MRI super-resolution using 3D generative adversarial networks.
76. Bressem KK, Adams LC, Erxleben C, Hamm B, Niehues SM, Vahldiek JL (2020) Comparing different deep learning architectures for classification of chest radiographs. Sci Rep 10:13590.
77. Dar SUH, Özbey M, Çatlı AB, Çukur T (2020) A Transfer-Learning Approach for Accelerated MRI Using Deep Neural Networks. Magn Reson Med 84:663–685.
78. Korkmaz Y, Dar SUH, Yurt M, Ozbey M, Cukur T (2022) Unsupervised MRI Reconstruction via Zero-Shot Learned Adversarial Transformers. IEEE Trans Med Imaging 41:1747–1763.
79. Güngör A, Dar SU, Öztürk Ş, Korkmaz Y, Bedel HA, Elmas G, Ozbey M, Çukur T (2023) Adaptive diffusion priors for accelerated MRI reconstruction. Med Image Anal 88:102872.

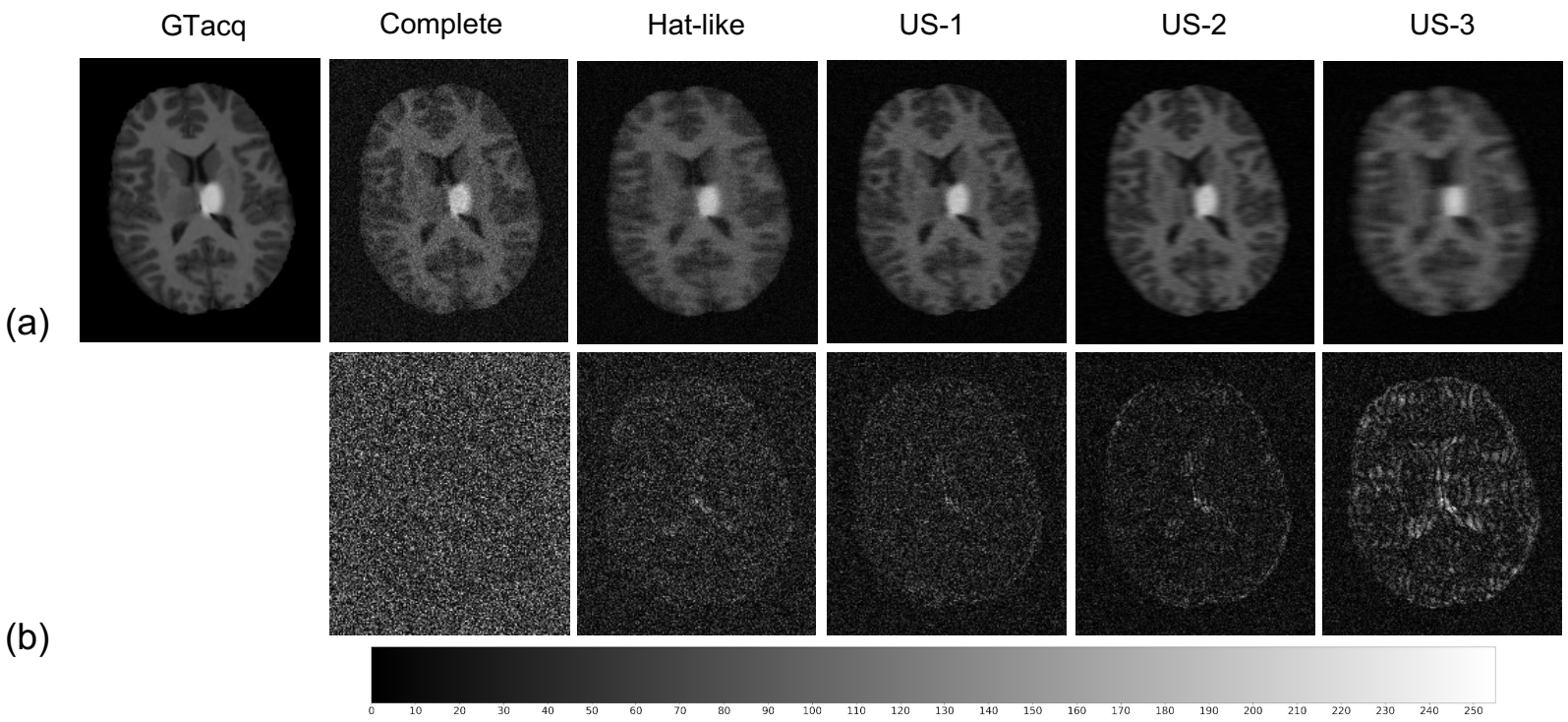

Fig. 1. (a) Acquired ground truth (GTacq) image and the low quality images generated using complete, hat-like, US-1, US-2, and US-3 protocols. (b) Pixel-by-pixel error maps between GTacq and low quality images.

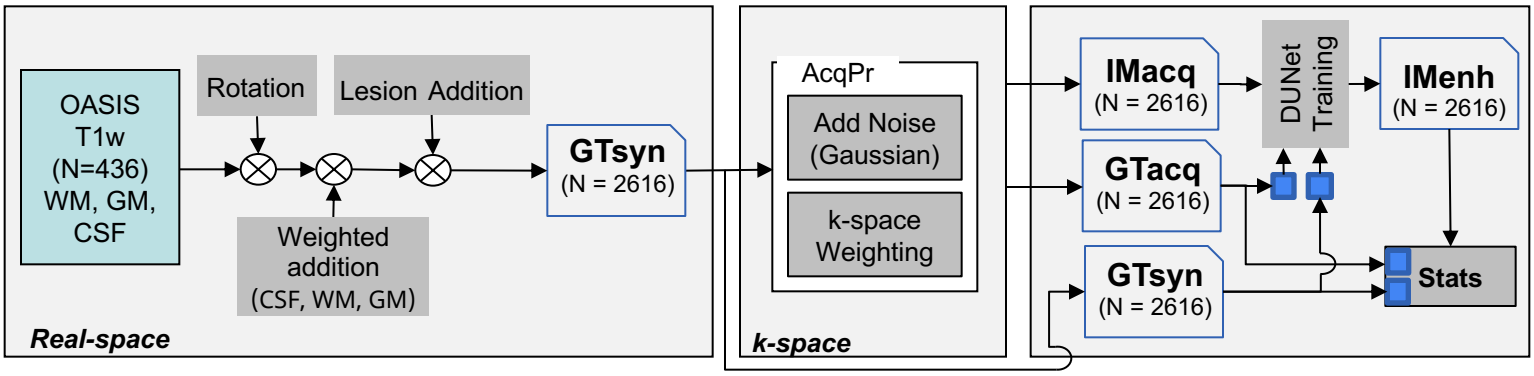

Fig. 2. Flowchart of the dataset synthesis procedure and DUNet Training.

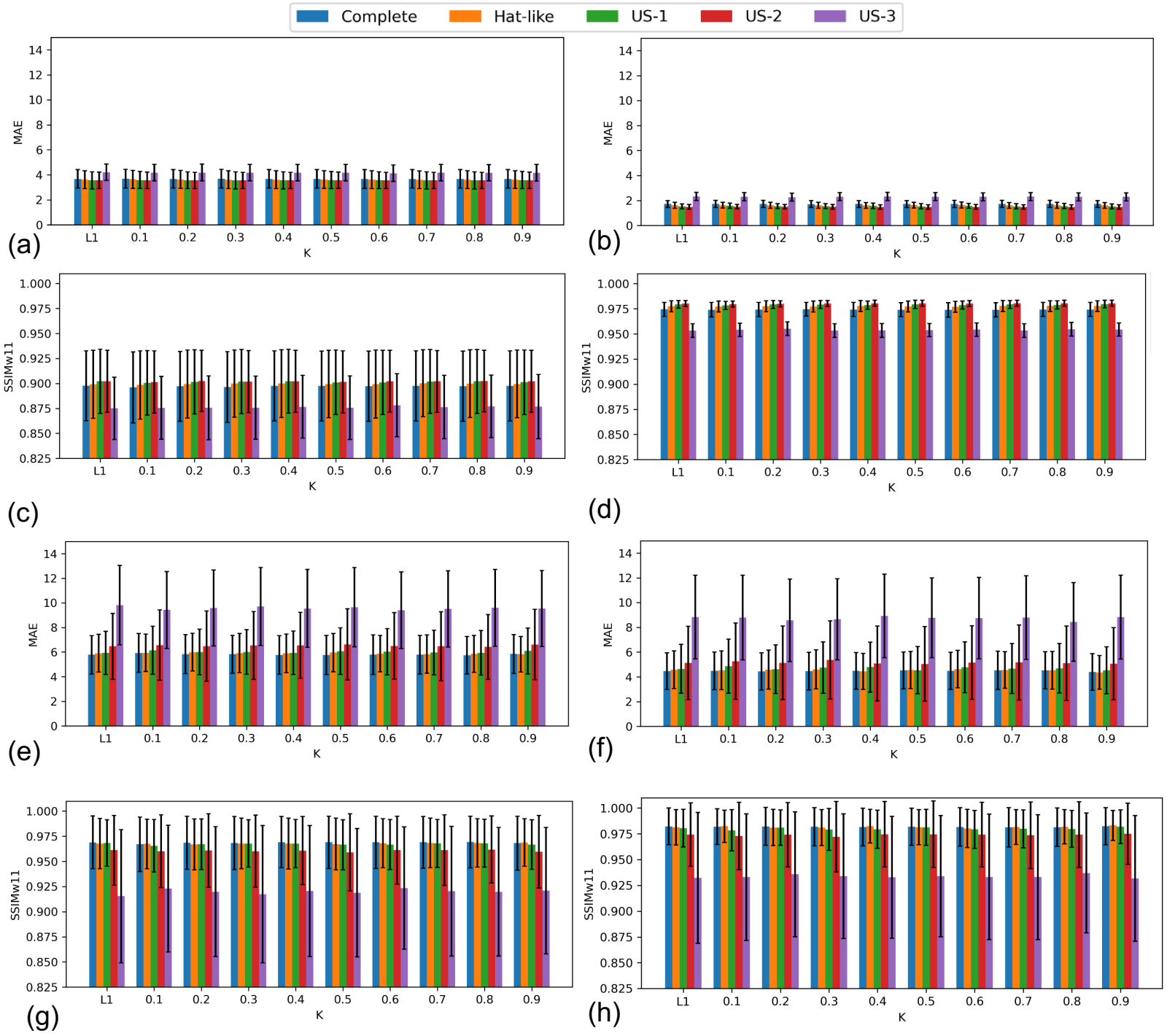

Fig. 3. MAE (a, b, e, f) and SSIM (c, d, g, h) of images enhanced by a DUNet trained with the CLF1 cost function ($\kappa \times L1 + (1-\kappa) \times L1_{Canny}$), with the GTacq (a, c, e, g) and the GTsyn (b, d, f, h) and the metrics calculated over the entire image (a, b, c, d) and lesion-focused ROI (e, f, g, h).

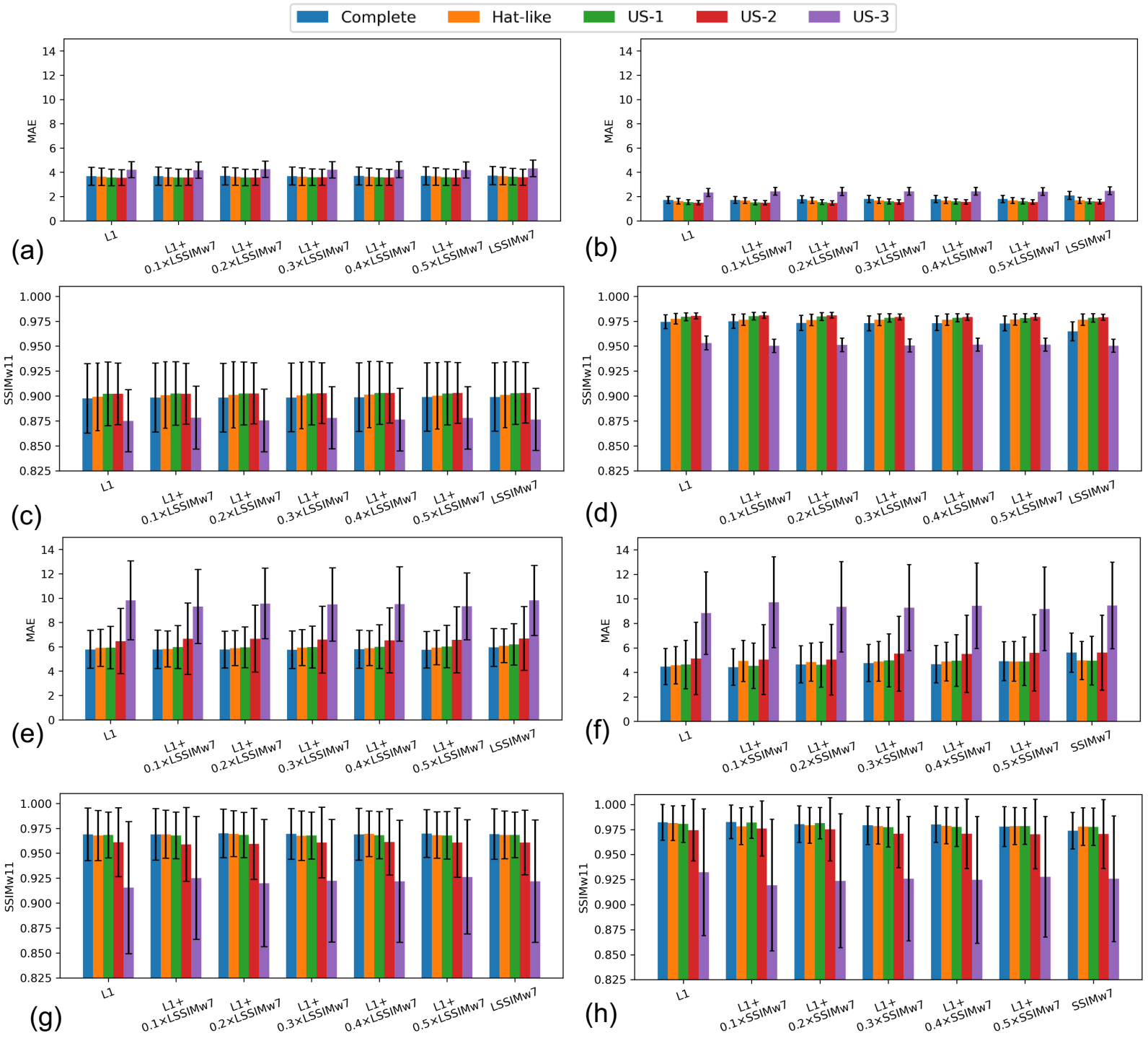

Fig. 4. MAE (a, b, e, f) and SSIM (c, d, g, h) of images enhanced by a DUNet trained with the CLF2 cost function (L1+λ×LSSIMw7 where LSSIM window size is 7), with the GTacq (a, c, e, g) and the GTsyn (b, d, f, h) and the metrics calculated over the entire image (a, b, c, d) and lesion-focused ROI (e, f, g, h).

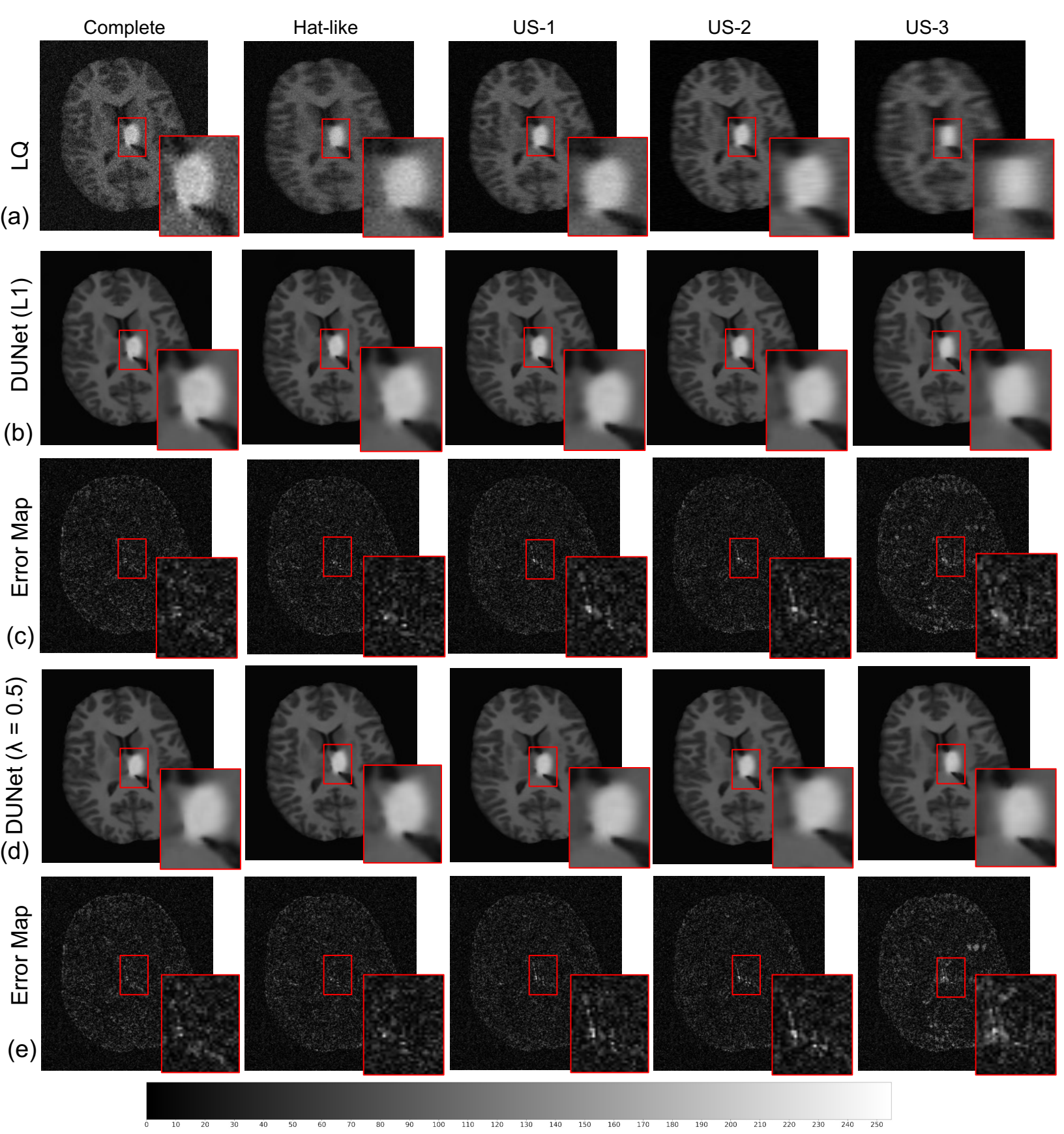

Fig. 5. The outcomes of enhancing the different Low Quality (LQ) input images (a) with DUNet trained with the Acquired Ground Truth (GTacq) and the CLF2 (L1+λ×LSSIMw7) for (b, c) λ = 0, i.e., a plain L1 loss function, and (d, e) with λ = 0.5, i.e., a composite loss function of L1+0.5×LSSIMw7. The difference maps in (c) and (e) are pixel-by-pixel differences of the output images to the corresponding ground truth, and their brightness is 5 times this of the images. The horizontal grayscale bar corresponds to all images and different maps.

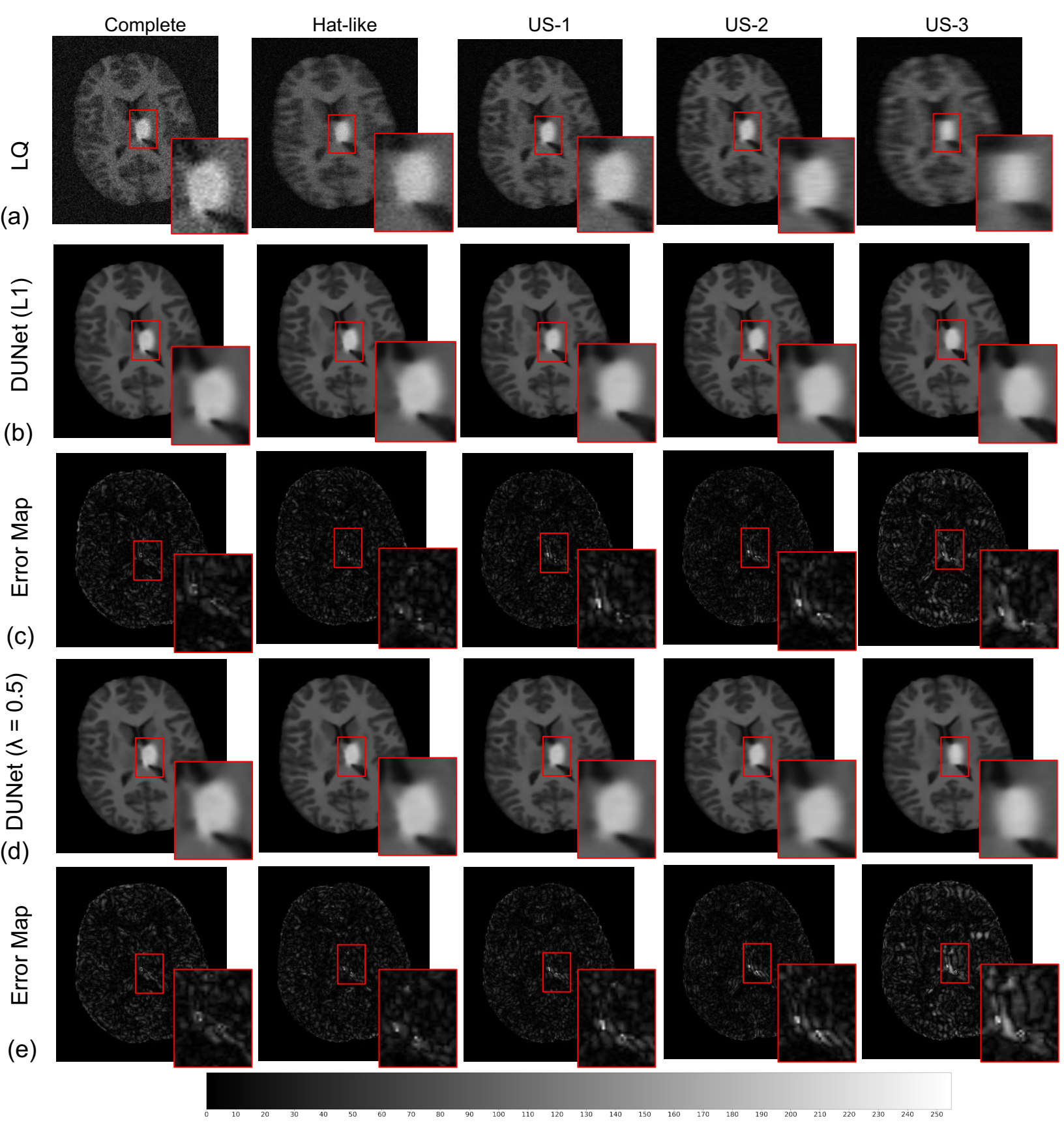

Fig. 6. The outcomes of enhancing the different Low Quality (LQ) input images (a) with DUNet trained with the Synthetic Ground Truth (GTsyn) and the CLF2 (L1+λ×LSSIMw7) for (b, c) λ = 0, i.e., a plain L1 loss function, and (d, e) with λ = 0.5, i.e., a composite loss function of L1+0.5×LSSIMw7. The difference maps in (c) and (e) are pixel-by-pixel differences of the output images to the corresponding ground truth, and their brightness is 5 times this of the images. The horizontal grayscale bar corresponds to all images and different maps.

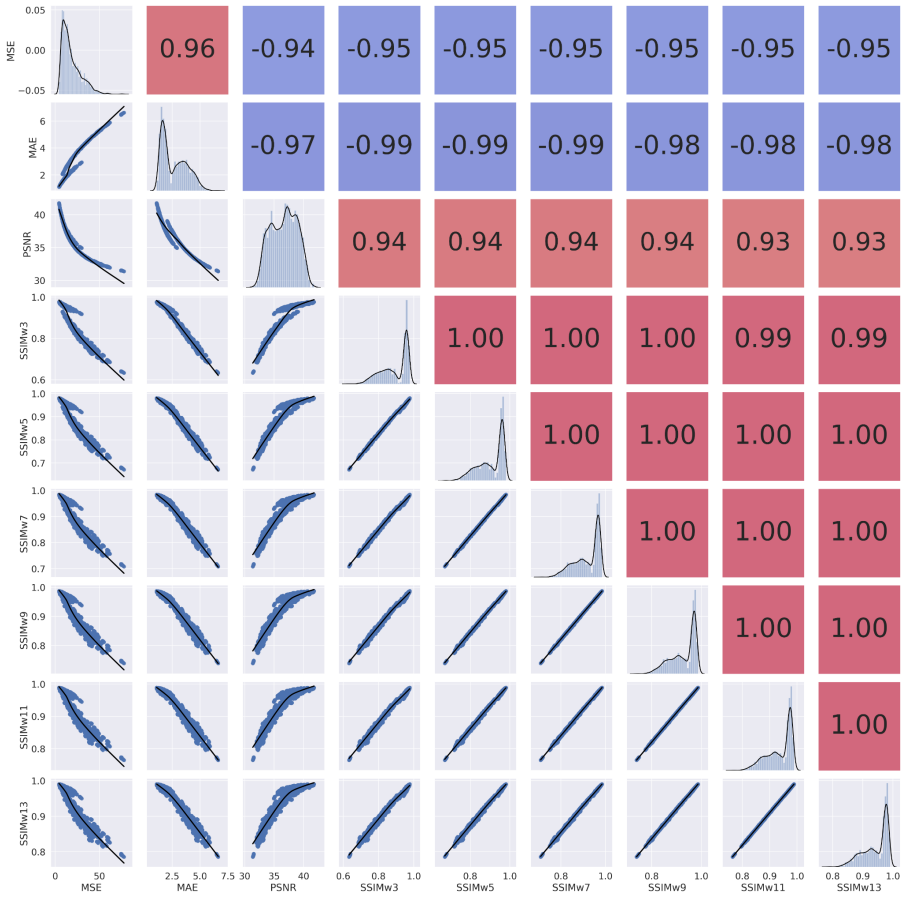

Fig. 7. Correlation scores (upper triangle matrix) and scatter plots (lower triangle matrix) for the 9 response variables. The diagonal elements of the matrix exhibit the distribution plots for the corresponding response variable. Correlation scores ∈ [-1.00, 1.00]; variables with a 1.00 are perfectly correlated, and the interpretation of analysis on one of the variables will be similar to its other perfectly correlated variable. Correlation scores are also color coded where red color means a positive correlation and blue color means a negative correlation.

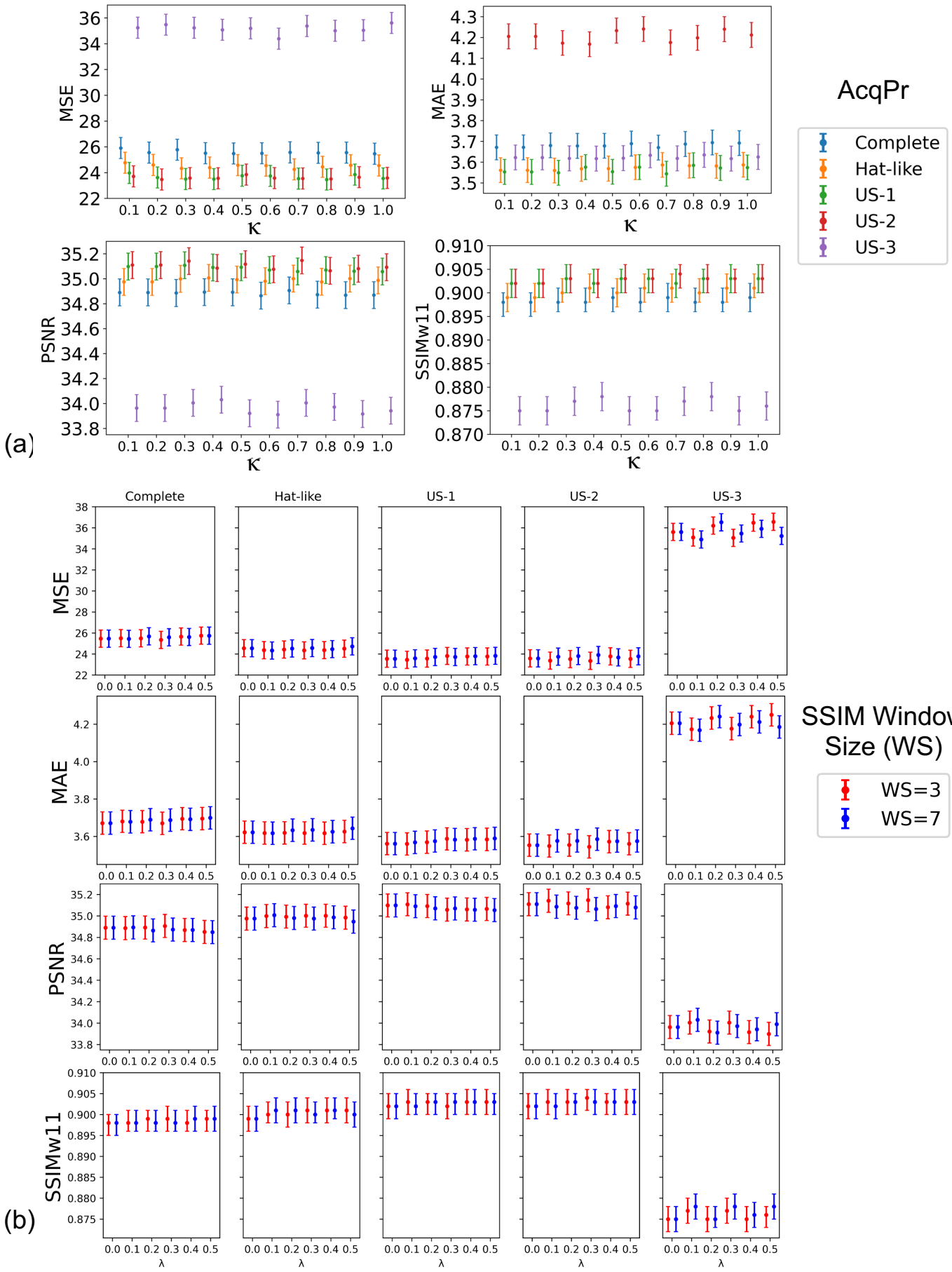

Fig. 8. Interaction plots for the mixed-effects model exhibiting how (a) the two factors κ and acquisition protocol (AcqPr), interact with each other for different response variables for the loss function $\kappa \times L1 + (1-\kappa) \times L1_{Canny}$ and (b) the three factors, λ, SSIM window size (WS), and acquisition protocol (AcqPr) interact with each other for different response variables when the loss function was $L1 + \lambda \times LSSIM$. For all possible combinations in (a) and (b), the plots report the predicted value and 95% confidence interval.

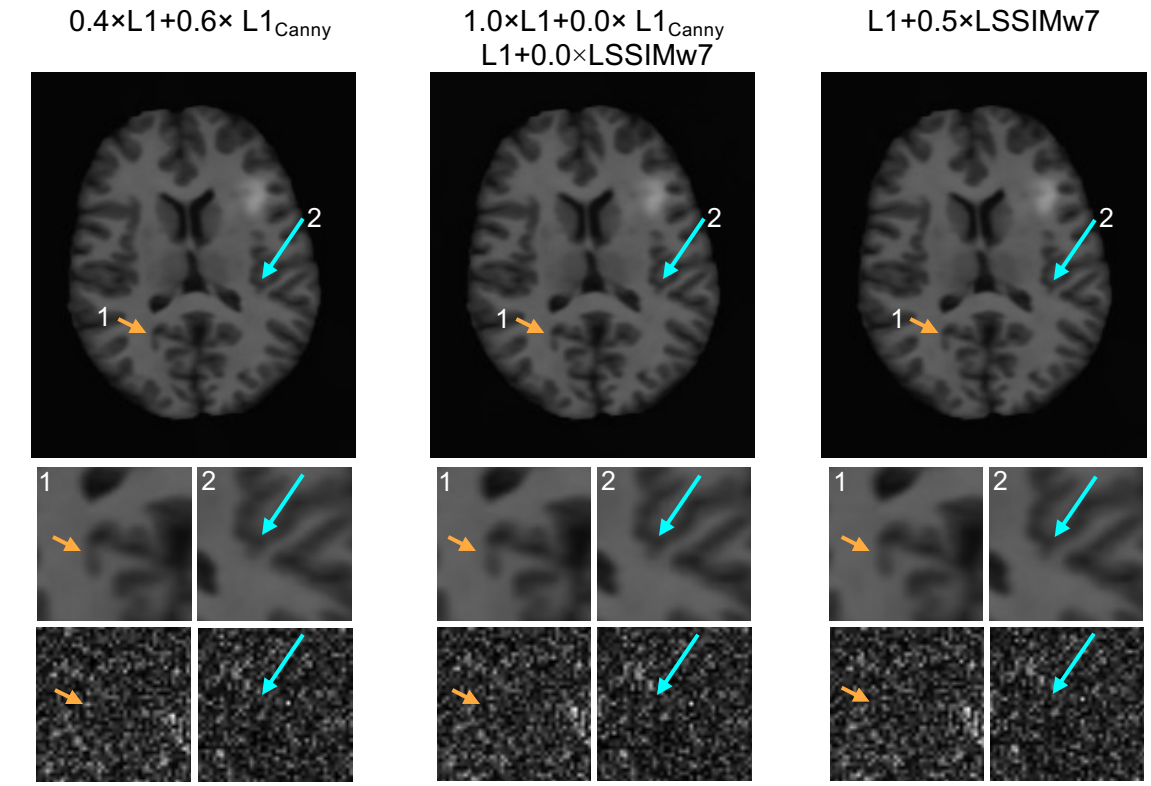

(a) SSIM = 0.9014 (b) SSIM = 0.9016 (c) SSIM = 0.9025

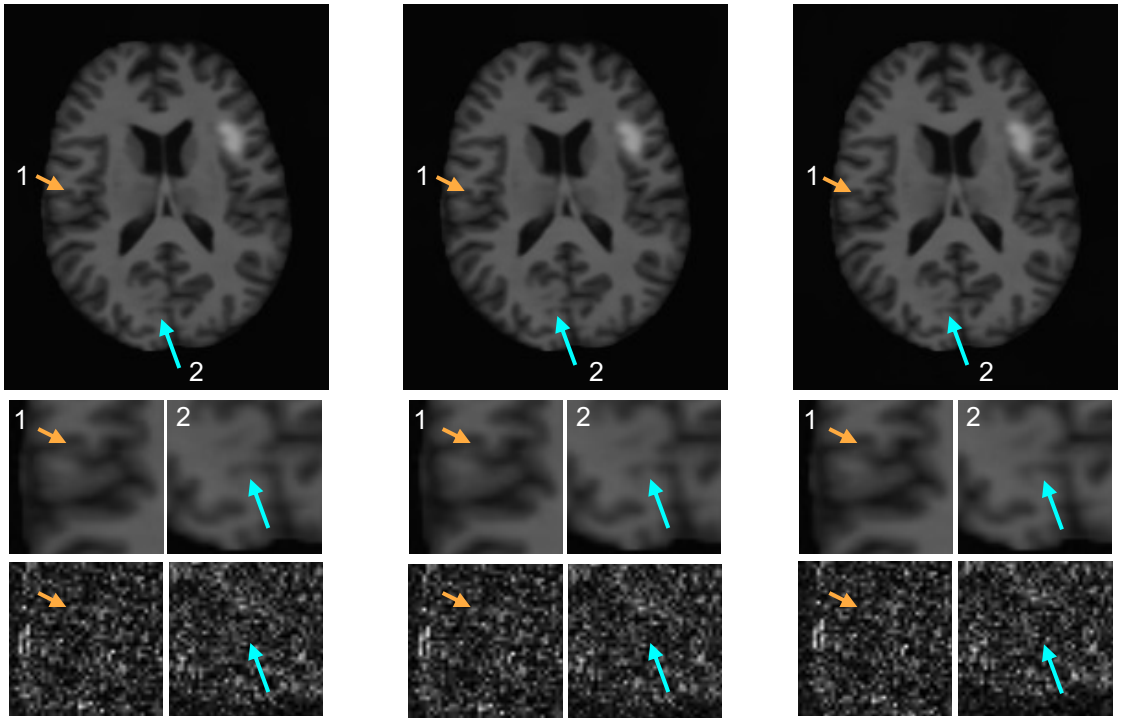

(d) SSIM = 0.9074 (e) SSIM = 0.9082 (f) SSIM = 0.9085

Fig. 9. Comparison of image enhancement with DUNet using different loss functions from the US-2 AcqPr. Images are enhanced using three different loss functions (a, d) CLF1 (i.e., $\kappa \times L1 + (1-\kappa) \times L1_{Canny}$) with κ=0.4, (b, e) plain L1 loss function (CLF1, κ=1; CLF2, λ = 0), and (c, f) CLF2 (i.e., $L1 + \lambda \times LSSIMw7$) with λ = 0.5. The arrows and zoomed-in areas highlight differences in structure when enhancement is done with different loss functions. The lower rows show zoomed-in regions with error maps relative to the GTacq. The entire image SSIM value with window size 11 is reported for all cases under the error maps.

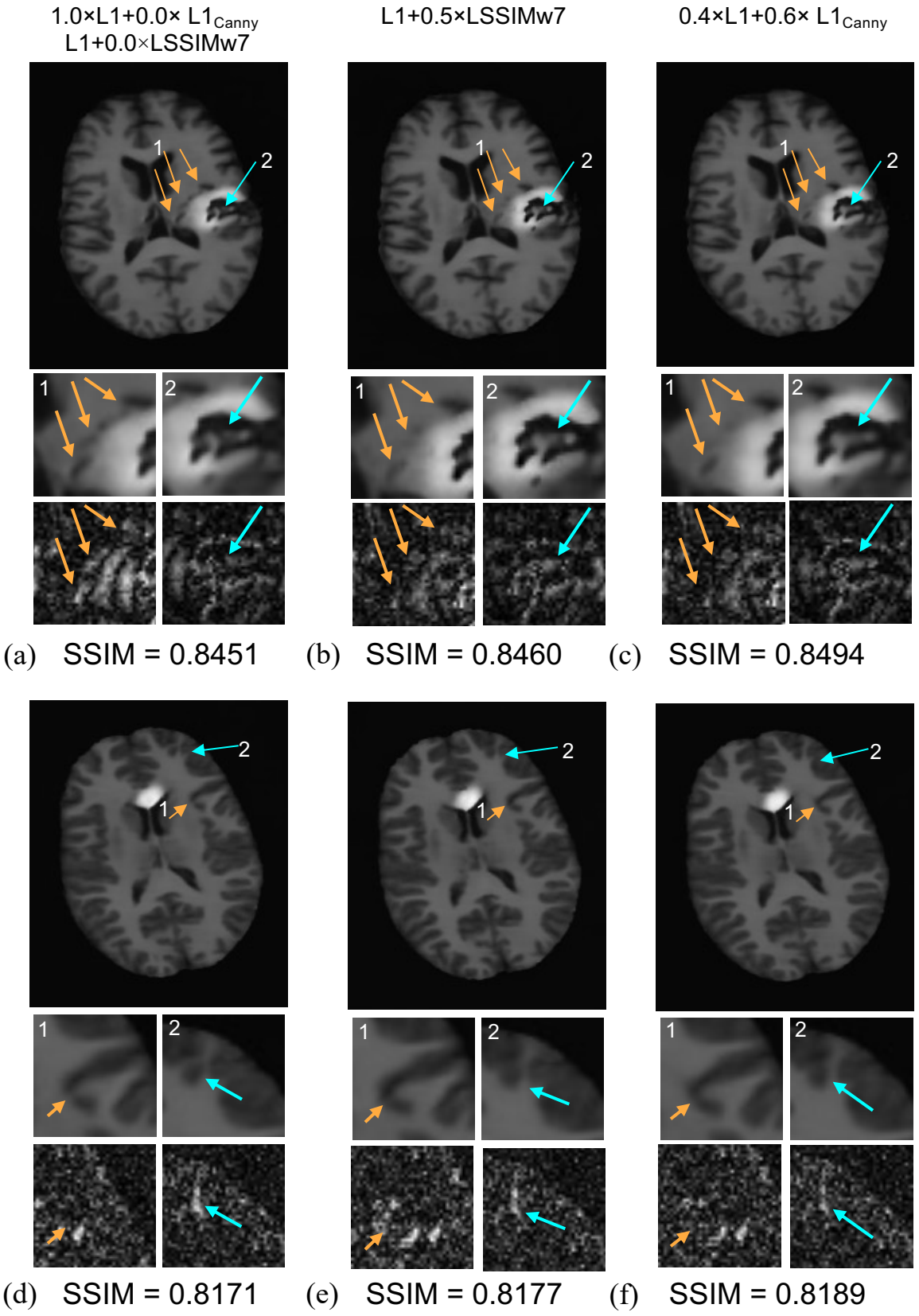

Fig. 10. Comparison of image enhancement with DUNet using different loss functions from the US-3 AcqPr. Images are enhanced using three different loss functions (a, d) plain L1 loss function (CLF1, κ=1; CLF2, λ = 0), (b, e) CLF2 (i.e., L1+λ×LSSIMw7) with λ = 0.5, and (c, f) CLF1 (i.e., κ×L1+(1-κ)×$L1_{Canny}$) with κ=0.4. The arrows and zoomed-in areas highlight differences in structure when enhancement is done with different loss functions. The lower rows show zoomed-in regions with error maps relative to the GTacq. The entire image SSIM value with window size 11 is reported for all cases under the error maps.

	Acronyms	Details	Cases
Acquisition	***Acquisition Protocols (AcqPr)***		***5***
	Complete	100% k-space, Nreps=10 per line	1
	Hat-like	100% k-space, Nreps=9 per line and 10% k-space (central), Nreps=19 per line	1
	US-1	20% central k-space; 20% random k-space; Nreps = 25 per line	1
	US-2	20% central k-space, Nreps=50 per line	1
	US-3	10% central k-space, 10% equidistant lines outside; Nreps=50 perline	1
Training	***Loss Functions (LF, CLFs)***		***24***
	L1	L1	1
	L2	L2	1
	LSSIM	SSIM Loss; LSSIM window $\in$ [3, 7]	2
	CLF1	$\kappa \times L1 + (1-\kappa) \times L1_{Canny}$ $\kappa \in$ [0.0 - 0.9; step = 0.1]	10
	CLF2	$L1 + \lambda \times LSSIM$; $\lambda \in$ [0.0 – 0.5; step = 0.1] and LSSIM window $\in$ [3, 7]	10
	Ground Truths (GT)		***2***
	GTacq	100% k-space, and Nreps=100	1
	GTsyn	100% k-space, Nreps = 1 and empty space signal set to 0	1
Metrics	***Metrics Region of Interest (MeROI)***		***2***
	Entire image	Evaluation metrics calculated over the entire image	1
	Lesion-focused ROI	Evaluation metrics calculated over the lesion-focused region	1

Table 1. Overview of the five acquisition protocols (AcqPr), the 24 loss functions (LF), the two ground truths (GT), and the two metrics region of interest (MeROI). The total cases per group are in bold italics. The evaluation metrics for the 240 (AcqPr×LF×GT) in silico experiments were calculated for the two MeROI, resulting to 480 cases (AcqPr×LF×GT×MeROI) used in statistical analysis.

Loss Function	GTacq					GTsyn				
	Complete	Hat-like	US-1	US-2	US-3	Complete	Hat-like	US-1	US-2	US-3
0.0×L1+1.0×$L1_{Canny}$	0.4653±0.0451	0.0846±0.0311	0.1756±0.0347	0.0849±0.0312	0.4170±0.0450	0.4455±0.0036	0.4471±0.0021	0.4433±0.0455	0.4466±0.0036	0.4472±0.0020
0.1×L1+0.9×$L1_{Canny}$	0.8479±0.0482	0.8508±0.0467	0.8523±0.0445	0.8525±0.0430	0.8249±0.0426	0.9598±0.0095	0.9639±0.0074	0.9641±0.0061	0.9652±0.0048	0.9361±0.0089
0.2×L1+0.8×$L1_{Canny}$	0.8495±0.0475	0.8519±0.0465	0.8534±0.0443	0.8540±0.0425	0.8251±0.0430	0.9603±0.0093	0.9642±0.0075	0.9656±0.0057	0.9656±0.0048	0.9374±0.0090
0.3×L1+0.7×$L1_{Canny}$	0.8486±0.0478	0.8525±0.0462	0.8542±0.0443	0.8530±0.0429	0.8253±0.0427	0.9606±0.0091	0.9638±0.0076	0.9653±0.0058	0.9657±0.0048	0.9353±0.0091
0.4×L1+0.6×$L1_{Canny}$	0.8499±0.0476	0.8523±0.0464	0.8544±0.0441	0.8532±0.0429	0.8261±0.0425	0.9602±0.0091	0.9645±0.0076	0.9644±0.0062	0.9663±0.0048	0.9354±0.0093
0.5×L1+0.5×$L1_{Canny}$	0.8498±0.0475	0.8517±0.0463	0.8529±0.0444	0.8525±0.0429	0.8253±0.0430	0.9599±0.0093	0.9638±0.0076	0.9656±0.0059	0.9665±0.0048	0.9356±0.0089
0.6×L1+0.4×$L1_{Canny}$	0.8496±0.0476	0.8519±0.0466	0.8530±0.0443	0.8535±0.0428	0.8279±0.0427	0.9596±0.0096	0.9635±0.0076	0.9643±0.0059	0.9659±0.0048	0.9364±0.0090
0.7×L1+0.3×$L1_{Canny}$	0.8497±0.0476	0.8528±0.0460	0.8540±0.0441	0.8534±0.0428	0.8257±0.0428	0.9598±0.0094	0.9647±0.0075	0.9655±0.0057	0.9662±0.0047	0.9352±0.0091
0.8×L1+0.2×$L1_{Canny}$	0.8497±0.0476	0.8524±0.0464	0.8542±0.0441	0.8537±0.0427	0.8265±0.0425	0.9602±0.0092	0.9645±0.0075	0.9649±0.0059	0.9663±0.0047	0.9365±0.0091
0.9×L1+0.1×$L1_{Canny}$	0.8499±0.0476	0.8520±0.0465	0.8531±0.0444	0.8534±0.0429	0.8262±0.0433	0.9603±0.0092	0.9645±0.0074	0.9660±0.0057	0.9663±0.0047	0.9364±0.0088
L1	0.8501±0.0474	0.8516±0.0465	0.8542±0.0442	0.8532±0.0428	0.8244±0.0422	0.9603±0.0093	0.9642±0.0075	0.9657±0.0057	0.9659±0.0048	0.9349±0.0093
L1+0.1×LSSIMw3	0.8508±0.0471	0.8531±0.0459	0.8552±0.0438	0.8547±0.0424	0.8267±0.0423	0.9580±0.0099	0.9633±0.0078	0.9662±0.0057	0.9672±0.0046	0.9323±0.0089
L1+0.2×LSSIMw3	0.8510±0.0472	0.8531±0.0460	0.8549±0.0438	0.8542±0.0425	0.8245±0.0422	0.9609±0.0092	0.9625±0.0080	0.9647±0.0059	0.9665±0.0048	0.9335±0.0089
L1+0.3×LSSIMw3	0.8518±0.0468	0.8538±0.0457	0.8541±0.0438	0.8553±0.0424	0.8269±0.0424	0.9473±0.0126	0.9631±0.0077	0.9548±0.0071	0.9548±0.0056	0.9333±0.0089
L1+0.4×LSSIMw3	0.8510±0.0470	0.8538±0.0458	0.8551±0.0438	0.8538±0.0422	0.8246±0.0424	0.9584±0.0100	0.9627±0.0079	0.9559±0.0071	0.9538±0.0057	0.9340±0.0088
L1+0.5×LSSIMw3	0.8514±0.0468	0.8540±0.0457	0.8551±0.0437	0.8547±0.0422	0.8250±0.0422	0.9484±0.0119	0.9632±0.0077	0.9544±0.0072	0.9546±0.0057	0.9335±0.0089
LSSIMw3	0.8520±0.0465	0.8540±0.0456	0.8553±0.0437	0.8548±0.0422	0.8270±0.0421	0.9579±0.0100	0.9629±0.0078	0.9641±0.0060	0.9642±0.0050	0.9277±0.0092
L1+0.1×LSSIMw7	0.8509±0.0470	0.8537±0.0460	0.8546±0.0440	0.8532±0.0422	0.8279±0.0427	0.9609±0.0092	0.9625±0.0080	0.9667±0.0056	0.9667±0.0047	0.9311±0.0090
L1+0.2×LSSIMw7	0.8508±0.0469	0.8537±0.0458	0.8547±0.0438	0.8537±0.0423	0.8249±0.0425	0.9584±0.0100	0.9624±0.0079	0.9661±0.0058	0.9671±0.0046	0.9324±0.0091
L1+0.3×LSSIMw7	0.8509±0.0470	0.8529±0.0459	0.8546±0.0439	0.8538±0.0424	0.8275±0.0423	0.9579±0.0100	0.9624±0.0081	0.9637±0.0061	0.9642±0.0048	0.9315±0.0089
L1+0.4×LSSIMw7	0.8512±0.0470	0.8543±0.0457	0.8552±0.0437	0.8545±0.0420	0.8258±0.0425	0.9581±0.0098	0.9625±0.0080	0.9638±0.0061	0.9638±0.0051	0.9323±0.0087
L1+0.5×LSSIMw7	0.8515±0.0468	0.8529±0.0459	0.8546±0.0439	0.8542±0.0423	0.8275±0.0424	0.9577±0.0100	0.9629±0.0078	0.9636±0.0061	0.9642±0.0049	0.9327±0.0088
LSSIMw7	0.8515±0.0468	0.8540±0.0455	0.8550±0.0436	0.8545±0.0423	0.8259±0.0423	0.9463±0.0124	0.9625±0.0080	0.9636±0.0060	0.9635±0.0049	0.9317±0.0088
L2	0.8475±0.0473	0.8514±0.0462	0.8526±0.0437	0.8513±0.0415	0.8226±0.0406	0.9576±0.0103	0.9623±0.0080	0.9614±0.0068	0.9627±0.0052	0.9321±0.0089

Table 2. The SSIM window 5 (mean ± standard deviation) was calculated over the entire image for the complete test set (N=516) for all possible combinations of the experiments with 24 loss functions, 5 AcqPr, and 2 GT. Loss functions that belong to the same combination are color coded together for better visualization: tan rows correspond to $\kappa \times L1+(1-\kappa) \times L1_{Canny}$ CLF, blue rows to $L1+\lambda \times LSSIMw3$ CLF, and green rows to $L1+\lambda \times LSSIMw7$ CLF. L1 loss is shared by all three groups and is reported in the tan rows.

Loss Function	GTacq					GTsyn				
	Complete	Hat-like	US-1	US-2	US-3	Complete	Hat-like	US-1	US-2	US-3
0.0×L1+1.0×$L1_{Canny}$	0.1664±0.0387	0.0014±0.0025	0.0104±0.0150	0.0067±0.0029	0.2774±0.0580	0.0027±0.0088	0.0010±0.0033	0.2158±0.0303	0.0039±0.0094	0.0009±0.0031
0.1×L1+0.9×$L1_{Canny}$	0.9190±0.0475	0.9182±0.0447	0.9126±0.0484	0.9018±0.0613	0.8490±0.0846	0.9585±0.0306	0.9588±0.0302	0.9486±0.0390	0.9376±0.0576	0.8797±0.0847
0.2×L1+0.8×$L1_{Canny}$	0.9215±0.0467	0.9175±0.0457	0.9158±0.0473	0.9037±0.0628	0.8463±0.0858	0.9592±0.0314	0.9563±0.0316	0.9537±0.0356	0.9399±0.0561	0.8845±0.0825
0.3×L1+0.7×$L1_{Canny}$	0.9209±0.0459	0.9187±0.0461	0.9169±0.0460	0.9018±0.0610	0.8421±0.0901	0.9590±0.0315	0.9564±0.0319	0.9503±0.0397	0.9362±0.0608	0.8806±0.0844
0.4×L1+0.6×$L1_{Canny}$	0.9225±0.0458	0.9185±0.0464	0.9168±0.0460	0.9026±0.0585	0.8462±0.0878	0.9582±0.0314	0.9589±0.0301	0.9506±0.0370	0.9407±0.0572	0.8797±0.0806
0.5×L1+0.5×$L1_{Canny}$	0.9224±0.0462	0.9178±0.0464	0.9145±0.0471	0.8998±0.0643	0.8437±0.0854	0.9583±0.0311	0.9568±0.0316	0.9544±0.0355	0.9414±0.0572	0.8815±0.0805
0.6×L1+0.4×$L1_{Canny}$	0.9222±0.0463	0.9194±0.0447	0.9147±0.0475	0.9038±0.0592	0.8499±0.0838	0.9581±0.0320	0.9549±0.0337	0.9504±0.0361	0.9399±0.0557	0.8809±0.0828
0.7×L1+0.3×$L1_{Canny}$	0.9220±0.0462	0.9196±0.0462	0.9169±0.0460	0.9041±0.0611	0.8461±0.0846	0.9574±0.0329	0.9577±0.0306	0.9515±0.0368	0.9390±0.0585	0.8789±0.0838
0.8×L1+0.2×$L1_{Canny}$	0.9228±0.0458	0.9199±0.0447	0.9172±0.0465	0.9052±0.0576	0.8457±0.0848	0.9574±0.0326	0.9578±0.0304	0.9515±0.0353	0.9402±0.0569	0.8850±0.0799
0.9×L1+0.1×$L1_{Canny}$	0.9206±0.0475	0.9205±0.0440	0.9149±0.0465	0.9008±0.0614	0.8467±0.0846	0.9595±0.0311	0.9605±0.0270	0.9554±0.0336	0.9416±0.0543	0.8779±0.0839
L1	0.9221±0.0469	0.9187±0.0457	0.9178±0.0446	0.9036±0.0600	0.8395±0.0863	0.9591±0.0313	0.9569±0.0314	0.9527±0.0365	0.9397±0.0560	0.8785±0.0850
L1+0.1×LSSIMw3	0.9223±0.0450	0.9192±0.0457	0.9184±0.0452	0.9031±0.0593	0.8455±0.0843	0.9541±0.0339	0.9530±0.0318	0.9518±0.0364	0.9402±0.0552	0.8552±0.0922
L1+0.2×LSSIMw3	0.9213±0.0466	0.9201±0.0441	0.9166±0.0460	0.9020±0.0626	0.8353±0.0897	0.9433±0.0303	0.9487±0.0345	0.9498±0.0361	0.9399±0.0562	0.8664±0.0869
L1+0.3×LSSIMw3	0.9225±0.0458	0.9178±0.0457	0.9127±0.0467	0.9043±0.0606	0.8499±0.0808	0.9393±0.0306	0.9500±0.0348	0.9284±0.0478	0.9096±0.0774	0.8637±0.0848
L1+0.4×LSSIMw3	0.9213±0.0455	0.9193±0.0438	0.9155±0.0460	0.8999±0.0603	0.8342±0.0872	0.9418±0.0300	0.9514±0.0341	0.9272±0.0487	0.9097±0.0797	0.8728±0.0807
L1+0.5×LSSIMw3	0.9217±0.0459	0.9200±0.0446	0.9164±0.0454	0.9022±0.0605	0.8421±0.0841	0.9372±0.0306	0.9526±0.0316	0.9274±0.0462	0.9071±0.0809	0.8642±0.0841
LSSIMw3	0.9229±0.0444	0.9182±0.0449	0.9160±0.0461	0.8999±0.0617	0.8506±0.0787	0.9396±0.0306	0.9478±0.0336	0.9459±0.0377	0.9329±0.0590	0.8489±0.0913
L1+0.1×LSSIMw7	0.9220±0.0461	0.9212±0.0447	0.9169±0.0452	0.8992±0.0628	0.8534±0.0822	0.9599±0.0294	0.9511±0.0325	0.9556±0.0333	0.9432±0.0521	0.8604±0.0857
L1+0.2×LSSIMw7	0.9239±0.0444	0.9220±0.0435	0.9173±0.0447	0.8995±0.0606	0.8461±0.0830	0.9555±0.0311	0.9529±0.0314	0.9541±0.0332	0.9421±0.0545	0.8669±0.0889
L1+0.3×LSSIMw7	0.9230±0.0458	0.9181±0.0452	0.9165±0.0458	0.9023±0.0600	0.8486±0.0822	0.9535±0.0321	0.9513±0.0318	0.9463±0.0376	0.9327±0.0593	0.8691±0.0832
L1+0.4×LSSIMw7	0.9220±0.0467	0.9214±0.0434	0.9170±0.0456	0.9031±0.0587	0.8484±0.0819	0.9551±0.0306	0.9523±0.0315	0.9464±0.0375	0.9326±0.0597	0.8685±0.0836
L1+0.5×LSSIMw7	0.9236±0.0438	0.9195±0.0426	0.9165±0.0463	0.9022±0.0602	0.8537±0.0786	0.9511±0.0327	0.9511±0.0330	0.9483±0.0360	0.9322±0.0589	0.8716±0.0821
LSSIMw7	0.9224±0.0456	0.9200±0.0443	0.9177±0.0451	0.9021±0.0583	0.8482±0.0823	0.9426±0.0324	0.9505±0.0316	0.9469±0.0363	0.9313±0.0590	0.8703±0.0832
L2	0.9191±0.0468	0.9199±0.0440	0.9165±0.0460	0.8995±0.0616	0.8463±0.0854	0.9574±0.0299	0.9571±0.0290	0.9471±0.0366	0.9383±0.0550	0.8832±0.0750

Table 3. The SSIM window 5 (mean ± standard deviation) was calculated over the lesion focused ROI for the complete test set (N=516) for all possible combinations of the experiments with 24 loss functions, 5 AcqPr, and 2 GT. Loss functions that belong to the same combination are color coded together for better visualization: tan rows correspond to $\kappa \times L1+(1-\kappa) \times L1_{Canny}$ CLF, blue rows to $L1+\lambda \times LSSIMw3$ CLF, and green rows to $L1+\lambda \times LSSIMw7$ CLF. L1 loss is shared by all three groups and is reported in the tan rows.

(a)

Response Variable	κ (F-ratio [p-value])	AcqPr (F-ratio [p-value])	κ x AcqPr (F-ratio [p-value])
MSE	0.33 [0.965]	1388.66 [0.000]	0.19 [1.000]
MAE	0.23 [0.990]	723.07 [0.000]	0.12 [1.000]
PSNR	0.31 [0.971]	696.97 [0.000]	0.11 [1.000]
SSIMw11	0.36 [0.950]	562.59 [0.000]	0.11 [1.000]

(b)

Response Variable	λ (F-ratio [p-value])	WS (F-ratio [p-value])	AcqPr (F-ratio [p-value])	λ x WS (F-ratio [p-value])	λ x AcqPr (F-ratio [p-value])	WS x AcqPr (F-ratio [p-value])	λ x WS x AcqPr (F-ratio [p-value])
MSE	1.42 [0.213]	0.14 [0.708]	1834.66 [0.000]	0.43 [0.826]	0.59 [0.917]	0.48 [0.748]	0.26 [1.000]
MAE	0.91 [0.467]	0.35 [0.550]	941.14 [0.000]	0.22 [0.953]	0.26 [1.000]	0.37 [0.826]	0.12 [1.000]
PSNR	0.80 [0.544]	0.44 [0.509]	910.21 [0.000]	0.18 [0.969]	0.18 [1.000]	0.32 [0.861]	0.10 [1.000]
SSIMw11	1.19 [0.307]	0.14 [0.701]	742.79 [0.000]	0.06 [0.997]	0.25 [1.000]	0.39 [0.814]	0.07 [1.000]

(c)

Response Variable	κ (F-ratio [p-value])	AcqPr (F-ratio [p-value])	κ x AcqPr (F-ratio [p-value])
MSE	8.96 [0.000]	37436.45 [0.000]	5.33 [0.00]
MAE	15.10 [0.000]	46815.19 [0.000]	7.97 [0.00]
PSNR	9.66 [0.000]	21505.09 [0.000]	3.52 [0.00]
SSIMw11	46.80 [0.000]	71357.28 [0.000]	14.49 [0.00]

(d)

Response Variable	λ (F-ratio [p-value])	WS (F-ratio [p-value])	AcqPr (F-ratio [p-value])	λ x WS (F-ratio [p-value])	λ x AcqPr (F-ratio [p-value])	WS x AcqPr (F-ratio [p-value])	λ x WS x AcqPr (F-ratio [p-value])
MSE	37.05 [0.000]	3.65 [0.055]	47825.78 [0.000]	11.27 [0.000]	15.58 [0.000]	12.61 [0.000]	7.01 [0.000]
MAE	60.00 [0.000]	23.39 [0.000]	61457.02 [0.000]	14.51 [0.000]	17.25 [0.000]	24.55 [0.000]	8.20 [0.000]
PSNR	24.21 [0.000]	13.40 [0.000]	27284.21 [0.000]	5.49 [0.000]	5.65 [0.000]	9.73 [0.000]	3.26 [0.000]
SSIMw11	155.68 [0.000]	19.19 [0.000]	96428.73 [0.000]	8.01 [0.000]	33.14 [0.000]	50.96 [0.000]	9.55 [0.000]

Table 4. The F-ratios and p-values (in square brackets) from the f-test performed with classical ANOVA (a, b) and mixed effects model (c, d) aka repeated measures. (a and c) report results for DUNet trained on the CLF1 = $\kappa \times L1 + (1-\kappa) \times L1_{Canny}$ when investigating the interaction of explanatory variables κ (n = 10; $\kappa \in [0.1 – 1.0]$) and acquisition protocol (AcqPr; n = 5). (b and d) report results for DUNet trained on the CLF2 = $L1 + \lambda \times LSSIM$ when investigating the interaction of explanatory variables λ (n=6; $\lambda \in [0.0 – 0.5]$), LSSIM window size (WS; n=2), and acquisition protocol (AcqPr; n=5). Higher F-ratios correspond to lower p-values and are more statistically significant.

Loss Function	MSE	MAE	PSNR	SSIMw3	SSIMw5	SSIMw7	SSIMw9	SSIMw11	SSIMw13
0.0×L1+1.0×$L1_{Canny}$	1115.54±231.28	22.70±2.61	29.92±0.33	0.4894±0.0480	0.4653±0.0451	0.4461±0.0420	0.4305±0.0392	0.4168±0.0366	0.4039±0.0340
0.1×L1+0.9×$L1_{Canny}$	25.90±10.31	3.70±0.75	34.83±1.37	0.8238±0.0525	0.8479±0.0482	0.8680±0.0434	0.8836±0.0392	0.8960±0.0356	0.9061±0.0325
0.2×L1+0.8×$L1_{Canny}$	25.55±10.06	3.68±0.74	34.88±1.36	0.8253±0.0518	0.8495±0.0475	0.8694±0.0427	0.8849±0.0385	0.8971±0.0350	0.9071±0.0319
0.3×L1+0.7×$L1_{Canny}$	25.78±10.21	3.69±0.75	34.84±1.37	0.8245±0.0521	0.8486±0.0478	0.8686±0.0430	0.8841±0.0389	0.8964±0.0353	0.9064±0.0322
0.4×L1+0.6×$L1_{Canny}$	25.50±10.10	3.68±0.74	34.89±1.37	0.8257±0.0519	0.8499±0.0476	0.8698±0.0428	0.8853±0.0386	0.8974±0.0351	0.9074±0.0320
0.5×L1+0.5×$L1_{Canny}$	25.48±10.12	3.68±0.74	34.89±1.37	0.8257±0.0519	0.8498±0.0475	0.8698±0.0427	0.8852±0.0385	0.8974±0.0350	0.9073±0.0320
0.6×L1+0.4×$L1_{Canny}$	25.50±10.16	3.67±0.75	34.88±1.38	0.8254±0.0520	0.8496±0.0476	0.8696±0.0428	0.8851±0.0386	0.8973±0.0351	0.9073±0.0320
0.7×L1+0.3×$L1_{Canny}$	25.57±10.15	3.68±0.74	34.88±1.37	0.8254±0.0520	0.8497±0.0476	0.8697±0.0428	0.8852±0.0386	0.8974±0.0351	0.9074±0.0320
0.8×L1+0.2×$L1_{Canny}$	25.53±10.13	3.67±0.74	34.88±1.38	0.8255±0.0520	0.8497±0.0476	0.8696±0.0428	0.8851±0.0386	0.8973±0.0351	0.9072±0.0321
0.9×L1+0.1×$L1_{Canny}$	25.55±10.10	3.68±0.74	34.88±1.37	0.8257±0.0519	0.8499±0.0476	0.8698±0.0428	0.8853±0.0386	0.8974±0.0351	0.9074±0.0320
L1	25.46±10.08	3.67±0.74	34.89±1.37	0.8258±0.0518	0.8501±0.0474	0.8700±0.0426	0.8855±0.0384	0.8976±0.0349	0.9076±0.0319
L1+0.1×LSSIMw3	25.50±10.09	3.68±0.74	34.89±1.37	0.8263±0.0516	0.8508±0.0471	0.8708±0.0422	0.8863±0.0381	0.8984±0.0346	0.9083±0.0316
L1+0.2×LSSIMw3	25.49±10.14	3.68±0.74	34.89±1.37	0.8265±0.0516	0.8510±0.0472	0.8710±0.0423	0.8864±0.0382	0.8985±0.0347	0.9084±0.0316
L1+0.3×LSSIMw3	25.34±9.96	3.67±0.74	34.91±1.36	0.8272±0.0513	0.8518±0.0468	0.8717±0.0419	0.8869±0.0378	0.8990±0.0343	0.9088±0.0314
L1+0.4×LSSIMw3	25.66±10.13	3.69±0.75	34.87±1.36	0.8264±0.0515	0.8510±0.0470	0.8709±0.0422	0.8863±0.0380	0.8984±0.0345	0.9083±0.0315
L1+0.5×LSSIMw3	25.75±10.11	3.69±0.74	34.85±1.35	0.8268±0.0513	0.8514±0.0468	0.8713±0.0420	0.8866±0.0378	0.8987±0.0343	0.9085±0.0313
LSSIMw3	25.98±10.18	3.71±0.75	34.82±1.34	0.8273±0.0512	0.8520±0.0465	0.8719±0.0417	0.8872±0.0375	0.8992±0.0340	0.9090±0.0311
L1+0.1×LSSIMw7	25.44±10.06	3.68±0.74	34.89±1.37	0.8264±0.0515	0.8509±0.0470	0.8709±0.0422	0.8863±0.0380	0.8984±0.0345	0.9083±0.0315
L1+0.2×LSSIMw7	25.68±10.09	3.69±0.74	34.86±1.35	0.8262±0.0514	0.8508±0.0469	0.8708±0.0421	0.8862±0.0379	0.8983±0.0344	0.9082±0.0314
L1+0.3×LSSIMw7	25.59±10.13	3.69±0.75	34.87±1.36	0.8263±0.0515	0.8509±0.0470	0.8709±0.0421	0.8864±0.0380	0.8985±0.0345	0.9084±0.0315
L1+0.4×LSSIMw7	25.62±10.11	3.69±0.75	34.87±1.36	0.8266±0.0515	0.8512±0.0470	0.8712±0.0421	0.8866±0.0380	0.8987±0.0345	0.9086±0.0315
L1+0.5×LSSIMw7	25.74±10.15	3.70±0.75	34.85±1.36	0.8267±0.0514	0.8515±0.0468	0.8715±0.0420	0.8868±0.0378	0.8989±0.0343	0.9087±0.0314
LSSIMw7	25.92±10.25	3.71±0.75	34.83±1.35	0.8268±0.0514	0.8515±0.0468	0.8715±0.0420	0.8869±0.0378	0.8989±0.0343	0.9088±0.0313
L2	26.16±10.30	3.74±0.74	34.79±1.34	0.8231±0.0515	0.8475±0.0473	0.8676±0.0426	0.8833±0.0385	0.8957±0.0350	0.9058±0.0320

SuppTable 1. Evaluation metrics (mean±standard deviation) calculated for entire image on entire test set (N=516) between DUNet enhanced images and acquired ground truth (GTacq), when enhancement is performed from complete k-space AcqPr images. DUNet was trained with loss functions shown in the table and the GTacq was used as the ground truth to train the network.

Loss Function	MSE	MAE	PSNR	SSIMw3	SSIMw5	SSIMw7	SSIMw9	SSIMw11	SSIMw13
0.0×L1+1.0×$L1_{Canny}$	2305.79±486.59	33.98±3.92	29.19±0.40	0.0931±0.0332	0.0846±0.0311	0.0787±0.0291	0.0732±0.0272	0.0677±0.0252	0.0621±0.0231
0.1×L1+0.9×$L1_{Canny}$	24.76±9.50	3.64±0.72	34.95±1.35	0.8264±0.0513	0.8508±0.0467	0.8708±0.0419	0.8863±0.0377	0.8985±0.0342	0.9085±0.0311
0.2×L1+0.8×$L1_{Canny}$	24.59±9.43	3.63±0.71	34.97±1.36	0.8274±0.0511	0.8519±0.0465	0.8719±0.0416	0.8873±0.0374	0.8994±0.0339	0.9093±0.0309
0.3×L1+0.7×$L1_{Canny}$	24.33±9.36	3.61±0.71	35.01±1.37	0.8279±0.0509	0.8525±0.0462	0.8725±0.0413	0.8878±0.0372	0.8999±0.0337	0.9097±0.0307
0.4×L1+0.6×$L1_{Canny}$	24.39±9.40	3.61±0.71	35.00±1.37	0.8277±0.0510	0.8523±0.0464	0.8723±0.0416	0.8877±0.0374	0.8998±0.0339	0.9097±0.0309
0.5×L1+0.5×$L1_{Canny}$	24.58±9.43	3.62±0.71	34.97±1.36	0.8272±0.0509	0.8517±0.0463	0.8717±0.0414	0.8871±0.0373	0.8993±0.0338	0.9092±0.0308
0.6×L1+0.4×$L1_{Canny}$	24.54±9.48	3.62±0.72	34.98±1.36	0.8273±0.0512	0.8519±0.0466	0.8719±0.0417	0.8873±0.0375	0.8994±0.0340	0.9093±0.0310
0.7×L1+0.3×$L1_{Canny}$	24.25±9.31	3.60±0.71	35.02±1.37	0.8282±0.0507	0.8528±0.0460	0.8727±0.0412	0.8881±0.0370	0.9001±0.0335	0.9100±0.0305
0.8×L1+0.2×$L1_{Canny}$	24.45±9.42	3.62±0.71	34.99±1.36	0.8278±0.0510	0.8524±0.0464	0.8723±0.0415	0.8877±0.0374	0.8998±0.0339	0.9096±0.0309
0.9×L1+0.1×$L1_{Canny}$	24.57±9.48	3.62±0.72	34.98±1.36	0.8274±0.0511	0.8520±0.0465	0.8720±0.0416	0.8873±0.0375	0.8995±0.0340	0.9094±0.0310
L1	24.55±9.45	3.62±0.72	34.97±1.36	0.8272±0.0511	0.8516±0.0465	0.8715±0.0417	0.8869±0.0375	0.8991±0.0340	0.9090±0.0310
L1+0.1×LSSIMw3	24.37±9.32	3.62±0.71	35.00±1.35	0.8285±0.0507	0.8531±0.0459	0.8730±0.0410	0.8883±0.0369	0.9004±0.0334	0.9102±0.0305
L1+0.2×LSSIMw3	24.42±9.37	3.62±0.71	34.99±1.36	0.8284±0.0507	0.8531±0.0460	0.8730±0.0411	0.8883±0.0369	0.9003±0.0335	0.9101±0.0305
L1+0.3×LSSIMw3	24.35±9.30	3.62±0.71	35.00±1.35	0.8289±0.0505	0.8538±0.0457	0.8737±0.0409	0.8889±0.0367	0.9009±0.0333	0.9106±0.0303
L1+0.4×LSSIMw3	24.37±9.37	3.62±0.72	35.00±1.36	0.8289±0.0506	0.8538±0.0458	0.8737±0.0409	0.8889±0.0368	0.9009±0.0333	0.9107±0.0303
L1+0.5×LSSIMw3	24.51±9.41	3.63±0.72	34.98±1.36	0.8290±0.0505	0.8540±0.0457	0.8739±0.0408	0.8891±0.0367	0.9010±0.0332	0.9108±0.0303
LSSIMw3	24.53±9.35	3.63±0.71	34.97±1.34	0.8292±0.0505	0.8540±0.0456	0.8739±0.0407	0.8892±0.0366	0.9011±0.0332	0.9109±0.0302
L1+0.1×LSSIMw7	24.33±9.39	3.62±0.72	35.01±1.37	0.8287±0.0508	0.8537±0.0460	0.8737±0.0410	0.8890±0.0369	0.9010±0.0334	0.9107±0.0304
L1+0.2×LSSIMw7	24.53±9.42	3.63±0.72	34.98±1.35	0.8287±0.0506	0.8537±0.0458	0.8737±0.0409	0.8890±0.0367	0.9010±0.0332	0.9108±0.0303
L1+0.3×LSSIMw7	24.56±9.41	3.63±0.72	34.98±1.35	0.8280±0.0507	0.8529±0.0459	0.8730±0.0410	0.8884±0.0369	0.9004±0.0334	0.9103±0.0304
L1+0.4×LSSIMw7	24.46±9.37	3.62±0.72	34.99±1.35	0.8292±0.0505	0.8543±0.0457	0.8742±0.0408	0.8894±0.0367	0.9013±0.0332	0.9111±0.0302
L1+0.5×LSSIMw7	24.73±9.42	3.64±0.72	34.95±1.34	0.8280±0.0506	0.8529±0.0459	0.8729±0.0410	0.8882±0.0369	0.9002±0.0334	0.9100±0.0305
LSSIMw7	25.32±9.57	3.68±0.72	34.86±1.31	0.8289±0.0503	0.8540±0.0455	0.8740±0.0406	0.8893±0.0364	0.9012±0.0330	0.9109±0.0300
L2	24.74±9.45	3.65±0.72	34.94±1.34	0.8266±0.0508	0.8514±0.0462	0.8715±0.0413	0.8869±0.0372	0.8991±0.0337	0.9090±0.0307

SuppTable 2. Evaluation metrics (mean±standard deviation) calculated for entire image on entire test set (N=516) between DUNet images and acquired ground truth (GTacq), when enhancement is performed from hat-like k-space AcqPr images. DUNet was trained with loss functions shown in the table and the GTacq was used as the ground truth to train the network.

Loss Function	MSE	MAE	PSNR	SSIMw3	SSIMw5	SSIMw7	SSIMw9	SSIMw11	SSIMw13
0.0×L1+1.0×$L1_{Canny}$	2184.68±459.23	32.57±3.77	29.39±0.38	0.1933±0.0365	0.1756±0.0347	0.1619±0.0325	0.1497±0.0303	0.1383±0.0280	0.1271±0.0257
0.1×L1+0.9×$L1_{Canny}$	23.97±8.80	3.59±0.68	35.03±1.30	0.8274±0.0495	0.8523±0.0445	0.8728±0.0397	0.8884±0.0357	0.9006±0.0324	0.9104±0.0295
0.2×L1+0.8×$L1_{Canny}$	23.62±8.72	3.57±0.68	35.09±1.32	0.8284±0.0493	0.8534±0.0443	0.8738±0.0394	0.8894±0.0354	0.9015±0.0321	0.9113±0.0292
0.3×L1+0.7×$L1_{Canny}$	23.50±8.70	3.56±0.68	35.10±1.32	0.8291±0.0493	0.8542±0.0443	0.8745±0.0395	0.8899±0.0355	0.9019±0.0322	0.9116±0.0293
0.4×L1+0.6×$L1_{Canny}$	23.50±8.69	3.56±0.68	35.11±1.32	0.8292±0.0492	0.8544±0.0441	0.8747±0.0393	0.8902±0.0353	0.9022±0.0320	0.9119±0.0291
0.5×L1+0.5×$L1_{Canny}$	23.75±8.75	3.57±0.68	35.06±1.31	0.8278±0.0494	0.8529±0.0444	0.8733±0.0396	0.8890±0.0356	0.9011±0.0322	0.9109±0.0293
0.6×L1+0.4×$L1_{Canny}$	23.74±8.73	3.57±0.68	35.07±1.31	0.8279±0.0493	0.8530±0.0443	0.8734±0.0395	0.8890±0.0355	0.9011±0.0322	0.9109±0.0293
0.7×L1+0.3×$L1_{Canny}$	23.53±8.68	3.56±0.68	35.10±1.31	0.8288±0.0492	0.8540±0.0441	0.8743±0.0393	0.8898±0.0354	0.9019±0.0320	0.9116±0.0292
0.8×L1+0.2×$L1_{Canny}$	23.46±8.65	3.56±0.68	35.11±1.32	0.8291±0.0492	0.8542±0.0441	0.8745±0.0393	0.8900±0.0354	0.9020±0.0320	0.9117±0.0292
0.9×L1+0.1×$L1_{Canny}$	23.85±8.77	3.58±0.68	35.05±1.31	0.8280±0.0494	0.8531±0.0444	0.8735±0.0396	0.8891±0.0356	0.9012±0.0323	0.9110±0.0294
L1	23.55±8.69	3.56±0.68	35.10±1.32	0.8290±0.0492	0.8542±0.0442	0.8746±0.0394	0.8901±0.0354	0.9021±0.0321	0.9118±0.0292
L1+0.1×LSSIMw3	23.45±8.63	3.56±0.68	35.11±1.31	0.8298±0.0490	0.8552±0.0438	0.8755±0.0390	0.8909±0.0350	0.9028±0.0317	0.9124±0.0289
L1+0.2×LSSIMw3	23.57±8.68	3.57±0.68	35.09±1.31	0.8295±0.0490	0.8549±0.0438	0.8753±0.0390	0.8907±0.0350	0.9027±0.0317	0.9124±0.0289
L1+0.3×LSSIMw3	23.82±8.71	3.59±0.68	35.06±1.30	0.8288±0.0489	0.8541±0.0438	0.8746±0.0389	0.8902±0.0350	0.9022±0.0317	0.9120±0.0288
L1+0.4×LSSIMw3	23.77±8.70	3.58±0.68	35.06±1.30	0.8295±0.0489	0.8551±0.0438	0.8754±0.0389	0.8908±0.0350	0.9028±0.0317	0.9124±0.0288
L1+0.5×LSSIMw3	23.76±8.74	3.58±0.68	35.07±1.30	0.8296±0.0489	0.8551±0.0437	0.8755±0.0389	0.8909±0.0349	0.9029±0.0316	0.9125±0.0288
LSSIMw3	23.82±8.76	3.59±0.68	35.05±1.30	0.8297±0.0488	0.8553±0.0437	0.8756±0.0388	0.8910±0.0348	0.9030±0.0315	0.9126±0.0287
L1+0.1×LSSIMw7	23.59±8.71	3.57±0.68	35.09±1.31	0.8292±0.0491	0.8546±0.0440	0.8749±0.0392	0.8904±0.0352	0.9024±0.0319	0.9121±0.0290
L1+0.2×LSSIMw7	23.72±8.72	3.58±0.68	35.07±1.31	0.8292±0.0489	0.8547±0.0438	0.8750±0.0389	0.8905±0.0350	0.9025±0.0317	0.9122±0.0288
L1+0.3×LSSIMw7	23.72±8.70	3.58±0.68	35.07±1.30	0.8291±0.0491	0.8546±0.0439	0.8750±0.0390	0.8905±0.0351	0.9025±0.0317	0.9122±0.0289
L1+0.4×LSSIMw7	23.80±8.74	3.59±0.68	35.06±1.30	0.8296±0.0489	0.8552±0.0437	0.8756±0.0389	0.8910±0.0349	0.9029±0.0316	0.9126±0.0288
L1+0.5×LSSIMw7	23.83±8.77	3.59±0.68	35.05±1.30	0.8291±0.0491	0.8546±0.0439	0.8750±0.0390	0.8905±0.0351	0.9025±0.0317	0.9122±0.0289
LSSIMw7	24.42±8.94	3.63±0.69	34.97±1.28	0.8294±0.0489	0.8550±0.0436	0.8754±0.0388	0.8909±0.0348	0.9029±0.0315	0.9125±0.0287
L2	23.88±8.70	3.60±0.68	35.04±1.29	0.8271±0.0488	0.8526±0.0437	0.8732±0.0390	0.8889±0.0350	0.9011±0.0317	0.9109±0.0289

SuppTable 3. Evaluation metrics (mean±standard deviation) calculated for entire image on entire test set (N=516) between DUNet image and acquired ground truth (GTacq), when enhancement is performed from US-1 undersampled AcqPr images. DUNet was trained with loss functions shown in the table and the GTacq was used as the ground truth to train the network.

Loss Function	MSE	MAE	PSNR	SSIMw3	SSIMw5	SSIMw7	SSIMw9	SSIMw11	SSIMw13
0.0×L1+1.0×$L1_{Canny}$	2256.60±476.77	33.65±3.89	29.18±0.40	0.0942±0.0334	0.0849±0.0312	0.0786±0.0293	0.0729±0.0273	0.0675±0.0253	0.0620±0.0233
0.1×L1+0.9×$L1_{Canny}$	23.71±8.35	3.56±0.66	35.09±1.27	0.8270±0.0482	0.8525±0.0430	0.8734±0.0383	0.8892±0.0344	0.9013±0.0312	0.9111±0.0284
0.2×L1+0.8×$L1_{Canny}$	23.47±8.25	3.55±0.65	35.13±1.27	0.8283±0.0478	0.8540±0.0425	0.8748±0.0378	0.8905±0.0339	0.9025±0.0307	0.9122±0.0279
0.3×L1+0.7×$L1_{Canny}$	23.57±8.29	3.55±0.65	35.11±1.27	0.8275±0.0481	0.8530±0.0429	0.8738±0.0382	0.8896±0.0343	0.9017±0.0311	0.9115±0.0283
0.4×L1+0.6×$L1_{Canny}$	23.56±8.31	3.55±0.65	35.12±1.27	0.8276±0.0481	0.8532±0.0429	0.8741±0.0381	0.8899±0.0343	0.9020±0.0310	0.9118±0.0282
0.5×L1+0.5×$L1_{Canny}$	23.85±8.41	3.57±0.66	35.08±1.26	0.8269±0.0481	0.8525±0.0429	0.8734±0.0382	0.8893±0.0343	0.9015±0.0310	0.9113±0.0282
0.6×L1+0.4×$L1_{Canny}$	23.57±8.32	3.55±0.66	35.11±1.27	0.8278±0.0481	0.8535±0.0428	0.8743±0.0381	0.8901±0.0342	0.9022±0.0310	0.9119±0.0282
0.7×L1+0.3×$L1_{Canny}$	23.54±8.29	3.55±0.66	35.11±1.27	0.8279±0.0480	0.8534±0.0428	0.8742±0.0380	0.8900±0.0342	0.9020±0.0309	0.9118±0.0282
0.8×L1+0.2×$L1_{Canny}$	23.51±8.31	3.55±0.66	35.12±1.27	0.8280±0.0480	0.8537±0.0427	0.8745±0.0380	0.8903±0.0341	0.9024±0.0309	0.9121±0.0281
0.9×L1+0.1×$L1_{Canny}$	23.64±8.36	3.56±0.65	35.10±1.27	0.8277±0.0480	0.8534±0.0429	0.8743±0.0381	0.8901±0.0342	0.9022±0.0310	0.9119±0.0282
L1	23.58±8.34	3.55±0.66	35.11±1.27	0.8276±0.0481	0.8532±0.0428	0.8741±0.0381	0.8900±0.0342	0.9021±0.0310	0.9119±0.0282
L1+0.1×LSSIMw3	23.37±8.24	3.55±0.66	35.14±1.28	0.8288±0.0477	0.8547±0.0424	0.8755±0.0376	0.8912±0.0337	0.9032±0.0305	0.9129±0.0278
L1+0.2×LSSIMw3	23.52±8.27	3.55±0.65	35.12±1.26	0.8284±0.0477	0.8542±0.0425	0.8750±0.0377	0.8907±0.0339	0.9028±0.0307	0.9125±0.0279
L1+0.3×LSSIMw3	23.35±8.29	3.54±0.66	35.15±1.28	0.8294±0.0478	0.8553±0.0424	0.8761±0.0377	0.8917±0.0338	0.9037±0.0306	0.9133±0.0278
L1+0.4×LSSIMw3	23.78±8.28	3.57±0.65	35.08±1.25	0.8280±0.0475	0.8538±0.0422	0.8747±0.0375	0.8905±0.0337	0.9026±0.0305	0.9123±0.0277
L1+0.5×LSSIMw3	23.54±8.24	3.56±0.65	35.11±1.26	0.8288±0.0475	0.8547±0.0422	0.8755±0.0375	0.8912±0.0337	0.9032±0.0305	0.9128±0.0277
LSSIMw3	24.03±8.45	3.59±0.66	35.04±1.25	0.8288±0.0476	0.8548±0.0422	0.8756±0.0375	0.8913±0.0336	0.9033±0.0304	0.9130±0.0276
L1+0.1×LSSIMw7	23.75±8.29	3.58±0.65	35.09±1.25	0.8274±0.0475	0.8532±0.0422	0.8742±0.0375	0.8901±0.0337	0.9022±0.0305	0.9120±0.0277
L1+0.2×LSSIMw7	23.81±8.30	3.58±0.66	35.08±1.25	0.8278±0.0476	0.8537±0.0423	0.8747±0.0376	0.8905±0.0337	0.9026±0.0305	0.9123±0.0278
L1+0.3×LSSIMw7	23.91±8.39	3.59±0.66	35.06±1.25	0.8278±0.0477	0.8538±0.0424	0.8748±0.0376	0.8906±0.0338	0.9027±0.0306	0.9124±0.0278
L1+0.4×LSSIMw7	23.68±8.30	3.57±0.65	35.09±1.25	0.8284±0.0473	0.8545±0.0420	0.8754±0.0373	0.8911±0.0334	0.9031±0.0303	0.9127±0.0275
L1+0.5×LSSIMw7	23.78±8.35	3.58±0.66	35.08±1.25	0.8282±0.0476	0.8542±0.0423	0.8752±0.0375	0.8910±0.0337	0.9030±0.0305	0.9127±0.0277
LSSIMw7	24.15±8.45	3.60±0.66	35.02±1.25	0.8285±0.0476	0.8545±0.0423	0.8754±0.0375	0.8911±0.0336	0.9031±0.0304	0.9128±0.0277
L2	24.06±8.22	3.61±0.64	35.03±1.21	0.8254±0.0467	0.8513±0.0415	0.8725±0.0369	0.8885±0.0331	0.9008±0.0300	0.9107±0.0273

SuppTable 4. Evaluation metrics (mean±standard deviation) calculated for entire image on entire test set (N=516) between DUNet images and acquired ground truth (GTacq), when enhancement is performed from US-2 undersampled AcqPr images. DUNet was trained with loss functions shown in the table and the GTacq was used as the ground truth to train the network.

Loss Function	MSE	MAE	PSNR	SSIMw3	SSIMw5	SSIMw7	SSIMw9	SSIMw11	SSIMw13
$0.0 \times L1 + 1.0 \times L1_{Canny}$	941.48±195.48	21.56±2.50	29.70±0.36	0.4385±0.0483	0.4170±0.0450	0.4075±0.0417	0.4031±0.0387	0.4010±0.0359	0.3999±0.0333
$0.1 \times L1 + 0.9 \times L1_{Canny}$	35.24±10.57	4.18±0.66	33.99±0.90	0.8064±0.0474	0.8249±0.0426	0.8443±0.0383	0.8613±0.0347	0.8755±0.0316	0.8874±0.0288
$0.2 \times L1 + 0.8 \times L1_{Canny}$	35.48±10.68	4.18±0.67	33.98±0.90	0.8065±0.0478	0.8251±0.0430	0.8445±0.0387	0.8614±0.0350	0.8756±0.0319	0.8875±0.0292
$0.3 \times L1 + 0.7 \times L1_{Canny}$	35.23±10.55	4.18±0.66	34.00±0.90	0.8067±0.0474	0.8253±0.0427	0.8446±0.0383	0.8615±0.0347	0.8757±0.0316	0.8876±0.0289
$0.4 \times L1 + 0.6 \times L1_{Canny}$	35.08±10.43	4.17±0.66	34.00±0.90	0.8073±0.0474	0.8261±0.0425	0.8456±0.0381	0.8625±0.0345	0.8766±0.0315	0.8883±0.0288
$0.5 \times L1 + 0.5 \times L1_{Canny}$	35.19±10.56	4.17±0.66	34.00±0.90	0.8068±0.0478	0.8253±0.0430	0.8446±0.0386	0.8615±0.0350	0.8757±0.0319	0.8875±0.0291
$0.6 \times L1 + 0.4 \times L1_{Canny}$	34.39±10.35	4.13±0.66	34.06±0.91	0.8089±0.0476	0.8279±0.0427	0.8473±0.0383	0.8641±0.0346	0.8781±0.0315	0.8897±0.0288
$0.7 \times L1 + 0.3 \times L1_{Canny}$	35.37±10.65	4.18±0.67	33.99±0.90	0.8070±0.0476	0.8257±0.0428	0.8452±0.0384	0.8621±0.0348	0.8763±0.0317	0.8881±0.0290
$0.8 \times L1 + 0.2 \times L1_{Canny}$	35.01±10.40	4.16±0.66	34.01±0.90	0.8077±0.0474	0.8265±0.0425	0.8460±0.0381	0.8629±0.0345	0.8770±0.0314	0.8887±0.0287
$0.9 \times L1 + 0.1 \times L1_{Canny}$	35.04±10.60	4.16±0.67	34.01±0.92	0.8074±0.0481	0.8262±0.0433	0.8457±0.0389	0.8626±0.0352	0.8768±0.0321	0.8886±0.0293
L1	35.61±10.50	4.21±0.65	33.96±0.88	0.8058±0.0470	0.8244±0.0422	0.8438±0.0378	0.8608±0.0342	0.8750±0.0312	0.8869±0.0285
L1+0.1×LSSIMw3	35.08±10.44	4.17±0.66	34.00±0.89	0.8079±0.0473	0.8267±0.0423	0.8461±0.0379	0.8630±0.0343	0.8770±0.0312	0.8888±0.0286
L1+0.2×LSSIMw3	36.21±10.68	4.23±0.66	33.92±0.86	0.8060±0.0472	0.8245±0.0422	0.8438±0.0379	0.8607±0.0343	0.8750±0.0312	0.8868±0.0286
L1+0.3×LSSIMw3	35.04±10.47	4.18±0.66	34.00±0.89	0.8081±0.0473	0.8269±0.0424	0.8462±0.0380	0.8630±0.0344	0.8771±0.0313	0.8888±0.0286
L1+0.4×LSSIMw3	36.49±10.80	4.24±0.67	33.92±0.87	0.8062±0.0474	0.8246±0.0424	0.8439±0.0381	0.8608±0.0345	0.8750±0.0315	0.8869±0.0288
L1+0.5×LSSIMw3	36.57±10.80	4.25±0.67	33.90±0.86	0.8063±0.0472	0.8250±0.0422	0.8445±0.0379	0.8615±0.0343	0.8756±0.0312	0.8874±0.0286
LSSIMw3	35.88±10.70	4.22±0.67	33.95±0.88	0.8079±0.0471	0.8270±0.0421	0.8464±0.0377	0.8632±0.0341	0.8773±0.0311	0.8890±0.0284
L1+0.1×LSSIMw7	34.89±10.60	4.17±0.67	34.03±0.91	0.8086±0.0476	0.8279±0.0427	0.8473±0.0383	0.8641±0.0347	0.8781±0.0316	0.8898±0.0289
L1+0.2×LSSIMw7	36.53±10.81	4.24±0.67	33.91±0.87	0.8064±0.0474	0.8249±0.0425	0.8443±0.0381	0.8613±0.0345	0.8755±0.0314	0.8874±0.0288
L1+0.3×LSSIMw7	35.46±10.54	4.20±0.67	33.97±0.89	0.8081±0.0473	0.8275±0.0423	0.8471±0.0378	0.8640±0.0342	0.8781±0.0311	0.8898±0.0284
L1+0.4×LSSIMw7	35.91±10.70	4.21±0.67	33.94±0.88	0.8070±0.0475	0.8258±0.0425	0.8451±0.0381	0.8621±0.0345	0.8763±0.0314	0.8881±0.0287
L1+0.5×LSSIMw7	35.23±10.55	4.18±0.67	33.99±0.89	0.8083±0.0474	0.8275±0.0424	0.8470±0.0380	0.8638±0.0344	0.8779±0.0313	0.8896±0.0286
LSSIMw7	37.45±11.16	4.31±0.68	33.81±0.86	0.8069±0.0472	0.8259±0.0423	0.8454±0.0379	0.8623±0.0343	0.8764±0.0312	0.8882±0.0285
L2	35.54±10.44	4.24±0.64	33.93±0.86	0.8038±0.0454	0.8226±0.0406	0.8422±0.0363	0.8593±0.0328	0.8737±0.0299	0.8857±0.0273

SuppTable 5. Evaluation metrics (mean±standard deviation) calculated for entire image on entire test set (N=516) between DUNet images and Acquired ground truth (GTacq), when enhancement is performed from US-3 undersampled AcqPr images. DUNet was trained with loss functions shown in the table and the GTacq was used as the ground truth to train the network.

Loss Function	MSE	MAE	PSNR	SSIMw3	SSIMw5	SSIMw7	SSIMw9	SSIMw11	SSIMw13
$0.0 \times L1 + 1.0 \times L1_{Canny}$	2268.27±477.17	31.19±3.56	30.35±0.13	0.4686±0.0038	0.4455±0.0036	0.4202±0.0037	0.3932±0.0040	0.3649±0.0044	0.3350±0.0049
$0.1 \times L1 + 0.9 \times L1_{Canny}$	10.78±3.61	1.73±0.28	38.41±1.21	0.9570±0.0091	0.9598±0.0095	0.9656±0.0087	0.9704±0.0079	0.9740±0.0071	0.9767±0.0066
$0.2 \times L1 + 0.8 \times L1_{Canny}$	10.68±3.55	1.72±0.28	38.45±1.20	0.9575±0.0089	0.9603±0.0093	0.9660±0.0086	0.9707±0.0077	0.9743±0.0071	0.9770±0.0065
$0.3 \times L1 + 0.7 \times L1_{Canny}$	10.58±3.50	1.71±0.28	38.48±1.19	0.9579±0.0088	0.9606±0.0091	0.9662±0.0084	0.9710±0.0076	0.9745±0.0069	0.9771±0.0064
$0.4 \times L1 + 0.6 \times L1_{Canny}$	10.70±3.54	1.72±0.28	38.44±1.19	0.9573±0.0088	0.9602±0.0091	0.9659±0.0084	0.9707±0.0076	0.9743±0.0069	0.9769±0.0064
$0.5 \times L1 + 0.5 \times L1_{Canny}$	10.72±3.57	1.72±0.28	38.45±1.19	0.9572±0.0089	0.9599±0.0093	0.9657±0.0085	0.9705±0.0077	0.9741±0.0070	0.9767±0.0065
$0.6 \times L1 + 0.4 \times L1_{Canny}$	10.83±3.67	1.73±0.29	38.40±1.21	0.9568±0.0092	0.9596±0.0096	0.9654±0.0088	0.9703±0.0080	0.9739±0.0072	0.9766±0.0067
$0.7 \times L1 + 0.3 \times L1_{Canny}$	10.77±3.64	1.73±0.29	38.42±1.21	0.9571±0.0090	0.9598±0.0094	0.9656±0.0087	0.9704±0.0078	0.9740±0.0071	0.9767±0.0066
$0.8 \times L1 + 0.2 \times L1_{Canny}$	10.72±3.55	1.72±0.28	38.43±1.19	0.9573±0.0089	0.9602±0.0092	0.9659±0.0085	0.9707±0.0077	0.9743±0.0070	0.9770±0.0064
$0.9 \times L1 + 0.1 \times L1_{Canny}$	10.66±3.55	1.72±0.28	38.46±1.20	0.9576±0.0088	0.9603±0.0092	0.9660±0.0084	0.9708±0.0076	0.9743±0.0069	0.9770±0.0064
L1	10.67±3.59	1.72±0.28	38.45±1.21	0.9575±0.0090	0.9603±0.0093	0.9661±0.0085	0.9708±0.0077	0.9744±0.0070	0.9771±0.0064
L1+0.1×LSSIMw3	11.29±3.76	1.78±0.29	38.21±1.21	0.9551±0.0094	0.9580±0.0099	0.9640±0.0091	0.9690±0.0083	0.9728±0.0075	0.9756±0.0069
L1+0.2×LSSIMw3	10.54±3.51	1.71±0.28	38.48±1.21	0.9580±0.0089	0.9609±0.0092	0.9666±0.0085	0.9713±0.0076	0.9748±0.0070	0.9774±0.0064
L1+0.3×LSSIMw3	14.08±4.71	2.02±0.34	37.35±1.18	0.9445±0.0117	0.9473±0.0126	0.9545±0.0118	0.9608±0.0106	0.9656±0.0096	0.9691±0.0088
L1+0.4×LSSIMw3	11.17±3.76	1.77±0.30	38.24±1.22	0.9553±0.0096	0.9584±0.0100	0.9645±0.0092	0.9695±0.0083	0.9733±0.0075	0.9760±0.0069
L1+0.5×LSSIMw3	14.00±4.54	2.02±0.33	37.35±1.16	0.9458±0.0111	0.9484±0.0119	0.9554±0.0111	0.9615±0.0101	0.9662±0.0091	0.9696±0.0084
LSSIMw3	11.34±3.78	1.79±0.30	38.18±1.22	0.9548±0.0096	0.9579±0.0100	0.9640±0.0092	0.9691±0.0083	0.9729±0.0075	0.9757±0.0069
L1+0.1×LSSIMw7	10.54±3.51	1.71±0.28	38.48±1.21	0.9580±0.0089	0.9609±0.0092	0.9666±0.0085	0.9713±0.0076	0.9748±0.0070	0.9774±0.0064
L1+0.2×LSSIMw7	11.17±3.76	1.77±0.30	38.24±1.22	0.9553±0.0096	0.9584±0.0100	0.9645±0.0092	0.9695±0.0083	0.9733±0.0075	0.9760±0.0069
L1+0.3×LSSIMw7	11.34±3.78	1.79±0.30	38.18±1.22	0.9548±0.0096	0.9579±0.0100	0.9640±0.0092	0.9691±0.0083	0.9729±0.0075	0.9757±0.0069
L1+0.4×LSSIMw7	11.29±3.76	1.78±0.29	38.20±1.21	0.9551±0.0094	0.9581±0.0098	0.9642±0.0091	0.9692±0.0082	0.9730±0.0074	0.9758±0.0068
L1+0.5×LSSIMw7	11.40±3.81	1.80±0.30	38.15±1.22	0.9545±0.0096	0.9577±0.0100	0.9639±0.0092	0.9690±0.0083	0.9728±0.0075	0.9756±0.0069
LSSIMw7	14.77±4.67	2.09±0.33	37.10±1.12	0.9437±0.0114	0.9463±0.0124	0.9535±0.0116	0.9599±0.0105	0.9648±0.0095	0.9684±0.0087
L2	11.36±3.85	1.80±0.30	38.15±1.21	0.9547±0.0099	0.9576±0.0103	0.9636±0.0094	0.9687±0.0085	0.9725±0.0077	0.9754±0.0071

SuppTable 6. Evaluation metrics (mean±standard deviation) calculated for entire image on entire test set (N=516) between DUNet images and synthetic ground truth (GTsyn), when enhancement is performed from complete k-space AcqPr images. DUNet was trained with loss functions shown in the table and the GTsyn was used as the ground truth to train the network.

Loss Function	MSE	MAE	PSNR	SSIMw3	SSIMw5	SSIMw7	SSIMw9	SSIMw11	SSIMw13
$0.0\times L1+1.0\times L1_{Canny}$	2269.81±477.30	31.18±3.55	30.36±0.13	0.4718±0.0018	0.4471±0.0021	0.4210±0.0026	0.3937±0.0032	0.3649±0.0037	0.3348±0.0043
$0.1\times L1+0.9\times L1_{Canny}$	9.40±2.77	1.62±0.24	38.85±1.11	0.9609±0.0074	0.9639±0.0074	0.9694±0.0067	0.9739±0.0059	0.9772±0.0053	0.9797±0.0049
$0.2\times L1+0.8\times L1_{Canny}$	9.30±2.77	1.61±0.24	38.89±1.12	0.9612±0.0075	0.9642±0.0075	0.9696±0.0068	0.9741±0.0060	0.9775±0.0054	0.9799±0.0050
$0.3\times L1+0.7\times L1_{Canny}$	9.42±2.81	1.62±0.24	38.85±1.12	0.9607±0.0076	0.9638±0.0076	0.9693±0.0069	0.9739±0.0061	0.9772±0.0055	0.9797±0.0050
$0.4\times L1+0.6\times L1_{Canny}$	9.25±2.77	1.61±0.24	38.92±1.12	0.9614±0.0076	0.9645±0.0076	0.9699±0.0068	0.9744±0.0060	0.9777±0.0054	0.9802±0.0049
$0.5\times L1+0.5\times L1_{Canny}$	9.46±2.85	1.63±0.24	38.83±1.12	0.9607±0.0077	0.9638±0.0076	0.9693±0.0069	0.9739±0.0061	0.9772±0.0055	0.9797±0.0050
$0.6\times L1+0.4\times L1_{Canny}$	9.49±2.83	1.63±0.24	38.82±1.12	0.9606±0.0075	0.9635±0.0076	0.9690±0.0068	0.9735±0.0061	0.9769±0.0055	0.9795±0.0050
$0.7\times L1+0.3\times L1_{Canny}$	9.22±2.77	1.61±0.24	38.93±1.13	0.9617±0.0074	0.9647±0.0075	0.9701±0.0067	0.9745±0.0060	0.9778±0.0054	0.9802±0.0049
$0.8\times L1+0.2\times L1_{Canny}$	9.30±2.81	1.61±0.24	38.90±1.12	0.9614±0.0075	0.9645±0.0075	0.9699±0.0067	0.9744±0.0060	0.9777±0.0054	0.9801±0.0049
$0.9\times L1+0.1\times L1_{Canny}$	9.23±2.76	1.61±0.24	38.92±1.12	0.9615±0.0074	0.9645±0.0074	0.9700±0.0067	0.9744±0.0059	0.9777±0.0053	0.9802±0.0049
L1	9.31±2.77	1.61±0.24	38.89±1.12	0.9612±0.0074	0.9642±0.0075	0.9696±0.0067	0.9741±0.0060	0.9775±0.0054	0.9799±0.0049
L1+0.1×LSSIMw3	9.62±2.86	1.65±0.24	38.76±1.13	0.9601±0.0078	0.9633±0.0078	0.9689±0.0070	0.9735±0.0062	0.9769±0.0056	0.9794±0.0051
L1+0.2×LSSIMw3	9.83±2.93	1.67±0.25	38.67±1.13	0.9593±0.0080	0.9625±0.0080	0.9682±0.0072	0.9729±0.0064	0.9764±0.0057	0.9789±0.0052
L1+0.3×LSSIMw3	9.71±2.89	1.66±0.25	38.72±1.13	0.9600±0.0077	0.9631±0.0077	0.9687±0.0069	0.9733±0.0062	0.9768±0.0055	0.9793±0.0051
L1+0.4×LSSIMw3	9.77±2.91	1.66±0.25	38.69±1.13	0.9595±0.0079	0.9627±0.0079	0.9684±0.0071	0.9731±0.0063	0.9765±0.0057	0.9791±0.0052
L1+0.5×LSSIMw3	9.68±2.86	1.65±0.24	38.73±1.12	0.9600±0.0077	0.9632±0.0077	0.9689±0.0069	0.9735±0.0062	0.9769±0.0055	0.9795±0.0050
LSSIMw3	9.81±2.89	1.67±0.25	38.67±1.12	0.9598±0.0078	0.9629±0.0078	0.9685±0.0070	0.9732±0.0062	0.9766±0.0056	0.9791±0.0051
L1+0.1×LSSIMw7	9.81±2.93	1.67±0.25	38.68±1.13	0.9594±0.0079	0.9625±0.0080	0.9682±0.0072	0.9729±0.0064	0.9764±0.0057	0.9790±0.0052
L1+0.2×LSSIMw7	9.84±2.93	1.67±0.25	38.66±1.13	0.9594±0.0079	0.9624±0.0079	0.9681±0.0072	0.9728±0.0064	0.9763±0.0057	0.9789±0.0052
L1+0.3×LSSIMw7	9.86±2.94	1.67±0.25	38.66±1.13	0.9592±0.0080	0.9624±0.0081	0.9682±0.0073	0.9729±0.0064	0.9764±0.0058	0.9790±0.0053
L1+0.4×LSSIMw7	9.88±2.94	1.68±0.25	38.64±1.13	0.9593±0.0079	0.9625±0.0080	0.9682±0.0072	0.9730±0.0064	0.9765±0.0057	0.9790±0.0052
L1+0.5×LSSIMw7	9.75±2.89	1.66±0.25	38.70±1.12	0.9597±0.0078	0.9629±0.0078	0.9686±0.0071	0.9733±0.0063	0.9767±0.0056	0.9793±0.0051
LSSIMw7	9.90±2.95	1.68±0.25	38.62±1.13	0.9592±0.0080	0.9625±0.0080	0.9683±0.0072	0.9730±0.0064	0.9765±0.0057	0.9790±0.0052
L2	9.84±2.96	1.68±0.25	38.63±1.13	0.9592±0.0079	0.9623±0.0080	0.9680±0.0072	0.9727±0.0064	0.9762±0.0058	0.9788±0.0053

SuppTable 7. Evaluation metrics (mean±standard deviation) calculated for entire image on entire test set (N=516) between DUNet images and Synthetic ground truth (GTsyn), when enhancement is performed from hat-like kspace AcqPr images. DUNet was trained with loss functions shown in the table and the GTsyn was used as the ground truth to train the network.

Loss Function	MSE	MAE	PSNR	SSIMw3	SSIMw5	SSIMw7	SSIMw9	SSIMw11	SSIMw13
0.0×L1+1.0×$L1_{Canny}$	1254.74±263.88	23.87±2.74	30.33±0.13	0.4631±0.0463	0.4433±0.0455	0.4315±0.0434	0.4219±0.0409	0.4122±0.0381	0.4024±0.0352
0.1×L1+0.9×$L1_{Canny}$	8.98±2.41	1.57±0.21	39.06±0.98	0.9606±0.0065	0.9641±0.0061	0.9701±0.0053	0.9750±0.0046	0.9784±0.0041	0.9808±0.0038
0.2×L1+0.8×$L1_{Canny}$	8.59±2.25	1.54±0.20	39.22±0.97	0.9621±0.0061	0.9656±0.0057	0.9715±0.0050	0.9761±0.0044	0.9794±0.0039	0.9817±0.0036
0.3×L1+0.7×$L1_{Canny}$	8.67±2.30	1.55±0.20	39.18±0.98	0.9617±0.0062	0.9653±0.0058	0.9712±0.0050	0.9759±0.0044	0.9792±0.0040	0.9815±0.0036
0.4×L1+0.6×$L1_{Canny}$	8.90±2.42	1.57±0.21	39.09±1.00	0.9609±0.0066	0.9644±0.0062	0.9704±0.0054	0.9752±0.0047	0.9786±0.0042	0.9810±0.0038
0.5×L1+0.5×$L1_{Canny}$	8.56±2.28	1.54±0.20	39.24±0.99	0.9621±0.0062	0.9656±0.0059	0.9715±0.0051	0.9761±0.0044	0.9794±0.0040	0.9817±0.0036
0.6×L1+0.4×$L1_{Canny}$	8.97±2.35	1.58±0.20	39.04±0.97	0.9606±0.0063	0.9643±0.0059	0.9704±0.0051	0.9753±0.0045	0.9787±0.0040	0.9811±0.0037
0.7×L1+0.3×$L1_{Canny}$	8.60±2.27	1.54±0.20	39.23±0.98	0.9620±0.0061	0.9655±0.0057	0.9714±0.0050	0.9760±0.0044	0.9794±0.0039	0.9817±0.0036
0.8×L1+0.2×$L1_{Canny}$	8.80±2.32	1.56±0.20	39.13±0.97	0.9614±0.0062	0.9649±0.0059	0.9708±0.0051	0.9756±0.0045	0.9789±0.0040	0.9813±0.0037
0.9×L1+0.1×$L1_{Canny}$	8.48±2.26	1.53±0.20	39.27±0.99	0.9624±0.0061	0.9660±0.0057	0.9718±0.0050	0.9764±0.0044	0.9797±0.0039	0.9819±0.0036
L1	8.56±2.25	1.53±0.20	39.24±0.97	0.9622±0.0060	0.9657±0.0057	0.9716±0.0050	0.9762±0.0044	0.9794±0.0039	0.9818±0.0036
L1+0.1×LSSIMw3	8.49±2.23	1.53±0.20	39.27±0.98	0.9626±0.0060	0.9662±0.0057	0.9720±0.0049	0.9766±0.0043	0.9798±0.0038	0.9821±0.0035
L1+0.2×LSSIMw3	8.86±2.35	1.57±0.21	39.08±0.98	0.9612±0.0062	0.9647±0.0059	0.9707±0.0052	0.9755±0.0045	0.9789±0.0041	0.9813±0.0037
L1+0.3×LSSIMw3	11.53±2.97	1.81±0.23	38.05±0.94	0.9511±0.0075	0.9548±0.0071	0.9623±0.0061	0.9685±0.0053	0.9728±0.0047	0.9759±0.0043
L1+0.4×LSSIMw3	11.27±2.94	1.78±0.23	38.15±0.95	0.9520±0.0075	0.9559±0.0071	0.9632±0.0061	0.9693±0.0053	0.9735±0.0047	0.9765±0.0043
L1+0.5×LSSIMw3	11.68±3.02	1.83±0.24	37.99±0.94	0.9508±0.0076	0.9544±0.0072	0.9620±0.0063	0.9681±0.0054	0.9725±0.0048	0.9756±0.0044
LSSIMw3	9.09±2.39	1.59±0.21	38.99±0.98	0.9604±0.0064	0.9641±0.0060	0.9702±0.0052	0.9751±0.0045	0.9785±0.0040	0.9809±0.0037
L1+0.1×LSSIMw7	8.36±2.20	1.52±0.20	39.32±0.99	0.9631±0.0060	0.9667±0.0056	0.9724±0.0049	0.9769±0.0043	0.9801±0.0038	0.9823±0.0035
L1+0.2×LSSIMw7	8.51±2.27	1.54±0.20	39.24±0.99	0.9625±0.0062	0.9661±0.0058	0.9719±0.0050	0.9765±0.0044	0.9797±0.0039	0.9820±0.0036
L1+0.3×LSSIMw7	9.18±2.44	1.60±0.21	38.96±0.99	0.9598±0.0066	0.9637±0.0061	0.9699±0.0053	0.9748±0.0046	0.9783±0.0041	0.9808±0.0038
L1+0.4×LSSIMw7	9.11±2.41	1.60±0.21	38.98±0.99	0.9600±0.0065	0.9638±0.0061	0.9700±0.0053	0.9749±0.0046	0.9784±0.0041	0.9808±0.0038
L1+0.5×LSSIMw7	9.17±2.43	1.60±0.21	38.95±0.99	0.9598±0.0065	0.9636±0.0061	0.9698±0.0053	0.9748±0.0046	0.9783±0.0041	0.9807±0.0038
LSSIMw7	9.26±2.42	1.61±0.21	38.90±0.97	0.9599±0.0064	0.9636±0.0060	0.9699±0.0052	0.9748±0.0046	0.9783±0.0041	0.9807±0.0037
L2	9.58±2.59	1.65±0.22	38.76±1.00	0.9576±0.0073	0.9614±0.0068	0.9680±0.0059	0.9732±0.0052	0.9769±0.0046	0.9795±0.0042

SuppTable 8. Evaluation metrics (mean±standard deviation) calculated for entire image on entire test set (N=516) between DUNet images and synthetic ground truth (GTsyn), when enhancement is performed from US-1 undersampled AcqPr images. DUNet was trained with loss functions shown in the table and the GTsyn was used as the ground truth to train the network.

Loss Function	MSE	MAE	PSNR	SSIMw3	SSIMw5	SSIMw7	SSIMw9	SSIMw11	SSIMw13
$0.0 \times L1 + 1.0 \times L1_{Canny}$	2259.69±475.56	31.14±3.56	30.36±0.13	0.4698±0.0037	0.4466±0.0036	0.4216±0.0037	0.3949±0.0040	0.3667±0.0044	0.3370±0.0048
$0.1 \times L1 + 0.9 \times L1_{Canny}$	8.56±2.13	1.50±0.18	39.37±0.89	0.9612±0.0055	0.9652±0.0048	0.9716±0.0040	0.9765±0.0034	0.9798±0.0030	0.9821±0.0027
$0.2 \times L1 + 0.8 \times L1_{Canny}$	8.47±2.09	1.50±0.18	39.38±0.89	0.9616±0.0054	0.9656±0.0048	0.9720±0.0039	0.9768±0.0034	0.9801±0.0030	0.9823±0.0027
$0.3 \times L1 + 0.7 \times L1_{Canny}$	8.48±2.13	1.50±0.18	39.40±0.90	0.9617±0.0054	0.9657±0.0048	0.9720±0.0039	0.9768±0.0034	0.9801±0.0030	0.9824±0.0027
$0.4 \times L1 + 0.6 \times L1_{Canny}$	8.29±2.07	1.48±0.18	39.48±0.90	0.9623±0.0055	0.9663±0.0048	0.9725±0.0039	0.9773±0.0034	0.9805±0.0030	0.9827±0.0027
$0.5 \times L1 + 0.5 \times L1_{Canny}$	8.28±2.06	1.48±0.18	39.50±0.90	0.9624±0.0054	0.9665±0.0048	0.9727±0.0040	0.9774±0.0034	0.9806±0.0030	0.9828±0.0027
$0.6 \times L1 + 0.4 \times L1_{Canny}$	8.41±2.09	1.49±0.18	39.42±0.90	0.9618±0.0055	0.9659±0.0048	0.9722±0.0040	0.9770±0.0034	0.9803±0.0030	0.9825±0.0027
$0.7 \times L1 + 0.3 \times L1_{Canny}$	8.32±2.06	1.48±0.18	39.46±0.90	0.9621±0.0055	0.9662±0.0047	0.9725±0.0039	0.9772±0.0033	0.9805±0.0030	0.9827±0.0027
$0.8 \times L1 + 0.2 \times L1_{Canny}$	8.28±2.05	1.48±0.18	39.48±0.90	0.9623±0.0054	0.9663±0.0047	0.9725±0.0039	0.9772±0.0033	0.9805±0.0029	0.9827±0.0027
$0.9 \times L1 + 0.1 \times L1_{Canny}$	8.32±2.08	1.48±0.18	39.46±0.90	0.9622±0.0054	0.9663±0.0047	0.9725±0.0039	0.9773±0.0034	0.9805±0.0030	0.9827±0.0027
L1	8.40±2.10	1.49±0.18	39.42±0.90	0.9618±0.0055	0.9659±0.0048	0.9722±0.0039	0.9770±0.0033	0.9803±0.0029	0.9826±0.0027
L1+0.1×LSSIMw3	8.12±2.01	1.47±0.18	39.55±0.90	0.9631±0.0053	0.9672±0.0046	0.9733±0.0038	0.9779±0.0033	0.9811±0.0029	0.9832±0.0027
L1+0.2×LSSIMw3	8.30±2.11	1.49±0.19	39.45±0.92	0.9626±0.0055	0.9665±0.0048	0.9727±0.0039	0.9774±0.0033	0.9807±0.0030	0.9829±0.0027
L1+0.3×LSSIMw3	11.60±2.80	1.77±0.21	38.17±0.83	0.9508±0.0065	0.9548±0.0056	0.9628±0.0045	0.9692±0.0038	0.9735±0.0033	0.9765±0.0031
L1+0.4×LSSIMw3	11.82±2.88	1.79±0.21	38.10±0.84	0.9499±0.0067	0.9538±0.0057	0.9620±0.0046	0.9685±0.0038	0.9729±0.0034	0.9759±0.0031
L1+0.5×LSSIMw3	11.73±2.84	1.79±0.21	38.13±0.84	0.9505±0.0066	0.9546±0.0057	0.9626±0.0046	0.9690±0.0038	0.9733±0.0033	0.9763±0.0031
LSSIMw3	8.97±2.25	1.55±0.19	39.17±0.90	0.9599±0.0057	0.9642±0.0050	0.9708±0.0041	0.9759±0.0035	0.9793±0.0031	0.9817±0.0028
L1+0.1×LSSIMw7	8.32±2.04	1.49±0.18	39.44±0.89	0.9625±0.0054	0.9667±0.0047	0.9729±0.0039	0.9776±0.0034	0.9808±0.0030	0.9830±0.0027
L1+0.2×LSSIMw7	8.10±2.02	1.47±0.18	39.55±0.90	0.9630±0.0053	0.9671±0.0046	0.9732±0.0038	0.9778±0.0033	0.9810±0.0029	0.9832±0.0027
L1+0.3×LSSIMw7	8.92±2.19	1.54±0.19	39.19±0.88	0.9600±0.0056	0.9642±0.0048	0.9708±0.0040	0.9759±0.0034	0.9793±0.0030	0.9817±0.0028
L1+0.4×LSSIMw7	9.05±2.26	1.55±0.19	39.14±0.90	0.9595±0.0058	0.9638±0.0051	0.9705±0.0042	0.9756±0.0035	0.9791±0.0031	0.9815±0.0029
L1+0.5×LSSIMw7	8.95±2.20	1.54±0.19	39.18±0.88	0.9599±0.0056	0.9642±0.0049	0.9709±0.0041	0.9759±0.0035	0.9794±0.0031	0.9817±0.0028
LSSIMw7	9.18±2.25	1.57±0.19	39.06±0.89	0.9592±0.0057	0.9635±0.0049	0.9703±0.0040	0.9755±0.0034	0.9790±0.0031	0.9814±0.0028
L2	9.16±2.28	1.58±0.19	39.05±0.90	0.9585±0.0060	0.9627±0.0052	0.9696±0.0042	0.9749±0.0036	0.9785±0.0031	0.9809±0.0029

SuppTable 9. Evaluation metrics (mean±standard deviation) calculated for entire image on entire test set (N=516) between DUNet images and synthetic ground truth (GTsyn), when enhancement is performed from US-2 undersampled AcqPr images. DUNet was trained with loss functions shown in the table and the GTsyn was used as the ground truth to train the network.

Loss Function	MSE	MAE	PSNR	SSIMw3	SSIMw5	SSIMw7	SSIMw9	SSIMw11	SSIMw13
$0.0\times L1+1.0\times L1_{Canny}$	2269.89±477.30	31.17±3.55	30.36±0.13	0.4721±0.0016	0.4472±0.0020	0.4210±0.0026	0.3936±0.0031	0.3649±0.0037	0.3348±0.0042
$0.1\times L1+0.9\times L1_{Canny}$	19.85±5.58	2.30±0.32	36.40±0.78	0.9382±0.0090	0.9361±0.0089	0.9417±0.0082	0.9483±0.0073	0.9541±0.0067	0.9587±0.0061
$0.2\times L1+0.8\times L1_{Canny}$	19.46±5.62	2.27±0.32	36.49±0.79	0.9393±0.0090	0.9374±0.0090	0.9431±0.0082	0.9496±0.0074	0.9552±0.0067	0.9598±0.0062
$0.3\times L1+0.7\times L1_{Canny}$	20.04±5.75	2.31±0.33	36.37±0.79	0.9378±0.0091	0.9353±0.0091	0.9408±0.0083	0.9474±0.0075	0.9532±0.0068	0.9579±0.0062
$0.4\times L1+0.6\times L1_{Canny}$	20.17±5.76	2.33±0.33	36.33±0.80	0.9376±0.0093	0.9354±0.0093	0.9410±0.0085	0.9476±0.0076	0.9534±0.0069	0.9581±0.0063
$0.5\times L1+0.5\times L1_{Canny}$	20.16±5.62	2.31±0.32	36.36±0.76	0.9377±0.0090	0.9356±0.0089	0.9414±0.0081	0.9481±0.0073	0.9538±0.0066	0.9585±0.0060
$0.6\times L1+0.4\times L1_{Canny}$	19.78±5.59	2.29±0.32	36.42±0.79	0.9385±0.0090	0.9364±0.0090	0.9420±0.0081	0.9485±0.0073	0.9543±0.0066	0.9589±0.0060
$0.7\times L1+0.3\times L1_{Canny}$	20.21±5.69	2.31±0.32	36.35±0.77	0.9374±0.0091	0.9352±0.0091	0.9409±0.0083	0.9475±0.0075	0.9534±0.0068	0.9581±0.0063
$0.8\times L1+0.2\times L1_{Canny}$	19.93±5.73	2.29±0.32	36.42±0.78	0.9384±0.0091	0.9365±0.0091	0.9422±0.0083	0.9489±0.0075	0.9546±0.0068	0.9592±0.0062
$0.9\times L1+0.1\times L1_{Canny}$	19.76±5.55	2.29±0.32	36.42±0.77	0.9385±0.0089	0.9364±0.0088	0.9420±0.0080	0.9486±0.0072	0.9544±0.0066	0.9590±0.0061
L1	20.49±5.85	2.33±0.33	36.32±0.78	0.9371±0.0093	0.9349±0.0093	0.9407±0.0084	0.9474±0.0076	0.9532±0.0068	0.9579±0.0063
L1+0.1×LSSIMw3	21.56±5.90	2.40±0.32	36.14±0.74	0.9348±0.0090	0.9323±0.0089	0.9381±0.0081	0.9449±0.0073	0.9510±0.0067	0.9558±0.0061
L1+0.2×LSSIMw3	21.05±5.79	2.37±0.32	36.20±0.76	0.9359±0.0090	0.9335±0.0089	0.9393±0.0080	0.9461±0.0072	0.9521±0.0065	0.9569±0.0060
L1+0.3×LSSIMw3	21.30±5.91	2.39±0.32	36.16±0.75	0.9357±0.0090	0.9333±0.0089	0.9391±0.0081	0.9460±0.0073	0.9519±0.0066	0.9567±0.0061
L1+0.4×LSSIMw3	20.79±5.71	2.37±0.32	36.22±0.76	0.9362±0.0089	0.9340±0.0088	0.9399±0.0080	0.9466±0.0072	0.9526±0.0065	0.9573±0.0060
L1+0.5×LSSIMw3	21.21±5.89	2.38±0.33	36.19±0.76	0.9359±0.0090	0.9335±0.0089	0.9394±0.0081	0.9462±0.0073	0.9522±0.0066	0.9569±0.0061
LSSIMw3	23.45±6.47	2.53±0.34	35.83±0.73	0.9312±0.0093	0.9277±0.0092	0.9334±0.0084	0.9405±0.0076	0.9469±0.0069	0.9521±0.0064
L1+0.1×LSSIMw7	21.94±6.04	2.43±0.33	36.06±0.74	0.9337±0.0092	0.9311±0.0090	0.9371±0.0082	0.9441±0.0074	0.9503±0.0067	0.9552±0.0062
L1+0.2×LSSIMw7	21.39±5.95	2.41±0.33	36.12±0.77	0.9349±0.0092	0.9324±0.0091	0.9382±0.0083	0.9451±0.0074	0.9512±0.0067	0.9561±0.0062
L1+0.3×LSSIMw7	21.74±5.90	2.42±0.33	36.07±0.74	0.9341±0.0090	0.9315±0.0089	0.9374±0.0080	0.9444±0.0072	0.9506±0.0066	0.9555±0.0060
L1+0.4×LSSIMw7	21.71±5.85	2.42±0.32	36.07±0.72	0.9345±0.0089	0.9323±0.0087	0.9384±0.0079	0.9454±0.0071	0.9514±0.0065	0.9563±0.0060
L1+0.5×LSSIMw7	21.46±5.86	2.41±0.32	36.11±0.74	0.9351±0.0090	0.9327±0.0088	0.9386±0.0080	0.9455±0.0072	0.9516±0.0065	0.9564±0.0060
LSSIMw7	22.01±5.91	2.47±0.32	35.97±0.73	0.9343±0.0090	0.9317±0.0088	0.9375±0.0080	0.9444±0.0072	0.9505±0.0065	0.9554±0.0060
L2	21.07±5.75	2.42±0.33	36.08±0.76	0.9347±0.0091	0.9321±0.0089	0.9379±0.0081	0.9448±0.0073	0.9509±0.0066	0.9558±0.0061

SuppTable 10. Evaluation metrics (mean±standard deviation) calculated for entire image on entire test set (N=516) between DUNet images and Synthetic ground truth (GTsyn), when enhancement is performed from US-3 undersampled AcqPr images. DUNet was trained with loss functions shown in the table and the GTsyn was used as the ground truth to train the network.

Loss Function	MSE	MAE	PSNR	SSIMw3	SSIMw5	SSIMw7	SSIMw9	SSIMw11	SSIMw13
$0.0\times L1+1.0\times L1_{Canny}$	7160.09±3198.60	74.71±19.66	27.89±0.47	0.1866±0.0453	0.1664±0.0387	0.1589±0.0351	0.1581±0.0320	0.1610±0.0297	0.1657±0.0280
$0.1\times L1+0.9\times L1_{Canny}$	61.84±35.21	5.93±1.57	32.08±1.55	0.8713±0.0569	0.9190±0.0475	0.9451±0.0385	0.9593±0.0316	0.9671±0.0271	0.9715±0.0242
$0.2\times L1+0.8\times L1_{Canny}$	59.83±34.49	5.84±1.60	32.18±1.60	0.8738±0.0563	0.9215±0.0467	0.9472±0.0377	0.9610±0.0310	0.9686±0.0264	0.9728±0.0234
$0.3\times L1+0.7\times L1_{Canny}$	59.34±32.79	5.82±1.53	32.18±1.62	0.8730±0.0557	0.9209±0.0459	0.9467±0.0371	0.9606±0.0306	0.9683±0.0263	0.9724±0.0235
$0.4\times L1+0.6\times L1_{Canny}$	58.68±34.21	5.77±1.57	32.32±3.37	0.8748±0.0556	0.9225±0.0458	0.9480±0.0367	0.9617±0.0300	0.9692±0.0255	0.9732±0.0227
$0.5\times L1+0.5\times L1_{Canny}$	58.59±34.93	5.77±1.59	32.34±3.36	0.8752±0.0561	0.9224±0.0462	0.9479±0.0371	0.9616±0.0304	0.9690±0.0260	0.9731±0.0232
$0.6\times L1+0.4\times L1_{Canny}$	59.03±35.07	5.80±1.61	32.21±1.74	0.8746±0.0562	0.9222±0.0463	0.9477±0.0372	0.9615±0.0304	0.9690±0.0259	0.9731±0.0231
$0.7\times L1+0.3\times L1_{Canny}$	58.85±33.80	5.80±1.57	32.17±1.51	0.8743±0.0561	0.9220±0.0462	0.9477±0.0370	0.9615±0.0302	0.9689±0.0258	0.9730±0.0230
$0.8\times L1+0.2\times L1_{Canny}$	58.21±32.80	5.75±1.52	32.25±1.59	0.8754±0.0556	0.9228±0.0458	0.9482±0.0368	0.9618±0.0302	0.9693±0.0257	0.9733±0.0228
$0.9\times L1+0.1\times L1_{Canny}$	60.07±34.90	5.85±1.58	32.14±1.49	0.8731±0.0567	0.9206±0.0475	0.9464±0.0385	0.9604±0.0315	0.9681±0.0269	0.9724±0.0238
L1	58.56±33.78	5.78±1.56	32.32±3.35	0.8747±0.0564	0.9221±0.0469	0.9476±0.0379	0.9614±0.0310	0.9689±0.0264	0.9730±0.0234
L1+0.1×LSSIMw3	58.52±32.69	5.78±1.53	32.29±3.33	0.8746±0.0550	0.9223±0.0450	0.9479±0.0360	0.9616±0.0294	0.9691±0.0250	0.9732±0.0223
L1+0.2×LSSIMw3	59.27±33.82	5.81±1.56	32.19±1.62	0.8738±0.0562	0.9213±0.0466	0.9471±0.0375	0.9610±0.0305	0.9686±0.0260	0.9728±0.0230
L1+0.3×LSSIMw3	58.56±33.09	5.80±1.53	32.18±1.53	0.8754±0.0553	0.9225±0.0458	0.9478±0.0370	0.9616±0.0303	0.9691±0.0257	0.9732±0.0228
L1+0.4×LSSIMw3	59.78±34.02	5.83±1.54	32.16±1.61	0.8734±0.0554	0.9213±0.0455	0.9471±0.0366	0.9610±0.0300	0.9686±0.0256	0.9728±0.0228
L1+0.5×LSSIMw3	59.29±35.19	5.81±1.59	32.27±3.41	0.8742±0.0556	0.9217±0.0459	0.9475±0.0367	0.9613±0.0300	0.9688±0.0255	0.9730±0.0227
LSSIMw3	60.87±32.54	5.93±1.48	32.01±1.49	0.8753±0.0544	0.9229±0.0444	0.9484±0.0355	0.9621±0.0289	0.9695±0.0246	0.9735±0.0219
L1+0.1×LSSIMw7	58.97±35.14	5.78±1.58	32.24±1.66	0.8743±0.0563	0.9220±0.0461	0.9477±0.0369	0.9615±0.0302	0.9690±0.0258	0.9731±0.0230
L1+0.2×LSSIMw7	58.06±32.75	5.76±1.52	32.21±1.47	0.8762±0.0548	0.9239±0.0444	0.9491±0.0352	0.9626±0.0285	0.9699±0.0243	0.9738±0.0217
L1+0.3×LSSIMw7	57.83±32.54	5.75±1.54	32.34±3.41	0.8754±0.0557	0.9230±0.0458	0.9484±0.0367	0.9620±0.0299	0.9694±0.0254	0.9734±0.0226
L1+0.4×LSSIMw7	58.82±33.47	5.79±1.57	32.32±3.39	0.8744±0.0564	0.9220±0.0467	0.9476±0.0375	0.9614±0.0306	0.9689±0.0260	0.9731±0.0230
L1+0.5×LSSIMw7	57.95±32.11	5.75±1.49	32.33±3.35	0.8758±0.0542	0.9236±0.0438	0.9490±0.0347	0.9625±0.0282	0.9698±0.0240	0.9738±0.0213
LSSIMw7	61.51±34.82	5.94±1.56	32.26±4.47	0.8746±0.0556	0.9224±0.0456	0.9480±0.0366	0.9617±0.0298	0.9692±0.0254	0.9732±0.0225
L2	61.23±35.68	5.92±1.62	32.18±3.35	0.8713±0.0565	0.9191±0.0468	0.9453±0.0377	0.9595±0.0309	0.9674±0.0265	0.9717±0.0236

SuppTable 11. Evaluation metrics (mean±standard deviation) calculated for lesion-focused ROI on entire test set (N=516) between DUNet images and acquired ground truth (GTacq), when enhancement is performed from complete k-space AcqPr images. DUNet was trained with loss functions shown in the table and the GTacq was used as the ground truth to train the network.

Loss Function	MSE	MAE	PSNR	SSIMw3	SSIMw5	SSIMw7	SSIMw9	SSIMw11	SSIMw13
0.0×L1+1.0×$L1_{Canny}$	13388.97±5886.04	105.39±26.36	27.93±0.76	0.0029±0.0041	0.0014±0.0025	0.0008±0.0016	0.0006±0.0010	0.0004±0.0006	0.0003±0.0231
0.1×L1+0.9×$L1_{Canny}$	61.99±33.85	5.95±1.52	32.04±1.55	0.8700±0.0551	0.9182±0.0447	0.9449±0.0355	0.9594±0.0289	0.9674±0.0246	0.9718±0.0311
0.2×L1+0.8×$L1_{Canny}$	63.15±33.76	5.99±1.53	32.02±1.51	0.8694±0.0559	0.9175±0.0457	0.9442±0.0364	0.9588±0.0297	0.9669±0.0253	0.9715±0.0309
0.3×L1+0.7×$L1_{Canny}$	61.46±36.02	5.92±1.59	32.06±1.53	0.8707±0.0562	0.9187±0.0461	0.9453±0.0366	0.9598±0.0297	0.9678±0.0252	0.9722±0.0307
0.4×L1+0.6×$L1_{Canny}$	61.05±34.79	5.91±1.57	32.20±3.30	0.8702±0.0566	0.9185±0.0464	0.9452±0.0368	0.9598±0.0299	0.9678±0.0253	0.9723±0.0309
0.5×L1+0.5×$L1_{Canny}$	61.85±33.18	5.96±1.55	32.02±1.52	0.8699±0.0561	0.9178±0.0464	0.9445±0.0371	0.9592±0.0302	0.9673±0.0257	0.9718±0.0308
0.6×L1+0.4×$L1_{Canny}$	60.56±32.41	5.87±1.48	32.09±1.53	0.8712±0.0549	0.9194±0.0447	0.9459±0.0353	0.9603±0.0286	0.9681±0.0243	0.9725±0.0310
0.7×L1+0.3×$L1_{Canny}$	59.92±33.75	5.84±1.55	32.13±1.57	0.8719±0.0565	0.9196±0.0462	0.9461±0.0364	0.9605±0.0293	0.9684±0.0247	0.9727±0.0305
0.8×L1+0.2×$L1_{Canny}$	60.15±32.13	5.85±1.49	32.22±3.32	0.8718±0.0553	0.9199±0.0447	0.9463±0.0352	0.9606±0.0285	0.9684±0.0242	0.9727±0.0309
0.9×L1+0.1×$L1_{Canny}$	59.37±31.09	5.82±1.44	32.13±1.40	0.8725±0.0547	0.9205±0.0440	0.9468±0.0347	0.9610±0.0280	0.9687±0.0237	0.9730±0.0310
L1	61.06±33.00	5.91±1.53	32.17±3.31	0.8705±0.0557	0.9187±0.0457	0.9452±0.0364	0.9597±0.0296	0.9677±0.0251	0.9722±0.0310
L1+0.1×LSSIMw3	60.23±31.91	5.89±1.48	32.17±3.28	0.8717±0.0556	0.9192±0.0457	0.9456±0.0364	0.9600±0.0296	0.9680±0.0251	0.9724±0.0305
L1+0.2×LSSIMw3	60.36±30.71	5.89±1.47	32.16±3.32	0.8723±0.0544	0.9201±0.0441	0.9463±0.0348	0.9606±0.0282	0.9683±0.0240	0.9727±0.0305
L1+0.3×LSSIMw3	61.75±31.98	5.96±1.50	32.10±3.30	0.8702±0.0553	0.9178±0.0457	0.9444±0.0367	0.9590±0.0300	0.9672±0.0254	0.9717±0.0303
L1+0.4×LSSIMw3	60.75±31.78	5.91±1.46	32.06±1.48	0.8712±0.0544	0.9193±0.0438	0.9458±0.0347	0.9602±0.0283	0.9681±0.0242	0.9725±0.0303
L1+0.5×LSSIMw3	60.03±29.89	5.88±1.40	32.13±3.29	0.8722±0.0550	0.9200±0.0446	0.9463±0.0356	0.9605±0.0291	0.9683±0.0247	0.9727±0.0303
LSSIMw3	61.89±32.13	5.98±1.46	31.95±1.35	0.8703±0.0550	0.9182±0.0449	0.9449±0.0359	0.9595±0.0293	0.9676±0.0249	0.9721±0.0302
L1+0.1×LSSIMw7	58.90±31.25	5.82±1.47	32.13±1.53	0.8732±0.0550	0.9212±0.0447	0.9473±0.0352	0.9614±0.0285	0.9690±0.0241	0.9732±0.0304
L1+0.2×LSSIMw7	59.82±29.92	5.88±1.44	32.06±1.49	0.8742±0.0544	0.9220±0.0435	0.9479±0.0340	0.9619±0.0273	0.9695±0.0230	0.9736±0.0303
L1+0.3×LSSIMw7	61.03±31.60	5.92±1.48	32.02±1.40	0.8700±0.0556	0.9181±0.0452	0.9448±0.0359	0.9594±0.0292	0.9674±0.0248	0.9720±0.0304
L1+0.4×LSSIMw7	60.10±31.62	5.89±1.44	32.05±1.50	0.8733±0.0546	0.9214±0.0434	0.9477±0.0337	0.9618±0.0270	0.9694±0.0228	0.9736±0.0302
L1+0.5×LSSIMw7	60.89±30.33	5.93±1.41	32.00±1.46	0.8712±0.0535	0.9195±0.0426	0.9461±0.0335	0.9604±0.0272	0.9682±0.0232	0.9725±0.0305
LSSIMw7	63.42±30.94	6.09±1.39	31.82±1.22	0.8719±0.0552	0.9200±0.0443	0.9464±0.0349	0.9606±0.0283	0.9684±0.0240	0.9727±0.0300
L2	60.06±30.44	5.89±1.47	32.17±3.31	0.8717±0.0544	0.9199±0.0440	0.9463±0.0348	0.9605±0.0284	0.9682±0.0243	0.9725±0.0307

SuppTable 12. Evaluation metrics (mean±standard deviation) calculated for lesion-focused ROI on entire test set (N=516) between DUNet images and acquired ground truth (GTacq), when enhancement is performed from hat-like k-space AcqPr images. DUNet was trained with loss functions shown in the table and the GTacq was used as the ground truth to train the network.

Loss Function	MSE	MAE	PSNR	SSIMw3	SSIMw5	SSIMw7	SSIMw9	SSIMw11	SSIMw13
0.0×L1+1.0×$L1_{Canny}$	12934.80±5710.40	102.79±26.15	27.94±0.76	0.0220±0.0223	0.0104±0.0150	0.0049±0.0101	0.0023±0.0066	0.0011±0.0043	0.0006±0.0257
0.1×L1+0.9×$L1_{Canny}$	69.65±52.86	6.15±1.95	32.05±1.62	0.8623±0.0599	0.9126±0.0484	0.9413±0.0380	0.9569±0.0308	0.9655±0.0262	0.9703±0.0295
0.2×L1+0.8×$L1_{Canny}$	65.63±47.47	6.00±1.85	32.22±3.34	0.8661±0.0582	0.9158±0.0473	0.9437±0.0371	0.9588±0.0299	0.9671±0.0252	0.9716±0.0292
0.3×L1+0.7×$L1_{Canny}$	65.85±44.93	6.00±1.81	32.14±1.48	0.8670±0.0575	0.9169±0.0460	0.9448±0.0356	0.9597±0.0282	0.9678±0.0236	0.9723±0.0293
0.4×L1+0.6×$L1_{Canny}$	64.62±43.83	5.95±1.77	32.14±1.45	0.8670±0.0573	0.9168±0.0460	0.9446±0.0358	0.9596±0.0286	0.9677±0.0241	0.9722±0.0291
0.5×L1+0.5×$L1_{Canny}$	67.90±50.80	6.07±1.91	32.24±3.42	0.8642±0.0586	0.9145±0.0471	0.9428±0.0368	0.9582±0.0295	0.9666±0.0249	0.9712±0.0293
0.6×L1+0.4×$L1_{Canny}$	67.01±48.45	6.03±1.88	32.12±1.62	0.8648±0.0586	0.9147±0.0475	0.9430±0.0370	0.9583±0.0296	0.9667±0.0250	0.9713±0.0293
0.7×L1+0.3×$L1_{Canny}$	64.37±44.25	5.96±1.81	32.15±1.61	0.8672±0.0572	0.9169±0.0460	0.9448±0.0357	0.9598±0.0284	0.9679±0.0239	0.9723±0.0292
0.8×L1+0.2×$L1_{Canny}$	64.31±46.94	5.94±1.81	32.29±3.33	0.8674±0.0586	0.9172±0.0465	0.9450±0.0358	0.9600±0.0284	0.9681±0.0238	0.9725±0.0292
0.9×L1+0.1×$L1_{Canny}$	67.93±50.10	6.09±1.87	32.19±3.36	0.8649±0.0580	0.9149±0.0465	0.9431±0.0363	0.9584±0.0291	0.9667±0.0245	0.9714±0.0294
L1	64.33±43.80	5.93±1.75	32.33±3.45	0.8679±0.0560	0.9178±0.0446	0.9455±0.0345	0.9603±0.0274	0.9683±0.0230	0.9726±0.0292
L1+0.1×LSSIMw3	63.09±41.31	5.92±1.71	32.15±1.47	0.8689±0.0566	0.9184±0.0452	0.9460±0.0349	0.9607±0.0277	0.9686±0.0232	0.9730±0.0289
L1+0.2×LSSIMw3	65.52±46.20	6.01±1.83	32.11±1.46	0.8664±0.0579	0.9166±0.0460	0.9446±0.0357	0.9597±0.0285	0.9678±0.0239	0.9722±0.0289
L1+0.3×LSSIMw3	68.73±48.21	6.14±1.90	32.01±1.59	0.8623±0.0580	0.9127±0.0467	0.9416±0.0365	0.9574±0.0292	0.9660±0.0245	0.9708±0.0288
L1+0.4×LSSIMw3	66.58±46.47	6.05±1.83	32.05±1.63	0.8654±0.0575	0.9155±0.0460	0.9436±0.0359	0.9587±0.0288	0.9670±0.0242	0.9716±0.0288
L1+0.5×LSSIMw3	65.06±42.77	6.01±1.69	32.06±1.51	0.8664±0.0564	0.9164±0.0454	0.9444±0.0354	0.9595±0.0282	0.9677±0.0237	0.9721±0.0288
LSSIMw3	66.74±44.75	6.08±1.75	32.00±1.54	0.8662±0.0575	0.9160±0.0461	0.9441±0.0359	0.9593±0.0286	0.9675±0.0240	0.9720±0.0287
L1+0.1×LSSIMw7	64.85±45.13	5.97±1.77	32.13±1.61	0.8669±0.0567	0.9169±0.0452	0.9448±0.0350	0.9598±0.0278	0.9679±0.0234	0.9723±0.0290
L1+0.2×LSSIMw7	64.03±41.11	5.95±1.68	32.22±3.34	0.8672±0.0565	0.9173±0.0447	0.9453±0.0343	0.9603±0.0271	0.9683±0.0228	0.9726±0.0288
L1+0.3×LSSIMw7	65.09±43.35	5.97±1.71	32.27±3.37	0.8666±0.0572	0.9165±0.0458	0.9445±0.0353	0.9596±0.0280	0.9677±0.0235	0.9722±0.0289
L1+0.4×LSSIMw7	65.37±45.31	6.00±1.80	32.20±3.33	0.8668±0.0569	0.9170±0.0456	0.9450±0.0353	0.9599±0.0281	0.9680±0.0236	0.9724±0.0288
L1+0.5×LSSIMw7	65.31±44.24	6.01±1.74	32.05±1.43	0.8663±0.0578	0.9165±0.0463	0.9446±0.0359	0.9597±0.0285	0.9679±0.0238	0.9723±0.0289
LSSIMw7	67.99±42.81	6.19±1.70	31.84±1.45	0.8678±0.0568	0.9177±0.0451	0.9455±0.0348	0.9604±0.0275	0.9683±0.0230	0.9726±0.0287
L2	64.82±43.46	5.98±1.81	32.24±3.33	0.8661±0.0576	0.9165±0.0460	0.9446±0.0355	0.9598±0.0280	0.9679±0.0233	0.9723±0.0289

SuppTable 13. Evaluation metrics (mean±standard deviation) calculated for lesion-focused ROI on entire test set (N=516) between DUNet image and acquired ground truth (GTacq), when enhancement is performed from US-1 undersampled AcqPr images. DUNet was trained with loss functions shown in the table and the GTacq was used as the ground truth to train the network.

Loss Function	MSE	MAE	PSNR	SSIMw3	SSIMw5	SSIMw7	SSIMw9	SSIMw11	SSIMw13
$0.0\times L1+1.0\times L1_{Canny}$	12994.42±5694.01	103.83±25.93	27.93±0.74	0.0108±0.0042	0.0067±0.0029	0.0047±0.0020	0.0038±0.0015	0.0033±0.0012	0.0030±0.0233
$0.1\times L1+0.9\times L1_{Canny}$	89.11±98.97	6.57±2.86	31.97±1.75	0.8488±0.0733	0.9018±0.0613	0.9332±0.0495	0.9505±0.0415	0.9600±0.0362	0.9654±0.0284
$0.2\times L1+0.8\times L1_{Canny}$	86.36±95.38	6.48±2.86	32.26±4.55	0.8507±0.0760	0.9037±0.0628	0.9348±0.0501	0.9517±0.0418	0.9609±0.0365	0.9662±0.0279
$0.3\times L1+0.7\times L1_{Canny}$	87.48±92.11	6.54±2.76	31.99±1.74	0.8487±0.0730	0.9018±0.0610	0.9333±0.0491	0.9506±0.0410	0.9601±0.0358	0.9656±0.0283
$0.4\times L1+0.6\times L1_{Canny}$	87.49±89.29	6.54±2.68	31.97±1.72	0.8495±0.0708	0.9026±0.0585	0.9341±0.0466	0.9513±0.0389	0.9607±0.0339	0.9661±0.0282
$0.5\times L1+0.5\times L1_{Canny}$	91.54±101.84	6.64±2.89	31.91±1.64	0.8468±0.0757	0.8998±0.0643	0.9317±0.0521	0.9492±0.0438	0.9590±0.0384	0.9646±0.0282
$0.6\times L1+0.4\times L1_{Canny}$	86.05±88.20	6.50±2.70	32.09±3.42	0.8508±0.0719	0.9038±0.0592	0.9350±0.0469	0.9519±0.0389	0.9612±0.0337	0.9665±0.0282
$0.7\times L1+0.3\times L1_{Canny}$	86.14±94.73	6.47±2.81	32.14±3.42	0.8512±0.0739	0.9041±0.0611	0.9351±0.0487	0.9520±0.0404	0.9612±0.0352	0.9664±0.0282
$0.8\times L1+0.2\times L1_{Canny}$	83.92±85.93	6.42±2.64	32.19±3.45	0.8526±0.0697	0.9052±0.0576	0.9359±0.0461	0.9526±0.0384	0.9618±0.0334	0.9670±0.0281
$0.9\times L1+0.1\times L1_{Canny}$	90.59±99.18	6.61±2.87	32.02±3.42	0.8474±0.0737	0.9008±0.0614	0.9326±0.0495	0.9501±0.0414	0.9597±0.0362	0.9651±0.0282
L1	84.98±86.50	6.46±2.69	32.01±1.86	0.8512±0.0718	0.9036±0.0600	0.9347±0.0479	0.9517±0.0398	0.9611±0.0346	0.9664±0.0282
L1+0.1×LSSIMw3	86.09±88.82	6.50±2.74	32.11±3.53	0.8501±0.0720	0.9031±0.0593	0.9344±0.0473	0.9515±0.0393	0.9610±0.0342	0.9663±0.0278
L1+0.2×LSSIMw3	87.28±90.42	6.56±2.73	32.02±3.38	0.8487±0.0764	0.9020±0.0626	0.9336±0.0496	0.9509±0.0412	0.9604±0.0357	0.9659±0.0279
L1+0.3×LSSIMw3	84.23±85.24	6.46±2.63	32.00±1.70	0.8517±0.0731	0.9043±0.0606	0.9354±0.0483	0.9523±0.0401	0.9615±0.0349	0.9668±0.0278
L1+0.4×LSSIMw3	90.21±95.86	6.66±2.77	31.81±1.54	0.8466±0.0722	0.8999±0.0603	0.9321±0.0483	0.9499±0.0402	0.9597±0.0351	0.9652±0.0277
L1+0.5×LSSIMw3	87.56±93.17	6.54±2.76	32.10±3.49	0.8494±0.0723	0.9022±0.0605	0.9335±0.0487	0.9508±0.0407	0.9604±0.0354	0.9659±0.0277
LSSIMw3	91.66±96.89	6.73±2.75	31.75±1.69	0.8465±0.0740	0.8999±0.0617	0.9319±0.0496	0.9497±0.0416	0.9595±0.0364	0.9651±0.0276
L1+0.1×LSSIMw7	91.38±104.01	6.66±2.93	31.88±1.72	0.8463±0.0745	0.8992±0.0628	0.9312±0.0511	0.9489±0.0427	0.9588±0.0371	0.9645±0.0277
L1+0.2×LSSIMw7	89.85±92.71	6.66±2.75	31.81±1.60	0.8461±0.0727	0.8995±0.0606	0.9318±0.0487	0.9496±0.0408	0.9594±0.0356	0.9650±0.0278
L1+0.3×LSSIMw7	87.76±93.19	6.58±2.74	32.07±3.45	0.8489±0.0719	0.9023±0.0600	0.9339±0.0483	0.9512±0.0404	0.9607±0.0354	0.9660±0.0278
L1+0.4×LSSIMw7	86.15±88.75	6.53±2.67	31.93±1.60	0.8496±0.0712	0.9031±0.0587	0.9346±0.0466	0.9518±0.0384	0.9612±0.0332	0.9665±0.0275
L1+0.5×LSSIMw7	87.95±91.84	6.58±2.72	32.03±3.46	0.8492±0.0724	0.9022±0.0602	0.9338±0.0482	0.9511±0.0400	0.9606±0.0348	0.9660±0.0277
LSSIMw7	89.16±89.29	6.68±2.62	31.79±1.46	0.8487±0.0713	0.9021±0.0583	0.9339±0.0458	0.9512±0.0377	0.9607±0.0325	0.9661±0.0277
L2	89.03±90.40	6.63±2.71	31.87±1.79	0.8462±0.0731	0.8995±0.0616	0.9316±0.0498	0.9493±0.0419	0.9591±0.0369	0.9647±0.0273

SuppTable 14. Evaluation metrics (mean±standard deviation) calculated for lesion-focused ROI on entire test set (N=516) between DUNet images and acquired ground truth (GTacq), when enhancement is performed from US-2 undersampled AcqPr images. DUNet was trained with loss functions shown in the table and the GTacq was used as the ground truth to train the network.

Loss Function	MSE	MAE	PSNR	SSIMw3	SSIMw5	SSIMw7	SSIMw9	SSIMw11	SSIMw13
0.0×L1+1.0×$L1_{Canny}$	5753.99±2361.93	67.54±16.28	27.86±0.51	0.2900±0.0532	0.2774±0.0580	0.2788±0.0597	0.2868±0.0592	0.2971±0.0573	0.3081±0.0333
0.1×L1+0.9×$L1_{Canny}$	160.78±115.44	9.42±3.11	30.23±1.39	0.8057±0.0825	0.8490±0.0846	0.8827±0.0792	0.9066±0.0712	0.9230±0.0630	0.9339±0.0288
0.2×L1+0.8×$L1_{Canny}$	165.77±113.45	9.58±3.09	30.18±1.54	0.8038±0.0832	0.8463±0.0858	0.8796±0.0806	0.9034±0.0728	0.9199±0.0647	0.9311±0.0292
0.3×L1+0.7×$L1_{Canny}$	168.75±119.58	9.71±3.17	30.09±1.14	0.8002±0.0865	0.8421±0.0901	0.8758±0.0852	0.9002±0.0770	0.9174±0.0683	0.9292±0.0289
0.4×L1+0.6×$L1_{Canny}$	163.88±117.00	9.54±3.17	30.21±1.36	0.8035±0.0859	0.8462±0.0878	0.8798±0.0821	0.9038±0.0738	0.9206±0.0652	0.9319±0.0288
0.5×L1+0.5×$L1_{Canny}$	166.17±117.33	9.64±3.22	30.24±3.33	0.8013±0.0833	0.8437±0.0854	0.8775±0.0800	0.9018±0.0721	0.9188±0.0639	0.9304±0.0291
0.6×L1+0.4×$L1_{Canny}$	158.75±118.63	9.41±3.12	30.22±1.24	0.8070±0.0826	0.8499±0.0838	0.8834±0.0777	0.9071±0.0693	0.9234±0.0608	0.9344±0.0288
0.7×L1+0.3×$L1_{Canny}$	162.09±112.97	9.51±3.11	30.16±1.08	0.8031±0.0820	0.8461±0.0846	0.8798±0.0797	0.9038±0.0724	0.9203±0.0646	0.9315±0.0290
0.8×L1+0.2×$L1_{Canny}$	165.23±117.10	9.60±3.13	30.25±3.28	0.8028±0.0831	0.8457±0.0848	0.8794±0.0795	0.9033±0.0719	0.9199±0.0640	0.9311±0.0287
0.9×L1+0.1×$L1_{Canny}$	163.28±112.84	9.54±3.09	30.17±1.09	0.8036±0.0829	0.8467±0.0846	0.8804±0.0788	0.9043±0.0708	0.9208±0.0629	0.9320±0.0293
L1	173.55±123.38	9.81±3.24	30.09±1.14	0.7971±0.0839	0.8395±0.0863	0.8736±0.0814	0.8982±0.0740	0.9154±0.0663	0.9273±0.0285
L1+0.1×LSSIMw3	164.61±117.88	9.60±3.12	30.13±1.34	0.8028±0.0816	0.8455±0.0843	0.8790±0.0797	0.9029±0.0725	0.9196±0.0647	0.9309±0.0286
L1+0.2×LSSIMw3	178.72±124.43	10.01±3.24	30.04±1.40	0.7938±0.0854	0.8353±0.0897	0.8694±0.0857	0.8944±0.0782	0.9121±0.0699	0.9244±0.0286
L1+0.3×LSSIMw3	160.04±112.28	9.45±3.05	30.17±1.08	0.8071±0.0792	0.8499±0.0808	0.8829±0.0755	0.9062±0.0683	0.9223±0.0607	0.9332±0.0286
L1+0.4×LSSIMw3	181.98±123.49	10.11±3.19	30.12±3.32	0.7933±0.0835	0.8342±0.0872	0.8679±0.0836	0.8928±0.0768	0.9106±0.0690	0.9230±0.0288
L1+0.5×LSSIMw3	168.62±106.37	9.79±2.87	30.01±0.99	0.7994±0.0812	0.8421±0.0841	0.8761±0.0795	0.9005±0.0722	0.9176±0.0644	0.9292±0.0286
LSSIMw3	162.49±102.52	9.61±2.91	30.11±1.37	0.8068±0.0781	0.8506±0.0787	0.8845±0.0724	0.9082±0.0641	0.9242±0.0562	0.9349±0.0284
L1+0.1×LSSIMw7	154.69±112.10	9.30±3.05	30.24±1.11	0.8103±0.0809	0.8534±0.0822	0.8863±0.0769	0.9094±0.0694	0.9252±0.0616	0.9357±0.0289
L1+0.2×LSSIMw7	162.62±108.60	9.55±2.91	30.22±3.27	0.8031±0.0813	0.8461±0.0830	0.8797±0.0782	0.9035±0.0713	0.9199±0.0638	0.9311±0.0288
L1+0.3×LSSIMw7	160.14±111.90	9.48±3.02	30.12±1.08	0.8050±0.0817	0.8486±0.0822	0.8824±0.0766	0.9061±0.0692	0.9224±0.0616	0.9333±0.0284
L1+0.4×LSSIMw7	160.85±111.16	9.51±3.06	30.15±1.20	0.8052±0.0810	0.8484±0.0819	0.8819±0.0764	0.9056±0.0688	0.9218±0.0612	0.9327±0.0287
L1+0.5×LSSIMw7	152.31±95.41	9.32±2.75	30.31±3.35	0.8095±0.0785	0.8537±0.0786	0.8871±0.0727	0.9104±0.0649	0.9262±0.0573	0.9367±0.0286
LSSIMw7	168.54±108.82	9.81±2.89	30.00±1.30	0.8043±0.0817	0.8482±0.0823	0.8819±0.0766	0.9057±0.0690	0.9219±0.0614	0.9327±0.0285
L2	159.52±108.34	9.49±2.97	30.14±1.17	0.8040±0.0823	0.8463±0.0854	0.8795±0.0807	0.9034±0.0729	0.9201±0.0644	0.9316±0.0273

SuppTable 15. Evaluation metrics (mean±standard deviation) calculated for lesion-focused ROI on entire test set set (N=516) between DUNet images and acquired ground truth (GTacq), when enhancement is performed from US-3 undersampled AcqPr images. DUNet was trained with loss functions shown in the table and the GTacq was used as the ground truth to train the network.

Loss Function	MSE	MAE	PSNR	SSIMw3	SSIMw5	SSIMw7	SSIMw9	SSIMw11	SSIMw13
0.0×L1+1.0×$L1_{Canny}$	13387.23±5920.33	105.30±26.59	28.09±3.25	0.0055±0.0131	0.0027±0.0088	0.0013±0.0057	0.0007±0.0032	0.0003±0.0015	0.0002±0.0010
0.1×L1+0.9×$L1_{Canny}$	38.93±30.11	4.49±1.53	34.03±2.03	0.9423±0.0358	0.9585±0.0306	0.9705±0.0252	0.9776±0.0207	0.9819±0.0173	0.9844±0.0148
0.2×L1+0.8×$L1_{Canny}$	38.14±28.77	4.44±1.51	34.12±2.15	0.9430±0.0355	0.9592±0.0314	0.9710±0.0265	0.9780±0.0219	0.9822±0.0184	0.9847±0.0157
0.3×L1+0.7×$L1_{Canny}$	38.55±28.43	4.46±1.51	34.07±2.13	0.9432±0.0360	0.9590±0.0315	0.9707±0.0264	0.9777±0.0219	0.9820±0.0185	0.9845±0.0159
0.4×L1+0.6×$L1_{Canny}$	38.85±27.89	4.49±1.48	34.01±2.03	0.9422±0.0352	0.9582±0.0314	0.9701±0.0264	0.9773±0.0218	0.9817±0.0182	0.9843±0.0156
0.5×L1+0.5×$L1_{Canny}$	39.27±27.76	4.52±1.49	33.98±2.11	0.9421±0.0358	0.9583±0.0311	0.9702±0.0259	0.9775±0.0214	0.9818±0.0179	0.9843±0.0154
0.6×L1+0.4×$L1_{Canny}$	38.60±28.18	4.48±1.49	34.01±2.09	0.9421±0.0363	0.9581±0.0320	0.9701±0.0268	0.9774±0.0222	0.9817±0.0186	0.9843±0.0160
0.7×L1+0.3×$L1_{Canny}$	39.65±29.28	4.53±1.54	34.01±2.15	0.9410±0.0368	0.9574±0.0329	0.9695±0.0277	0.9769±0.0229	0.9813±0.0192	0.9840±0.0164
0.8×L1+0.2×$L1_{Canny}$	39.80±28.69	4.54±1.50	33.97±2.04	0.9410±0.0370	0.9574±0.0326	0.9696±0.0272	0.9769±0.0223	0.9813±0.0187	0.9840±0.0160
0.9×L1+0.1×$L1_{Canny}$	37.43±27.98	4.40±1.47	34.15±2.06	0.9436±0.0355	0.9595±0.0311	0.9713±0.0259	0.9783±0.0213	0.9824±0.0179	0.9848±0.0154
L1	38.14±28.52	4.46±1.48	34.05±1.98	0.9433±0.0358	0.9591±0.0313	0.9709±0.0260	0.9780±0.0213	0.9822±0.0178	0.9847±0.0153
L1+0.1×LSSIMw3	43.91±32.71	4.74±1.61	33.71±1.99	0.9372±0.0379	0.9541±0.0339	0.9669±0.0287	0.9748±0.0238	0.9796±0.0201	0.9825±0.0173
L1+0.2×LSSIMw3	60.79±40.68	5.59±1.65	32.75±3.40	0.9216±0.0388	0.9433±0.0303	0.9589±0.0250	0.9682±0.0211	0.9739±0.0181	0.9775±0.0160
L1+0.3×LSSIMw3	68.66±38.76	6.06±1.54	32.05±1.34	0.9190±0.0380	0.9393±0.0306	0.9550±0.0257	0.9649±0.0216	0.9712±0.0186	0.9752±0.0164
L1+0.4×LSSIMw3	64.22±38.18	5.82±1.53	32.30±1.43	0.9211±0.0376	0.9418±0.0300	0.9572±0.0250	0.9667±0.0212	0.9727±0.0182	0.9765±0.0160
L1+0.5×LSSIMw3	69.88±39.03	6.11±1.57	32.12±3.29	0.9162±0.0373	0.9372±0.0306	0.9536±0.0260	0.9639±0.0221	0.9704±0.0190	0.9747±0.0167
LSSIMw3	64.35±38.39	5.79±1.56	32.37±1.54	0.9185±0.0380	0.9396±0.0306	0.9557±0.0257	0.9657±0.0218	0.9719±0.0187	0.9759±0.0164
L1+0.1×LSSIMw7	37.91±28.14	4.43±1.49	34.11±2.04	0.9439±0.0343	0.9599±0.0294	0.9715±0.0243	0.9785±0.0200	0.9825±0.0168	0.9850±0.0144
L1+0.2×LSSIMw7	41.80±29.75	4.65±1.51	33.79±1.94	0.9384±0.0355	0.9555±0.0311	0.9682±0.0262	0.9758±0.0217	0.9804±0.0183	0.9832±0.0158
L1+0.3×LSSIMw7	44.18±30.59	4.77±1.52	33.64±1.95	0.9360±0.0365	0.9535±0.0321	0.9664±0.0273	0.9743±0.0228	0.9791±0.0192	0.9821±0.0166
L1+0.4×LSSIMw7	42.13±30.35	4.67±1.52	33.76±1.93	0.9378±0.0348	0.9551±0.0306	0.9678±0.0258	0.9755±0.0214	0.9801±0.0180	0.9829±0.0156
L1+0.5×LSSIMw7	46.48±32.86	4.90±1.59	33.45±1.93	0.9337±0.0364	0.9511±0.0327	0.9645±0.0281	0.9727±0.0235	0.9779±0.0199	0.9811±0.0172
LSSIMw7	60.21±37.83	5.61±1.59	32.58±1.55	0.9202±0.0423	0.9426±0.0324	0.9585±0.0262	0.9680±0.0216	0.9738±0.0182	0.9774±0.0159
L2	39.72±26.73	4.60±1.43	33.81±1.90	0.9407±0.0335	0.9574±0.0299	0.9696±0.0254	0.9769±0.0212	0.9812±0.0180	0.9838±0.0156

SuppTable 16. Evaluation metrics (mean±standard deviation) calculated for lesion-focused ROI on entire test set (N=516) between DUNet images and synthetic ground truth (GTsyn), when enhancement is performed from complete k-space AcqPr images. DUNet was trained with loss functions shown in the table and the GTsyn was used as the ground truth to train the network.

Loss Function	MSE	MAE	PSNR	SSIMw3	SSIMw5	SSIMw7	SSIMw9	SSIMw11	SSIMw13
0.0×L1+1.0×$L1_{Canny}$	13393.99±5920.49	105.43±26.54	28.07±3.25	0.0021±0.0056	0.0010±0.0033	0.0005±0.0019	0.0003±0.0010	0.0002±0.0005	0.0001±0.0043
0.1×L1+0.9×$L1_{Canny}$	39.65±32.60	4.53±1.58	33.97±1.96	0.9422±0.0377	0.9588±0.0302	0.9709±0.0237	0.9780±0.0189	0.9823±0.0156	0.9848±0.0049
0.2×L1+0.8×$L1_{Canny}$	40.17±29.56	4.58±1.57	34.04±3.60	0.9397±0.0375	0.9563±0.0316	0.9689±0.0258	0.9765±0.0212	0.9811±0.0175	0.9840±0.0050
0.3×L1+0.7×$L1_{Canny}$	41.10±31.49	4.61±1.59	33.86±2.00	0.9395±0.0383	0.9564±0.0319	0.9690±0.0256	0.9766±0.0209	0.9811±0.0174	0.9839±0.0050
0.4×L1+0.6×$L1_{Canny}$	37.81±26.72	4.44±1.46	34.07±2.04	0.9426±0.0362	0.9589±0.0301	0.9710±0.0241	0.9782±0.0196	0.9824±0.0162	0.9850±0.0049
0.5×L1+0.5×$L1_{Canny}$	39.62±28.56	4.54±1.50	33.92±1.92	0.9399±0.0378	0.9568±0.0316	0.9694±0.0255	0.9769±0.0207	0.9815±0.0171	0.9842±0.0050
0.6×L1+0.4×$L1_{Canny}$	41.09±29.32	4.62±1.52	33.81±1.93	0.9386±0.0391	0.9549±0.0337	0.9675±0.0274	0.9754±0.0224	0.9803±0.0185	0.9833±0.0050
0.7×L1+0.3×$L1_{Canny}$	39.43±27.51	4.55±1.48	33.90±1.97	0.9415±0.0364	0.9577±0.0306	0.9699±0.0248	0.9772±0.0203	0.9817±0.0169	0.9844±0.0049
0.8×L1+0.2×$L1_{Canny}$	39.19±28.51	4.53±1.52	33.98±2.05	0.9411±0.0368	0.9578±0.0304	0.9701±0.0246	0.9775±0.0200	0.9819±0.0165	0.9846±0.0049
0.9×L1+0.1×$L1_{Canny}$	36.11±23.85	4.36±1.36	34.16±1.94	0.9442±0.0332	0.9605±0.0270	0.9722±0.0216	0.9792±0.0176	0.9832±0.0146	0.9856±0.0049
L1	40.42±29.35	4.57±1.52	33.89±1.95	0.9402±0.0379	0.9569±0.0314	0.9693±0.0253	0.9768±0.0207	0.9813±0.0172	0.9841±0.0049
L1+0.1×LSSIMw3	45.03±32.68	4.78±1.59	33.64±1.95	0.9356±0.0384	0.9530±0.0318	0.9662±0.0258	0.9744±0.0213	0.9793±0.0178	0.9824±0.0051
L1+0.2×LSSIMw3	50.21±38.53	5.05±1.73	33.30±1.88	0.9311±0.0405	0.9487±0.0345	0.9625±0.0287	0.9713±0.0238	0.9769±0.0198	0.9804±0.0052
L1+0.3×LSSIMw3	48.44±36.72	4.97±1.72	33.41±1.94	0.9329±0.0408	0.9500±0.0348	0.9637±0.0289	0.9723±0.0240	0.9777±0.0201	0.9812±0.0051
L1+0.4×LSSIMw3	47.48±36.67	4.91±1.69	33.49±1.92	0.9339±0.0404	0.9514±0.0341	0.9648±0.0280	0.9732±0.0232	0.9783±0.0194	0.9816±0.0052
L1+0.5×LSSIMw3	45.75±33.88	4.83±1.61	33.55±1.92	0.9349±0.0383	0.9526±0.0316	0.9661±0.0257	0.9743±0.0212	0.9793±0.0176	0.9824±0.0050
LSSIMw3	52.00±38.39	5.20±1.72	33.08±1.92	0.9299±0.0394	0.9478±0.0336	0.9620±0.0280	0.9709±0.0233	0.9765±0.0196	0.9801±0.0051
L1+0.1×LSSIMw7	48.02±35.58	4.93±1.68	33.48±1.94	0.9332±0.0393	0.9511±0.0325	0.9647±0.0265	0.9730±0.0219	0.9782±0.0183	0.9814±0.0052
L1+0.2×LSSIMw7	45.41±31.73	4.84±1.56	33.53±1.86	0.9356±0.0371	0.9529±0.0314	0.9660±0.0259	0.9742±0.0214	0.9792±0.0179	0.9823±0.0052
L1+0.3×LSSIMw7	46.82±34.47	4.90±1.63	33.48±1.97	0.9335±0.0382	0.9513±0.0318	0.9650±0.0261	0.9734±0.0216	0.9785±0.0181	0.9817±0.0053
L1+0.4×LSSIMw7	45.98±32.61	4.88±1.58	33.46±1.94	0.9350±0.0374	0.9523±0.0315	0.9656±0.0260	0.9738±0.0216	0.9788±0.0182	0.9819±0.0052
L1+0.5×LSSIMw7	46.23±33.46	4.90±1.63	33.46±1.92	0.9337±0.0391	0.9511±0.0330	0.9646±0.0271	0.9731±0.0223	0.9784±0.0186	0.9817±0.0051
LSSIMw7	47.54±32.81	4.97±1.56	33.31±1.79	0.9329±0.0371	0.9505±0.0316	0.9641±0.0264	0.9726±0.0221	0.9779±0.0187	0.9812±0.0052
L2	38.53±24.68	4.56±1.35	33.80±1.83	0.9406±0.0338	0.9571±0.0290	0.9694±0.0238	0.9768±0.0195	0.9813±0.0164	0.9840±0.0053

SuppTable 17. Evaluation metrics (mean±standard deviation) calculated for lesion-focused ROI on entire test set (N=516) between DUNet images and synthetic ground truth (GTsyn), when enhancement is performed from hat-like k-space AcqPr images. DUNet was trained with loss functions shown in the table and the GTsyn was used as the ground truth to train the network.

Loss Function	MSE	MAE	PSNR	SSIMw3	SSIMw5	SSIMw7	SSIMw9	SSIMw11	SSIMw13
0.0×L1+1.0×$L1_{Canny}$	7320.44±3159.92	77.12±19.30	27.79±0.46	0.2231±0.0342	0.2158±0.0303	0.2182±0.0273	0.2222±0.0240	0.2261±0.0209	0.2295±0.0352
0.1×L1+0.9×$L1_{Canny}$	51.20±54.34	4.86±2.18	33.99±3.79	0.9291±0.0489	0.9486±0.0390	0.9639±0.0303	0.9731±0.0241	0.9785±0.0199	0.9817±0.0038
0.2×L1+0.8×$L1_{Canny}$	45.06±45.06	4.63±1.96	34.21±3.72	0.9351±0.0454	0.9537±0.0356	0.9679±0.0271	0.9762±0.0211	0.9810±0.0171	0.9838±0.0036
0.3×L1+0.7×$L1_{Canny}$	48.30±50.68	4.75±2.08	34.10±3.73	0.9314±0.0494	0.9503±0.0397	0.9650±0.0311	0.9740±0.0247	0.9792±0.0203	0.9823±0.0036
0.4×L1+0.6×$L1_{Canny}$	48.87±48.00	4.79±2.02	33.91±2.43	0.9311±0.0472	0.9506±0.0370	0.9654±0.0286	0.9743±0.0226	0.9794±0.0186	0.9824±0.0038
0.5×L1+0.5×$L1_{Canny}$	43.69±43.63	4.53±1.91	34.28±2.48	0.9359±0.0449	0.9544±0.0355	0.9684±0.0272	0.9766±0.0213	0.9813±0.0173	0.9841±0.0036
0.6×L1+0.4×$L1_{Canny}$	48.91±48.99	4.77±2.05	34.07±3.72	0.9309±0.0458	0.9504±0.0361	0.9653±0.0281	0.9742±0.0223	0.9793±0.0184	0.9823±0.0037
0.7×L1+0.3×$L1_{Canny}$	47.29±47.23	4.67±2.01	34.14±2.42	0.9325±0.0467	0.9515±0.0368	0.9661±0.0283	0.9748±0.0223	0.9799±0.0183	0.9829±0.0036
0.8×L1+0.2×$L1_{Canny}$	47.29±48.23	4.69±2.01	34.05±2.46	0.9326±0.0444	0.9515±0.0353	0.9660±0.0274	0.9747±0.0217	0.9798±0.0179	0.9828±0.0037
0.9×L1+0.1×$L1_{Canny}$	42.98±40.49	4.53±1.89	34.34±3.79	0.9368±0.0426	0.9554±0.0336	0.9692±0.0258	0.9773±0.0202	0.9819±0.0164	0.9845±0.0036
L1	45.95±46.11	4.64±1.98	34.13±2.40	0.9341±0.0459	0.9527±0.0365	0.9670±0.0283	0.9756±0.0223	0.9805±0.0183	0.9834±0.0036
L1+0.1×LSSIMw3	47.84±47.01	4.72±1.98	34.04±2.36	0.9329±0.0455	0.9518±0.0364	0.9663±0.0281	0.9750±0.0219	0.9801±0.0177	0.9831±0.0035
L1+0.2×LSSIMw3	49.20±50.28	4.79±2.00	33.92±2.28	0.9306±0.0452	0.9498±0.0361	0.9649±0.0281	0.9739±0.0222	0.9791±0.0183	0.9822±0.0037
L1+0.3×LSSIMw3	78.24±85.25	6.00±2.70	32.63±1.96	0.9055±0.0598	0.9284±0.0478	0.9483±0.0388	0.9607±0.0326	0.9682±0.0286	0.9728±0.0043
L1+0.4×LSSIMw3	79.97±88.74	6.05±2.76	32.58±1.84	0.9042±0.0615	0.9272±0.0487	0.9473±0.0393	0.9599±0.0331	0.9675±0.0291	0.9722±0.0043
L1+0.5×LSSIMw3	81.77±84.18	6.21±2.62	32.34±1.73	0.9048±0.0583	0.9274±0.0462	0.9472±0.0372	0.9597±0.0312	0.9673±0.0274	0.9721±0.0044
LSSIMw3	55.41±55.73	5.09±2.12	33.53±2.25	0.9261±0.0474	0.9459±0.0377	0.9618±0.0294	0.9714±0.0236	0.9771±0.0197	0.9805±0.0037
L1+0.1×LSSIMw7	42.83±40.79	4.53±1.85	34.38±3.75	0.9374±0.0421	0.9556±0.0333	0.9693±0.0255	0.9773±0.0197	0.9820±0.0159	0.9846±0.0035
L1+0.2×LSSIMw7	44.79±41.05	4.62±1.83	34.09±2.27	0.9354±0.0421	0.9541±0.0332	0.9682±0.0254	0.9765±0.0196	0.9813±0.0158	0.9841±0.0036
L1+0.3×LSSIMw7	54.49±53.92	4.98±2.16	33.85±3.72	0.9265±0.0471	0.9463±0.0376	0.9620±0.0296	0.9715±0.0238	0.9772±0.0199	0.9806±0.0038
L1+0.4×LSSIMw7	53.57±52.60	4.96±2.11	33.77±2.39	0.9264±0.0474	0.9464±0.0375	0.9623±0.0292	0.9719±0.0234	0.9775±0.0195	0.9808±0.0038
L1+0.5×LSSIMw7	51.30±49.79	4.90±1.98	33.75±2.21	0.9285±0.0455	0.9483±0.0360	0.9638±0.0278	0.9730±0.0220	0.9784±0.0182	0.9816±0.0038
LSSIMw7	52.51±49.93	4.95±1.99	33.69±2.28	0.9271±0.0458	0.9469±0.0363	0.9625±0.0283	0.9720±0.0226	0.9776±0.0187	0.9810±0.0037
L2	51.12±50.25	4.93±2.03	33.85±3.64	0.9269±0.0470	0.9471±0.0366	0.9630±0.0282	0.9725±0.0225	0.9780±0.0189	0.9812±0.0042

SuppTable 18. Evaluation metrics (mean±standard deviation) calculated for lesion-focused ROI on entire test set (N=516) between DUNet images and synthetic ground truth (GTsyn), when enhancement is performed from US-1 undersampled AcqPr images. DUNet was trained with loss functions shown in the table and the GTsyn was used as the ground truth to train the network.

Loss Function	MSE	MAE	PSNR	SSIMw3	SSIMw5	SSIMw7	SSIMw9	SSIMw11	SSIMw13
$0.0\times L1+1.0\times L1_{Canny}$	13315.58±5878.46	105.01±26.46	28.07±3.25	0.0077±0.0136	0.0039±0.0094	0.0021±0.0059	0.0011±0.0031	0.0007±0.0014	0.0005±0.0048
$0.1\times L1+0.9\times L1_{Canny}$	69.92±95.20	5.26±3.08	33.93±2.64	0.9150±0.0719	0.9376±0.0576	0.9558±0.0454	0.9666±0.0376	0.9729±0.0326	0.9768±0.0027
$0.2\times L1+0.8\times L1_{Canny}$	66.58±90.54	5.13±2.98	34.06±2.61	0.9177±0.0700	0.9399±0.0561	0.9576±0.0439	0.9680±0.0361	0.9741±0.0311	0.9778±0.0027
$0.3\times L1+0.7\times L1_{Canny}$	72.41±99.79	5.37±3.16	33.89±3.95	0.9136±0.0758	0.9362±0.0608	0.9546±0.0478	0.9657±0.0395	0.9722±0.0342	0.9762±0.0027
$0.4\times L1+0.6\times L1_{Canny}$	65.46±93.34	5.07±3.03	34.15±2.75	0.9187±0.0707	0.9407±0.0572	0.9581±0.0449	0.9685±0.0369	0.9745±0.0317	0.9782±0.0027
$0.5\times L1+0.5\times L1_{Canny}$	65.37±92.77	5.04±3.01	34.20±2.81	0.9192±0.0718	0.9414±0.0572	0.9586±0.0448	0.9687±0.0371	0.9746±0.0323	0.9781±0.0027
$0.6\times L1+0.4\times L1_{Canny}$	66.53±88.92	5.16±2.96	34.12±3.96	0.9175±0.0688	0.9399±0.0557	0.9577±0.0438	0.9682±0.0362	0.9743±0.0312	0.9780±0.0027
$0.7\times L1+0.3\times L1_{Canny}$	67.64±92.75	5.16±3.03	34.07±2.76	0.9168±0.0725	0.9390±0.0585	0.9568±0.0458	0.9674±0.0377	0.9736±0.0323	0.9774±0.0027
$0.8\times L1+0.2\times L1_{Canny}$	66.17±89.55	5.10±3.00	34.37±4.94	0.9179±0.0706	0.9402±0.0569	0.9578±0.0447	0.9682±0.0369	0.9743±0.0319	0.9780±0.0027
$0.9\times L1+0.1\times L1_{Canny}$	64.30±87.28	5.06±2.92	34.14±2.79	0.9194±0.0678	0.9416±0.0543	0.9589±0.0425	0.9692±0.0347	0.9751±0.0297	0.9786±0.0027
L1	65.77±90.72	5.13±2.95	33.99±2.60	0.9171±0.0700	0.9397±0.0560	0.9576±0.0438	0.9681±0.0359	0.9743±0.0308	0.9780±0.0027
L1+0.1×LSSIMw3	65.98±88.78	5.12±2.95	34.17±4.03	0.9180±0.0693	0.9402±0.0552	0.9580±0.0433	0.9684±0.0360	0.9745±0.0313	0.9781±0.0027
L1+0.2×LSSIMw3	66.97±95.73	5.14±3.04	34.03±2.68	0.9174±0.0710	0.9399±0.0562	0.9577±0.0439	0.9683±0.0361	0.9744±0.0310	0.9780±0.0027
L1+0.3×LSSIMw3	103.90±135.69	6.68±3.63	32.37±2.11	0.8840±0.0911	0.9096±0.0774	0.9342±0.0635	0.9501±0.0537	0.9595±0.0475	0.9652±0.0031
L1+0.4×LSSIMw3	106.26±141.44	6.71±3.69	32.35±1.99	0.8841±0.0945	0.9097±0.0797	0.9337±0.0656	0.9494±0.0556	0.9588±0.0492	0.9645±0.0031
L1+0.5×LSSIMw3	108.51±141.34	6.86±3.68	32.20±1.91	0.8817±0.0947	0.9071±0.0809	0.9317±0.0667	0.9478±0.0566	0.9576±0.0500	0.9636±0.0031
LSSIMw3	74.40±94.91	5.53±3.03	33.66±3.85	0.9095±0.0725	0.9329±0.0590	0.9524±0.0469	0.9642±0.0391	0.9711±0.0341	0.9753±0.0028
L1+0.1×LSSIMw7	63.26±82.83	5.04±2.84	34.21±3.98	0.9210±0.0659	0.9432±0.0521	0.9603±0.0400	0.9702±0.0323	0.9759±0.0275	0.9793±0.0027
L1+0.2×LSSIMw7	63.98±87.03	5.04±2.88	34.25±3.94	0.9202±0.0672	0.9421±0.0545	0.9591±0.0435	0.9692±0.0363	0.9750±0.0316	0.9786±0.0027
L1+0.3×LSSIMw7	74.91±95.82	5.52±3.06	33.55±2.63	0.9094±0.0733	0.9327±0.0593	0.9520±0.0471	0.9638±0.0392	0.9708±0.0341	0.9750±0.0028
L1+0.4×LSSIMw7	75.64±101.44	5.51±3.15	33.72±3.91	0.9096±0.0726	0.9326±0.0597	0.9520±0.0476	0.9638±0.0397	0.9707±0.0347	0.9749±0.0029
L1+0.5×LSSIMw7	76.41±99.53	5.58±3.11	33.47±2.55	0.9088±0.0720	0.9322±0.0589	0.9517±0.0474	0.9634±0.0398	0.9704±0.0348	0.9746±0.0028
LSSIMw7	75.88±97.70	5.61±3.06	33.44±2.49	0.9077±0.0725	0.9313±0.0590	0.9513±0.0470	0.9634±0.0393	0.9705±0.0344	0.9747±0.0028
L2	67.75±91.55	5.27±2.93	33.76±2.51	0.9158±0.0682	0.9383±0.0550	0.9564±0.0433	0.9672±0.0358	0.9734±0.0310	0.9772±0.0029

SuppTable 19. Evaluation metrics (mean±standard deviation) calculated for lesion-focused ROI on entire test set (N=516) between DUNet images and synthetic ground truth (GTsyn), when enhancement is performed from US-2 undersampled AcqPr images. DUNet was trained with loss functions shown in the table and the GTsyn was used as the ground truth to train the network.

Loss Function	MSE	MAE	PSNR	SSIMw3	SSIMw5	SSIMw7	SSIMw9	SSIMw11	SSIMw13
0.0×L1+1.0×$L1_{Canny}$	13394.51±5920.39	105.44±26.54	28.07±3.25	0.0018±0.0052	0.0009±0.0031	0.0005±0.0017	0.0002±0.0009	0.0002±0.0005	0.0001±0.0042
0.1×L1+0.9×$L1_{Canny}$	147.19±119.52	8.79±3.41	30.72±1.61	0.8664±0.0823	0.8797±0.0847	0.9010±0.0790	0.9193±0.0704	0.9331±0.0614	0.9430±0.0061
0.2×L1+0.8×$L1_{Canny}$	141.25±119.94	8.57±3.33	30.94±3.52	0.8705±0.0810	0.8845±0.0825	0.9052±0.0770	0.9227±0.0690	0.9358±0.0606	0.9453±0.0062
0.3×L1+0.7×$L1_{Canny}$	141.44±112.81	8.65±3.28	30.72±1.57	0.8667±0.0828	0.8806±0.0844	0.9019±0.0783	0.9201±0.0695	0.9339±0.0605	0.9439±0.0062
0.4×L1+0.6×$L1_{Canny}$	150.04±121.01	8.93±3.38	30.58±1.53	0.8662±0.0793	0.8797±0.0806	0.9010±0.0751	0.9192±0.0671	0.9329±0.0590	0.9427±0.0063
0.5×L1+0.5×$L1_{Canny}$	143.87±115.18	8.77±3.22	30.59±1.46	0.8678±0.0786	0.8815±0.0805	0.9026±0.0752	0.9205±0.0673	0.9339±0.0589	0.9436±0.0060
0.6×L1+0.4×$L1_{Canny}$	143.52±114.79	8.74±3.29	30.65±1.54	0.8677±0.0808	0.8809±0.0828	0.9018±0.0772	0.9196±0.0692	0.9332±0.0609	0.9430±0.0060
0.7×L1+0.3×$L1_{Canny}$	145.60±120.91	8.78±3.38	30.65±1.49	0.8648±0.0823	0.8789±0.0838	0.9008±0.0778	0.9192±0.0693	0.9330±0.0606	0.9429±0.0063
0.8×L1+0.2×$L1_{Canny}$	135.72±111.51	8.43±3.18	30.81±1.70	0.8708±0.0797	0.8850±0.0799	0.9062±0.0740	0.9239±0.0661	0.9371±0.0581	0.9463±0.0062
0.9×L1+0.1×$L1_{Canny}$	148.67±125.02	8.83±3.39	30.64±1.60	0.8649±0.0824	0.8779±0.0839	0.8992±0.0782	0.9177±0.0698	0.9317±0.0611	0.9418±0.0061
L1	148.34±121.25	8.84±3.37	30.63±1.70	0.8641±0.0834	0.8785±0.0850	0.9003±0.0798	0.9186±0.0719	0.9323±0.0633	0.9421±0.0063
L1+0.1×LSSIMw3	184.09±155.25	9.82±3.78	30.26±1.38	0.8442±0.0889	0.8552±0.0922	0.8779±0.0879	0.8986±0.0802	0.9151±0.0716	0.9274±0.0061
L1+0.2×LSSIMw3	168.58±139.55	9.40±3.57	30.51±3.42	0.8537±0.0848	0.8664±0.0869	0.8887±0.0821	0.9084±0.0741	0.9237±0.0653	0.9348±0.0060
L1+0.3×LSSIMw3	175.46±144.86	9.64±3.60	30.29±1.44	0.8513±0.0825	0.8637±0.0848	0.8860±0.0808	0.9059±0.0733	0.9214±0.0650	0.9328±0.0061
L1+0.4×LSSIMw3	160.75±127.89	9.26±3.39	30.43±1.47	0.8587±0.0788	0.8728±0.0807	0.8951±0.0762	0.9142±0.0687	0.9287±0.0606	0.9391±0.0060
L1+0.5×LSSIMw3	174.94±145.52	9.55±3.67	30.37±1.53	0.8510±0.0838	0.8642±0.0841	0.8868±0.0791	0.9066±0.0719	0.9220±0.0643	0.9332±0.0061
LSSIMw3	203.50±175.39	10.33±4.02	30.23±3.50	0.8377±0.0889	0.8489±0.0913	0.8720±0.0873	0.8933±0.0802	0.9101±0.0723	0.9227±0.0064
L1+0.1×LSSIMw7	180.21±148.48	9.72±3.71	30.30±1.50	0.8475±0.0837	0.8604±0.0857	0.8833±0.0811	0.9036±0.0738	0.9195±0.0657	0.9311±0.0062
L1+0.2×LSSIMw7	168.76±141.51	9.35±3.69	30.50±1.75	0.8544±0.0865	0.8669±0.0889	0.8891±0.0837	0.9086±0.0756	0.9237±0.0669	0.9348±0.0062
L1+0.3×LSSIMw7	162.99±132.99	9.29±3.51	30.44±1.77	0.8560±0.0816	0.8691±0.0832	0.8914±0.0781	0.9109±0.0704	0.9259±0.0621	0.9367±0.0060
L1+0.4×LSSIMw7	168.16±136.03	9.44±3.49	30.45±3.42	0.8553±0.0816	0.8685±0.0836	0.8906±0.0788	0.9099±0.0714	0.9247±0.0633	0.9354±0.0060
L1+0.5×LSSIMw7	159.68±128.72	9.18±3.41	30.50±1.54	0.8582±0.0807	0.8716±0.0821	0.8937±0.0768	0.9129±0.0687	0.9277±0.0602	0.9383±0.0060
LSSIMw7	168.81±137.90	9.46±3.53	30.37±1.63	0.8571±0.0811	0.8703±0.0832	0.8921±0.0783	0.9112±0.0708	0.9258±0.0628	0.9364±0.0060
L2	139.30±107.33	8.67±3.13	30.65±1.57	0.8679±0.0740	0.8832±0.0750	0.9047±0.0702	0.9224±0.0632	0.9355±0.0558	0.9448±0.0061

SuppTable 20. Evaluation metrics (mean±standard deviation) calculated for lesion-focused ROI on entire test set (N=516) between DUNet images and synthetic ground truth (GTsyn), when enhancement is performed from US-3 underssampled AcqPr images. DUNet was trained with loss functions shown in the table and the GTsyn was used as the ground truth to train the network.